DISS. ETH NO. 22285

DROPLET MICROFLUIDICS FOR CELL-BASED ASSAYS

A thesis submitted to attain the degree of

DOCTOR OF SCIENCES of ETH ZURICH

(Dr. sc. ETH Zurich)

presented by

DOMINIK EICHER

MSc ETH Biology, ETH Zurich

born on *11.03.1984*

citizen of *Baden AG, Switzerland*

accepted on the recommendation of

Prof. Dr. Uwe Sauer, examiner
Prof. Dr. Petra Dittrich, co-examiner
Dr. Christoph Merten, co-examiner

2014

ABSTRACT

Microfluidic chips allow the precise manipulation of liquids in channel networks at the micrometer scale. Aqueous droplets within an immiscible oil phase can be produced in such systems via flow-focusing or cross-flow shearing and are used as massively parallelized miniaturized reaction vessels to carry out chemical or biological reactions with throughputs in excess of a million samples per hour. However, sample diversity has thus far been created via the encapsulation of single cells from genetically encoded libraries such as yeast deletion libraries, whereas the creation of chemical diversity in microfluidic droplets has been a long-standing limitation in the field of droplet-based microfluidics. This specifically limits the use of such systems in cell-based screens, which require many different conditions to be tested. This dissertation describes the establishment of a new and fully integrated droplet-based microfluidic system that allows the systematic generation of combinatorial mixtures in water-in-oil plugs hosting human live cells. The system is based on individually actuatable pins of a Braille display, which open and close valves in microfluidic channels and thereby control the generation of mixtures of liquids injected from different inlets. As a first application for our approach we conducted a small scale chemical genetics screen of matrix metalloproteinase (MMP) activity with the future goal of investigating the regulation of individual MMPs. The new device enabled the production and measurement of 686 individual sample and label plugs, which were used to encode the sample sequence and to prevent cross-contamination between samples. The sample plug sequence consisted of five replicates of all possible combinatorial mixtures of twelve compounds, which resulted in 79 unique sample mixtures that were co-encapsulated with cells in culture. Less than a million cells are required to carry out such an experiment, which enables the use of rare biological samples such as primary cells or dissociated cells from tumor biopsies. Furthermore, our new microfluidic system permits the addition of assay substrates at a later time point (e.g. after incubation) with the use of a newly developed fusion chip, which is fully compatible with cell-based assays in non-surfactant-stabilized plugs, something that was previously not shown.

As cells encapsulated in droplets can at most be cultivated for a few days, a further aim of this dissertation was the development of a microfluidic device, which combines droplet-based microfluidics with open tissue culture. The so-called semi-compartmentalization approach allows the combination of droplet-based microfluidics with long-term cell culture. Here, the permeability of the chip material polydimethylsiloxane (PDMS) to certain small molecules is exploited to deliver

drugs from plugs incubated in a microfluidic channel to cells in their close vicinity. Cells are no longer confined to the small volumes of plugs and can be accessed continuously, which enables medium exchange and washing steps. The practicability of this approach was shown by producing plugs containing tetracycline and incubating them inside a channel. During incubation tetracycline diffused out of the plugs and into the surrounding PDMS. We then seeded HeLa cells expressing green fluorescent protein (GFP) under the control of tetracycline in an adjacent channel or on the other side of a thin PDMS membrane. GFP expression as observed by fluorescence microscopy was only visible in positions where tetracycline plugs were incubated. Besides long incubation times and washing steps, this approach also allows imaging of cells at high magnification using a standard light microscope, which is not easily achieved within plugs because cells drift around in the plug.

In conclusion, the microfluidic modules described in this dissertation can be used individually or in combination to study biological systems in a wide range of applications. The low number of cells required permits combinatorial drug screens to be carried out directly on rare samples such as tumor biopsy-derived cells without the need of cell proliferation beforehand, which allows completely new applications in personalized medicine. Furthermore, the semi-compartmentalization approach can be used to stimulate subpopulations of cells within large tissue cultures, which is of particular interest for investigations of cell-to-cell signaling or chemotaxis.

ZUSAMMENFASSUNG

Mikrofluidikchips ermöglichen die präzise Handhabung von Flüssigkeiten in Kanalstrukturen im Mikrometerbereich und können genutzt werden, um wässrige Tröpfchen in einer nichtmischbaren Ölphase zu produzieren. Die Tröpfchen werden durch das Fokussieren oder Abscheren der wässrigen Phase durch die Ölphase produziert und können als miniaturisierte Reaktionsgefässe für chemische und biologische Reaktionen mit einem Durchsatz von über einer Million Proben pro Stunde verwendet werden. Proben mit unterschiedlicher Zusammensetzung wurden bislang durch die Einkapselung einzelner Zellen aus genetisch kodierten Probenbibliotheken wie Hefe-Gendeletionsbibliotheken erzäugt. Hingegen stellt die Erzeugung chemischer Diversität in Tropfen ein ungelöstes Problem im Fachgebiet der tropfen-basierten Mikrofluidik dar. Dies limitiert insbesondere die Verwendung solcher Systeme in zellbasierten Screens, welche das Prüfen vieler verschiedener Bedingungen erfordern. Diese Dissertation beschreibt die Entwicklung eines neuen vollintegrierten tropfen-basierten Mikrofluidiksystems, welches die systematische Erzeugung kombinatorischer Mischungen in Tröpfchen, die lebende menschliche Zellen enthalten, ermöglicht. Das System basiert auf individuell ansteuerbaren Stiften einer Braillezeile, die das Öffnen und Schliessen von Ventilen in Mikrokanälen erlauben und so die Generierung von Mischungen aus verschiedenen eingespritzten Lösungen kontrollieren. In einer Machbarkeitsstudie wurde die Regulation von Matrixmetalloproteinasen (MMP) mit einem limitierten chemisch-genetischen Screen enzymatischer MMP-Aktivität untersucht. Der neu entwickelte Chip ermöglichte die Herstellung kombinatorischer Mischungen ausgehend von zwölf Wirkstoffen, d.h. es wurden 79 individuelle Mischungen generiert, welche zusammen mit Zellen in Tröpfchen eingekapselt wurden. Alle Probemischungen wurden in fünffacher Ausführung hergestellt und ihre Reihenfolge mit zusätzlichen fluoreszenten Tröpfchen kodiert. So konnten insgesamt 686 Tröpfchen pro Experiment gemessen werden. Gleichzeitig waren zur Durchführung jedes Experiments weniger als eine Million Zellen nötig, was die Verwendung seltener Proben wie Primärzellen oder dissoziierter Zellen aus Tumorbiopsien erlaubt. Ausserdem ermöglicht unser Versuchsaufbau, durch die Verwendung eines neuentwickelten Fusionschips, die Zugabe von Versuchssubstraten zu einem späteren Zeitpunkt (beispielsweise nach einer Inkubationszeit). Letzterer ist vollkommen kompatibel mit zellbasierten Versuchen in Tröpfchen, die nicht durch grenzflächenaktive Stoffe stabilisiert wurden, was bis dato nicht gezeigt wurde.

Da in Tröpfchen eingekapselte Zellen maximal ein paar Tage überleben, war ein weiteres Ziel dieser Dissertation die Entwicklung eines neuen Mikrofluidikchips, welcher tröpfchenbasierte Mikrofluidik mit offener Zellkultur verbindet. Der sogenannte Semi-Kompartimentierungs-Chip ermöglicht die Verknüpfung tröpfchen-basierter Mikrofluidik mit Langzeit-Zellkultur. Zu diesem Zwecke wurde die chemische Permeabilität des Chipmaterials Polydimethylsiloxan (PDMS) ausgenutzt, um Wirkstoffe aus Tröpfchen, welche in einem Mikrokanal inkubiert wurden, zu Zellen zu transportieren, die auf der anderen Seite einer dünnen PDMS-Schicht wachsen. Die Zellen sind nicht länger im kleinen Volumen der Tröpfchen eingeschlossen, womit ständig auf sie zugegriffen werden kann, um z.B. das Nährmedium auszutauschen oder um die Zellen zu waschen. Die Machbarkeit dieses Versuchsaufbaus wurde gezeigt, indem Tröfchen mit Tetracyclin hergestellt wurden, welche in einem Kanal inkubiert wurden. Während der Inkubation diffundierte Tetracyclin aus den Tropfen und in die PDMS-Membran. HeLa-Zellen, die das grün fluoreszierende Protein (GFP) unter der Kontrolle von Tetracyclin exprimieren, wurden auf der gegenüberliegenden Seite einer PDMS-Membran gesät und erneut inkubiert. An den Stellen, wo Tetracyclin-Tröpfchen inkubiert wurden konnte GFP-Expression anhand von Fluorezenz gemessen werden. Neben der längeren Inkubationszeit erlaubt dieser Versuchsaufbaus auch Zellen mit einem normalen Lichtmikroskop bei hoher Vergrösserung abzubilden, was in Tröpfchen schwer machbar ist, weil die Zelle aus dem Fokus driften.

Abschliessend kann man sagen, dass die hier beschriebenen Mikrofluidikmodule, einzeln oder in Kombination, für das Studium vieler verschiedener biologischer Systeme benutzt werden können. Die geringe Anzahl benötigter Zellen erlaubt es kombinatorische Wirkstoff-Screens direkt mit seltenen Proben wie Zellen aus Tumorbiopsien durchzuführen, ohne dass diese vorweg noch amplifiziert werden müssten. Dies könnte völlig neue Anwendungen in der personalisierten Medizin erlauben. Der Semi-Kompartimentierungs-Chip kann zudem verwendet werden, um kleine Zell-Subpopulationen inmitten grösserer Zellkulturen anzuregen. In Kombination mit dem Kombinatorik-Chip brächte dies in Studien über Zell-Zell-Interaktionen oder Chemotaxis neue Möglichkeiten.

ACKNOWLEDGEMENTS

I would like to thank all the people that made the work described in this thesis possible. First of all I thank Dr. Christoph Merten, who agreed to take me on as a predoctoral fellow in his group and thus enabled my stay at EMBL. He provided the initial project ideas and ongoing guidance and feedback, including very open and fruitful discussions, which lead to this thesis. Many thanks also go to all active and former members of the Merten group, who created a nice work atmosphere in the lab and during coffee breaks. Special thanks go to Ramesh, who made the initial designs of the Braille chip, to Federica for "R support" and Nirupama for teaching me how to culture mammalian cells and her help in the semi-compartmentalization project.

I thank Prof. Dr. Uwe Sauer for his continued mentoring and for agreeing to be my external thesis supervisor at ETH Zürich. He was also part of my thesis advisory committee together with Dr. Nassos Typas, Dr. Lars Steinmetz and Dr. Jan Ellenberg, to all of whom I am very grateful for helping me to stay on track and helping me become a better scientist. I also thank Prof. Dr. Petra Dittrich for agreeing to be co-examiner and Prof. Dr. Matthias Peter as the chair for the defense of this thesis.

I would like to thank the people in the EMBL core facilities and other research groups for their valued support, specifically: Joe Lewis and Kerstin Putzker in the Chemical Biology Core Facility for helping me set up plate reader screens, Alfredo Castello in the Hentze group for providing HeLa cells, Swati Tyagi in the Lemke group and Tilman Plass in the Schultz group for providing fluorescent dyes, Gary Male in the Müller group for providing competent cells and the people in the Steinmetz group for initial support when setting things up at EMBL. Additional thanks go to the Studienstiftung des Deutschen Volkes for granting me a dissertation stipend.

Very special thanks go to my friends in Heidelberg for their moral support (homebrew!) and a stress-free environment in the times outside of the lab, i.e. listening patiently to my "hardships". Very special thanks go to my friends and family in Baden, whose unconditional support I have been able to rely on in the past 30 years and for providing an oasis to retreat to in times of distress. Very special thanks go to Franka, with whom I am starting a family as I am writing this and without whose support this endeavor would have been immensely harder! Who else would have proofread this? ☺

CONTENTS

1 GENERAL INTRODUCTION

1.1 Microfluidics

Microfluidics comprises various approaches that allow actuation and handling of minute amounts of fluids (nL - μL) at the μm scale (Whitesides, 2006). Typically microfluidic devices consist of channel networks with channel dimensions of 10-500 μm in which liquids can be actuated by different means. One of the simplest approaches that has been used for decades – and that could be considered microfluidic – is paper chromatography (Martin and Synge, 1941). Here minute amounts of analytes flow through μm scale porous networks made by the microscopic paper structure and are actuated by wicking and capillary action along the paper fibers. Nowadays paper microfluidic devices are mainly produced as low-cost and disposable one-use diagnostic devices similar to pregnancy tests to measure multiple analytes from urine (Martinez et al., 2007). More sophisticated microfluidic analysis systems made from polymers were developed with the purpose of miniaturizing existing lab scale experimental setups, to reduce sample reagent consumption and thereby cost, but also to gain sensitivity, throughput and multiplexing capabilities. Microfluidic approaches are sometimes also referred to as lab-on-a-chip (LOC) or micro total analysis systems (μTAS). The latter term was introduced by Manz et al. almost 25 years ago to distinguish them from larger total analysis systems being developed at the time with "unconvincing" results (Manz et al., 1990). Liquids in microfluidic devices are generally actuated by external pumps, e.g. syringe pumps, pressurized air or peristaltic pumping based on valving (Eicher and Merten, 2011).

One of the enabling technologies for modern microfluidics was developed in the 1990s in the Whitesides lab and is termed soft lithography (Xia and Whitesides, 1998). It is based on earlier photolithographic techniques developed to fabricate microelectronic devices (Nall and Lathrop, 1958). Soft lithography allows fast prototyping of new microfluidic chip designs by replica molding and is described in detail in the **Materials and Methods** section of this thesis. Briefly, it allows repetitive manufacture of identical microfluidic chips by using microscale structures patterned onto a silicon wafer as a negative mold. The time required from mold fabrication to the use of a finished microfluidic chip is at most one day. Molds are filled with polydimethylsiloxane (PDMS) and baked. The cured PDMS chip can be cut out using a scalpel. Molds can be re-filled with PDMS and thus can be reused many times (Duffy et al., 1998). PDMS was used as the base material for all microfluidic chips presented in this work. It has many advantages when used for microfluidic chip production in the context of biological and biomedical applications. The cured polymer is biocompatible and highly gas permeable which allows the culturing of cells on-chip and the performance of many biochemical assays. Since PDMS has optical properties similar to

that of glass, microfluidic devices made from this material are transparent and processes carried out on-chip can be monitored directly under a standard light microscope. Additionally, it is very flexible and easy to handle which makes it very amenable to use in the development of new prototype chips (Xia and Whitesides, 1998).

1.2 Single-phase microfluidics

Microfluidic chips are generally made up of channel networks for liquid flow which at these scales is governed by viscous forces. This means that the parallel injection of two miscible fluids does not lead to convective mixing as it is the case for turbulent flow at the macroscopic level (Avila et al., 2011). Rather, the two liquids form a laminar co-flow in which mixing can only occur via diffusion of molecules from one liquid stream to the other. The mathematical basis for this flow behavior in a pipe is given by **Eq. 1**, in which Re is the Reynolds number, ϱ is the density of the fluid, ℓ is a characteristic length scale (e.g. channel width), v is the velocity of the fluid and η is the dynamic viscosity of the fluid (Vyawahare et al., 2010):

$$\mathrm{Re} = \frac{\varrho v \ell}{\eta} \qquad \textbf{Eq. 1}$$

At $Re < 2000$ laminar flow dominates over turbulent flow. Different numbers have been mentioned for Re, but conditions in most microfluidic devices result in $Re < 5$ (Avila et al., 2011; Vyawahare et al., 2010). The occurrence of laminar flow can therefore be easily induced by reducing channel dimensions and/or increasing the viscosity of the fluids involved. An additional measure describing the diffusion behavior of two liquids is given by the Péclet number (Pe), where ℓ is a characteristic length scale, v is the velocity of the fluid and D is the mass diffusion coefficient (Vyawahare et al., 2010):

$$\mathrm{Pe} = \frac{v \ell}{D} \qquad \textbf{Eq. 2}$$

At $\mathrm{Pe} > 1$ fluid flow is dominated by convection, while at $\mathrm{Pe} < 1$ diffusion dominates. In microfluidic devices this ratio can be most easily influenced by changing the channel dimensions and the velocity at which the fluids are transported through the channel. Lastly, the capillary number (Ca) represents another important determinant for how liquids travel through microfluidic channels (Link et al., 2004):

$$\mathrm{Ca} = \frac{\eta v}{\gamma} \qquad \textbf{Eq. 3}$$

Here η is the dynamic viscosity of the fluid, v is the characteristic velocity of the fluid and γ is surface or interfacial tension between two fluids. This last metric is especially important when dealing with more than one liquid phase, as is the case in droplet-based microfluidics described in detail below (cf. section **1.3**).

The physical parameters at play in microfluidic devices allow experimental setups that were previously not feasible when using standard laboratory equipment. For instance, laminar flow systems have been used to expose different parts of single cells and of developing *Drosophila melanogaster*, *Danio rerio* and *Arabidopsis thaliana* embryos to diverse temperature regimes and stimulants which resulted in the induction of different cellular phenotypes in regions exposed to different factors (Choudhury et al., 2012; Lucchetta et al., 2005; Meier et al., 2010; Takayama et al., 2001). More complicated gradients have been produced by integrating gradient generators into the chip design. They allow the stable generation of gradients in different shapes (shallow, steep, one-sided, etc.) (Jeon et al., 2000). Cells or animals placed in such streams can thus be exposed to many spatial and temporal changes in experimental conditions with full control by the user.

Chemotaxis studies profit greatly from such stable gradient microfluidic devices by allowing the instantaneous and continuous generation of linear gradients, which was previously not possible. In an early study by Jeon et al., neutrophils were cultured in a 500 μm wide chamber perfused with differently shaped gradients of the chemokine interleukin-8 (IL-8; **Figure 1.1 A**) (Li Jeon et al., 2002). As expected, the neutrophils migrated along the chemokine gradient toward the higher concentration of IL-8. Different shapes of gradients resulted in different migration behavior for the cells, i.e. migration stopped abruptly when the highest concentration stream was directly adjacent to one with no IL-8 ("cliff gradient"), but continued if the concentration slowly decayed ("hill gradient"). The microfluidics approach chosen here allows fast changes between such configurations. However, the cells cultured under constant flow are subjected to shear forces which might influence their behavior. Therefore, in a more recent publication, cells were only indirectly exposed to chemical gradients by separating the culture chamber from the flow channel by a nanoporous polycarbonate membrane (VanDersarl et al., 2011). Compounds diffused through the porous membrane and into the culture chamber with a delay of merely 45 seconds which allows fast condition changes while eliminating flow exposure.

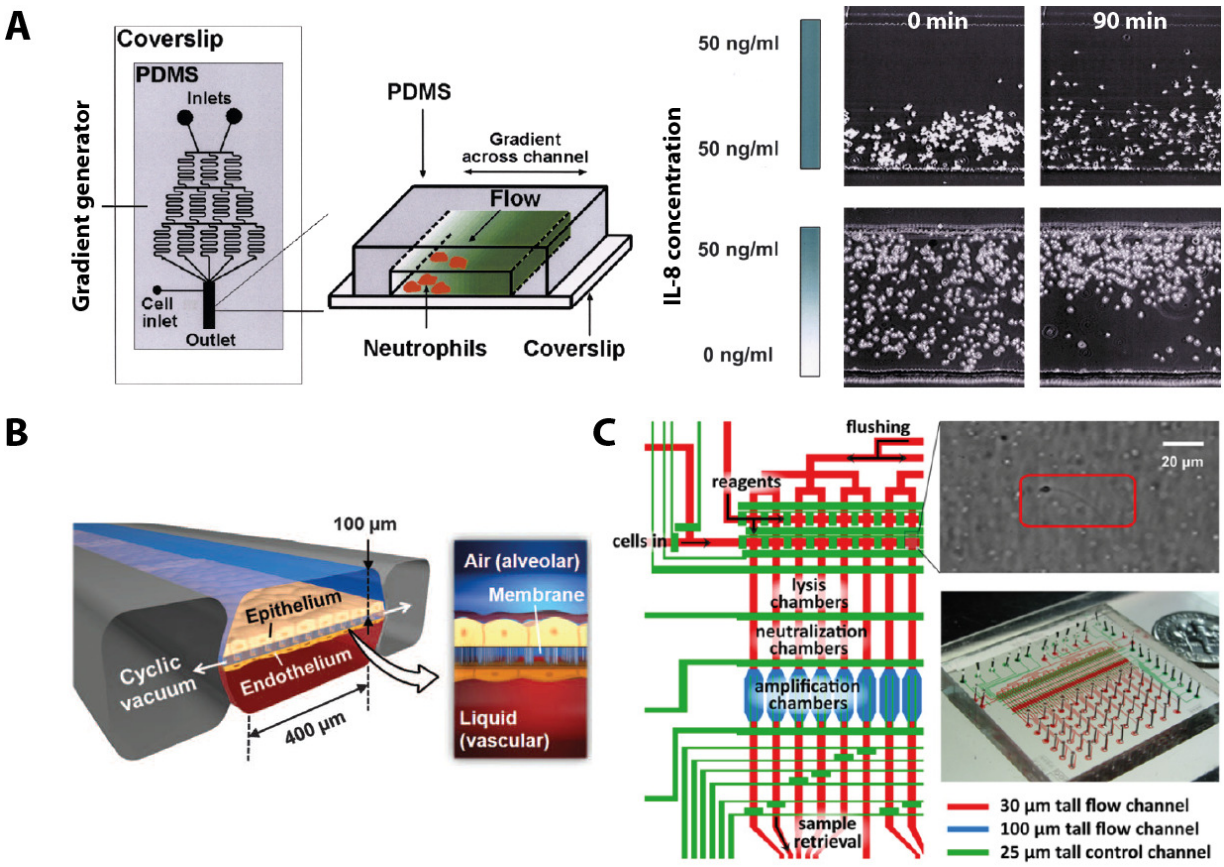

Figure 1.1 Single-phase microfluidics. A) Schematic of a gradient generator for neutrophil chemotaxis studies allowing the generation of a stable chemokines (left). Neutrophil migration when cells are seeded in one half of the channel and exposed to equal homogeneous IL-8 concentrations (top right) and when cells are seeded homogeneously but exposed to an IL-8 gradient over the width of the channel (bottom right). **B)** Lung-on-a-chip device: the central channel is divided by a porous PDMS membrane onto which epithelial cells are deposited from one side and endothelial cells from the other. A vacuum can be created in the two side channels to simulate breathing motions. **C)** An overview for the chip design used to sequence individual sperm. Aqueous flow channels are depicted in red and blue, pressurized air control channels in green. Individual sperm cells are trapped and treated in consecutive chambers, intermittently actuated by the valves formed by the control channels. A sperm cell and a photo of the chip are shown on the right. Reproduced with permission from (Huh et al., 2012a) © AAAS, (Li Jeon et al., 2002) © Nature Publishing Group ,(Wang et al., 2012a) © Elsevier

The same kind of porous PDMS membranes were employed in biomimetic organ-on-a-chip devices that have so far been developed for lung, kidney and liver (Huh et al., 2012b). The design of the lung-on-a-chip device developed by Huh et al. is quite simple but allows the simulation of many lung functions while it also serves as a model system for lung disease (Huh et al., 2012a; Huh et al., 2010). It consists of three parallel channels: two outer channels in which a vacuum can be produced and a larger middle channel which is separated into two parts by a porous PDMS membrane (**Figure 1.1 B**). Two different cell types (epithelial and endothelial) are deposited on

either side of this membrane and grown to confluence. The middle channel allows full control over the environment in which these cells are grown (drugs, growth factors, pathogens, immune cells). So the epithelial cells can be grown in air and the endothelial cells in liquid, just as they would be in the alveoli of the lung. By applying a vacuum to the outer channels, the user can simulate breathing and the physical stress exerted onto the cells. Thus this chip can be used as a test system for pathogenicity and pharmaceutical intervention in lungs.

Even though laminar flow allows different areas of a contiguous flow chamber to be exposed to different chemical environments, the number of different conditions is very limited. Real compartmentalization can only be achieved in separate channels or with the use of valves. Quake and fellows developed valving technology which employs pressurized air-filled channels to close off liquid filled channels located in a layer directly below the air channels. In this way they created isolated compartments in which reactions could be carried out separated from each other (Unger et al., 2000). Such valves have been assembled into complex networks of channels and individually addressable chambers that have been employed for various purposes: e.g. single (sperm) cell whole genome analysis, single cell intracellular molecule analysis and single DNA molecule digital PCR, (Eyer et al., 2012; Heyries et al., 2011; Wang et al., 2012a). The number of individually addressable compartments which can be generated in this way is limited by the space required on-chip to connect the hundreds of individual inlets to external equipment but this can be optimized by the use of multiplexing valves, i.e. few valves are used in combination to allow complex flow control patterns in a space-efficient manner (Gómez-Sjöberg et al., 2007). For applications requiring even higher numbers of compartmentalized samples with diverse compositions, e.g. large numbers of cells, droplet microfluidics is the method of choice. It is described in the next section.

1.3 Sample compartmentalization in droplet-based microfluidics

Droplet-based microfluidics is a specialized form of microfluidics, which is sometimes also referred to as segmented flow microfluidics, when using large droplets that fill a channel completely. Here, mono-disperse water-in-oil emulsions are produced that consist of individual aqueous droplets acting as miniature reaction vessels with volumes of pL to μL. Droplets can be stabilized by lowering their surface tension with the use of surfactants, which can be mixed into the carrier oil phase and can be produced by different means:

i. Droplet break-off can be achieved at the tip of a tapered capillary that sits within an immiscible oil phase. The oil phase can be present as a bulk reservoir in a vessel into

which droplets are formed or in a larger capillary into which the aqueous capillary is in-inserted (Umbanhowar et al., 2000). The latter approach can also be used to create double or even triple emulsions (Chu et al., 2007; Utada et al., 2005) (**Figure 1.2 A**).

ii. Alternatively, droplets can be produced by creating crossflow at a T junction between two perpendicular microfluidic channels. Droplets are formed by flow shearing of the discontinuous aqueous phase by the continuous oil phase (Thorsen et al., 2001) (**Figure 1.2 B**).

iii. Droplets can also be produced by flow focusing the aqueous phase from two sides by the oil phase followed by a narrow constriction leading into a wider channel (Anna et al., 2003) (**Figure 1.2 C**).

In this work we used the latter two methods for on-chip droplet production. Droplets can be produced at frequencies in a range of Hz-kHz, depending on channel geometries and relative flow rates applied. One microfluidic chip can contain multiple of these drop makers, allowing the production of multiple droplet species simultaneously.

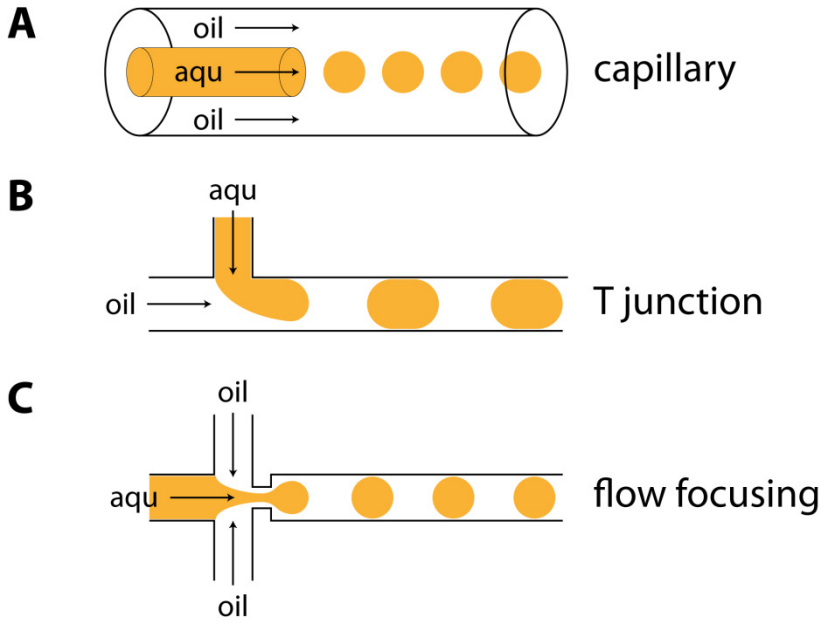

Figure 1.2 Droplet production by capillaries (**A**), at a T junction (**B**), by flow focusing (**C**).

In literature many terms are used to refer to water-in-oil compartments, some with overlapping use: droplets, plugs, slugs, segmented flow, digital microfluidics. For clarity in this work, I define the following two terms (**Figure 1.3**):

- **Droplets** are surfactant-stabilized and can therefore be produced at high frequencies without the need of an oil spacer to prevent droplet coalescence (cf. section **1.3.2**; **Figure**

1.3 A). Because they are stabilized, they can be incubated in densely packed delay lines (**Figure 1.3 B**) or as dense emulsions off-chip in a microcentrifuge tube (**Figure 1.3 C**). By doing so, droplet populations mix and cannot be analyzed in the order they were produced in (**Figure 1.3 D**) and thus require sample encoding.

- **Plugs** are non-surfactant-stabilized and thus have to be spaced out by carrier phase to prevent coalescence and sample mixing. This means that they cannot be produced at very high frequencies. Plugs can be incubated and stored by filling them into long tubing, which allows sample readout in the order of production and thus individual labels for every sample are not necessary (**Figure 1.3 E-G**).

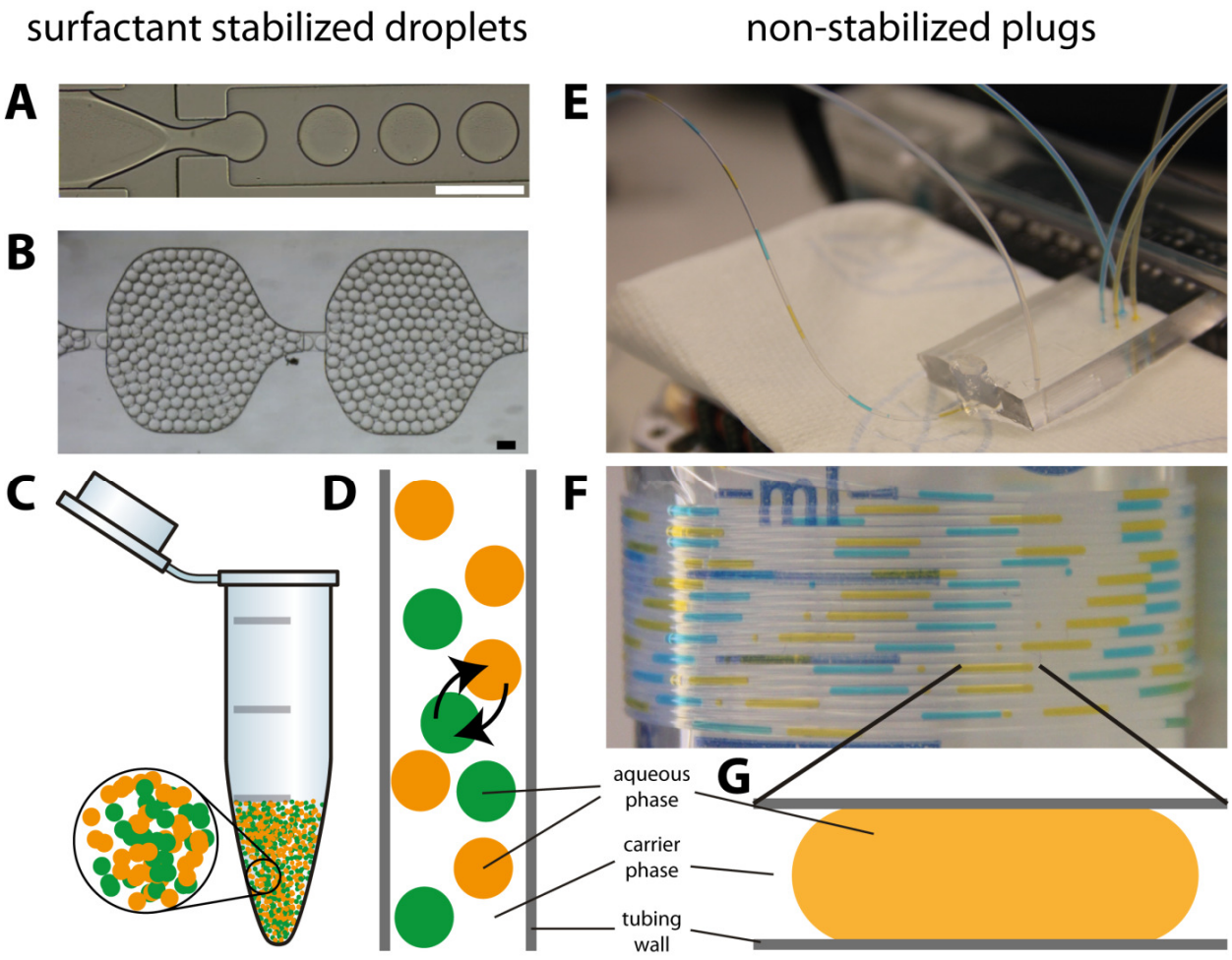

Figure 1.3 Droplets vs plugs. Surfactant-stabilized droplet production at kHz frequencies (**A**), droplet incubation at high densities in a delay line (**B**), storage off-chip in a microcentrifuge tube (**C**), changing positions during downstream processing (**D**). Non-surfactant-stabilized plug production into a long tubing (**E**), incubation/storage in the tubing (**F**) where plugs span the whole width preventing changes in plug sequence during downstream processing (**G**). (Scale bars: 200 µm)

1.3.1 Microfluidic modules for droplet manipulation

A variety of microfluidic modules have been developed to manipulate droplets after they have been produced. Droplets containing assay reagents can be incubated in dedicated delay lines or arrays of droplet traps that ensure equal incubation times for the thousands of droplets generally produced in such experiments (Frenz et al., 2009; Huebner et al., 2009). Alternatively, droplets can be collected in tubing or reaction vessels and incubated off-chip. This however requires re-injection of droplets onto an additional microfluidic chip for further processing and analysis of droplet contents. Fluorescent or fluorogenic reagents used as reporter molecules in biochemical assays in droplets can be detected directly in microfluidic channels using standard fluorescence microscopy and image analysis (Song and Ismagilov, 2003).

With the help of electrodes embedded on-chip, droplets can be sorted based on their content when coupled to optical detection of reaction products (e.g. fluorescent reporters) using lasers and a spectroscopic readout (Baret et al., 2009; Link et al., 2006). This allows the enrichment of rare samples from a large population of samples reminiscent of fluorescence-activated cell sorting (FACS), but in this case additionally allows sorting based on fluorescence in medium surrounding cells. Droplets can also be split into replicates with the same composition for multiplexing purposes via bifurcations in the microfluidic channels (Adamson et al., 2006; Link et al., 2004). Most relevant to this work however is droplet coalescence which is described in detail below.

1.3.2 Droplet fusion devices

Previous contributions in the field have resulted in many different solutions to achieve droplet fusion. The aim of all of the developed modules is to merge an existing collection of droplets with an external aqueous phase or a distinct droplet species. In order to fuse two aqueous surfactant-stabilized droplets in oil one has to devise a way to get them into close proximity to each other and decrease their surface tension, either chemically, based on chip geometry, through electrocoalescence or through a mixture of both. In the following I will describe current solutions in the literature and their limitations.

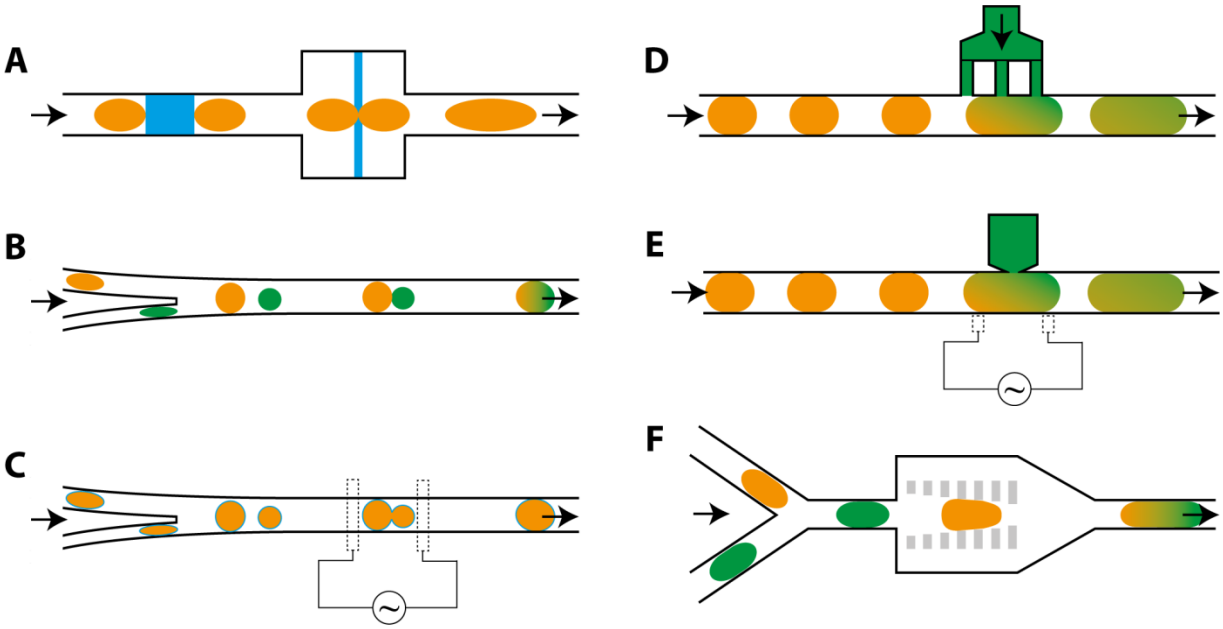

Figure 1.4 Microfluidic modules for droplet fusion. Droplets can be fused in different ways: passive droplet fusion based on channel geometry for non-stabilized droplets (**A**, **B** & **F**), with the help of electrodes for surfactant-stabilized droplets (**C** & **E**) and by directly injecting substrate droplets into an existing train of surfactant-stabilized or non-stabilized droplets (**D** & **E**).

Plugs coalesce when brought into close proximity. A small bridge of liquid is formed between the two surfaces, followed by interface destabilization and fusion (Eggers et al., 1999; Mazutis et al., 2009). Consecutive non-surfactant-stabilized droplets can be fused by removing the continuous oil phase around them and bringing the droplets into close contact. This can be easily achieved passively by simply widening a channel section or by removing carrier oil via a channel away from the center of the channel. The latter allows control over the rate of volume reduction between the droplets (**Figure 1.4 A** (Tan et al., 2004)). Non-surfactant-stabilized droplets of different sizes can also be passively merged by simply merging two channels with different widths containing droplets into one (**Figure 1.4 B** (Song et al., 2003). This approach, however, is dependent on exact synchronization and close spacing of the two droplet species to ensure a one to one pairing and contact between two droplets. This may only work for a very stringent set of parameters. In a similar setup, albeit with a more sophisticated geometry, pairwise coalescence could be performed at high frequency (kHz) and efficiency (99%) between a surfactant-stabilized and a non-surfactant-stabilized population of droplets (Mazutis et al., 2009). The addition of surfactant after fusion allows the collection of fused droplets for incubation off-chip and re-injection into a second device without additional coalescence, showing the robustness of this approach.

Droplets can also be fused by electrocoalescence. In a first approach, Link et al. produced two droplet populations of opposite charge by letting the water phase flow over electrodes and thereby capacitively charging the water-oil interface (Link et al., 2006). At a junction (still within the electric field generated by the electrodes) the two droplet populations coalesced. Ahn et al. described a similar method where they brought two surfactant-stabilized droplet populations of distinct chemical composition together in an alternating sequence at the junction of two individual inlets. Pairs of consecutive droplets are then fused through the induction of an electric field across the microfluidic channel generated by a pair of electrodes (**Figure 1.4 C**) (Ahn et al., 2006). The AC electric field induces a transient dipole in the droplet and vibrations of the droplet surface corresponding to the pulse frequency applied while the droplets pass the electrodes, facilitating droplet coalescence (Eow and Ghadiri, 2003).

The systems described above rely on the one-to-one pairing of two droplet species within a similar size range. To fuse droplets of different sizes and compositions other methods have to be applied for reliable fusion with minimal cross-contamination. The Ismagilov lab described a microfluidic device for substrate injection from a continuous phase into a train of large preformed plugs, superseding the need of droplet synchronization (**Figure 1.4 D** (Li et al., 2007)). Picoinjectors combine the latter approach with electrodes to allow the use of surfactant-stabilized droplets. Here, substrate release from a pressurized channel forming a T junction with the droplet channel is triggered upon droplet detection by an electrode allowing accurate control over dispensed amounts down to subpicolitre volumes (**Figure 1.4 E** (Abate et al., 2010)). This approach also allows consecutive addition of different compounds to the same droplet.

A final category of fusion devices is formed by the use of pillars in the channel geometry (**Figure 1.4 F**). In the simplest case, the pillars are built into a widening of a simple microfluidic channel taking the form of a flow permissive funnel. The droplets stop because they are being squeezed into the funnel and so their internal pressure (ΔP_d; Laplace pressure: pressure difference between the inside and the outside of a curved surface) rises caused by increased surface tension. At the same time the external pressure (ΔP) acting on the droplet – caused by the oil flow – drops because the oil can flow around the chamber through the side channels. As long as $\Delta P_d > \Delta P$ the droplet remains in the merging chamber. When a subsequent droplet enters the merging chamber it blocks flow through the narrow side channels causing the external pressure to rise, so that $\Delta P_d < \Delta P$. The two droplets merge since their surface tension is high and are being pushed towards the end of the funnel. When exiting the chamber, the droplet tip

relaxes towards a spherical shape driven by surface tension, which further pulls the droplet out of the chamber (Niu et al., 2008).

Pillars can also be used to fuse droplets of distinct composition by including a drop maker just upstream of the pillar chamber. In this configuration, incoming plugs fuse with freshly produced substrate droplets (Clausell-Tormos et al., 2008). Reliable one-to-one droplet fusion can additionally be achieved by integrating the drop maker directly in to the fusion chamber (El Debs et al., 2012). Cell encapsulation into droplets and consecutive droplet fusion poses a challenge that we want to address in this work.

1.3.3 Cells in droplets

Water-in-oil droplets have been used to compartmentalize many chemical and biochemical assays in very small volumes: e.g. PCR and protein crystallization (Chen et al., 2005; Schaerli et al., 2009). But droplets do not serve exclusively as reaction vessels for chemical and biochemical reactions; they can also be used to encapsulate cells together with reagents to perform cell-based assays on-chip. The first cell encapsulation experiments were performed over a decade ago. It was shown that individual bacteria could be encapsulated and that they could form a growing culture, which could be detected via the fluorescence of constitutively expressed green fluorescence protein (GFP) (Martin et al., 2003). A similar study showed that individual mammalian cells could be photolyzed by laser and their β-galactosidase content could be assayed using the fluorogenic substrate fluorescein di-β-D-galactopyranoside (FDG) which is enzymatically converted to fluorescein (He et al., 2005).

Many screens, however, have been based on the encapsulation of single cells into droplets. Most of these screens measured thousands of droplets with the same composition of cells and reagents, e.g. to show the diagnostic detection of rare surface markers via fluorogenic antibodies outperforming standard FACS (Joensson et al., 2009). Others measured the cytotoxicity of different concentrations of mitomycin C on individual human monocytic U937 cells (a fluorescently encoded library of one compound) (Brouzes et al., 2009). In order to create biological diversity in the samples Agresti et al. used a diverse yeast library to screen for enzymatically improved horseradish peroxidase in a directed evolution screen, which resulted in a 100-fold more efficient enzyme while costing a fraction of standard microtiter plate-based screening methods (Agresti et al., 2010). A further example for the screening of biological libraries was presented by El Debs et al. Here, individual hybridoma cells secreting antibodies able to inhibit angiotensin converting enzyme 1 (ACE-1) within a 10,000-fold larger population of non-inhibitors could be detected and the population could be enriched for high secretors (El

Debs et al., 2012). Droplet-based microfluidics is therefore well suited for the detection of rare samples within very large and diverse libraries.

When culturing cells in droplets for longer durations, droplet size becomes a limiting factor. Mammalian cell survival in droplets is limited by the depletion of nutrients and accumulation of cytotoxic waste products produced by the cells themselves within the surrounding medium. Nevertheless, Clausell-Tormos et al. showed that mammalian cells can survive several days in droplets, which was comparable to cultures grown at similar densities in microtiter plates (**Figure 1.5 A**). Moreover, it was shown that encapsulated eggs of the nematode *Caenorhabditis elegans* and the zebra fish *Danio rerio* hatched and formed an embryo in the droplet (**Figure 1.5 B**) (Clausell-Tormos et al., 2008; Funfak et al., 2007).

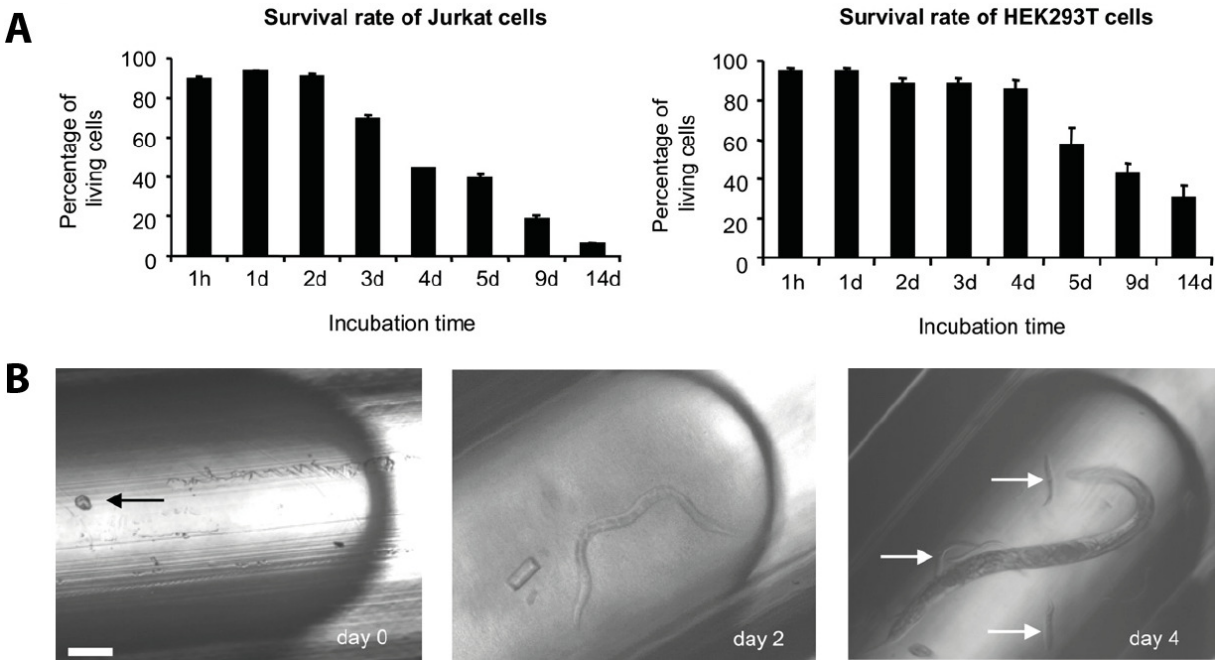

Figure 1.5 Cells and nematodes in plugs. A) Jurkat and HEK293T cells were encapsulated into 660 pL plugs and their survival assessed at different time points after encapsulation. **B)** An individual *C. elegans* egg (black arrow) was encapsulated in a plug, hatched and eventually gave rise to second generation offspring (white arrows) all within the same plug (scale bar:100 µm). Reproduced with permission from (Clausell-Tormos et al., 2008) © Elsevier

Since bacteria grow at much higher rates than mammalian cells the issue of nutrient depletion is exacerbated, but could be alleviated with the development of microdroplet chemostats (Jakiela et al., 2013). Analogous to a large-scale chemostat the medium can be continuously renewed by splitting off waste droplets and coalescence with droplets containing fresh medium. This works well for bacteria because they are present at very high numbers per droplet. It is not very practicable for mammalian cells however, since too many cells would be lost during every

washing step. Even if this is potentially preventable by applying filters, this setup – like all other published approaches – allows the cultivation of cells with very limited flexibility in the chemical composition of droplets. In other words, the setup only works if the medium for all samples is the same.

Generally, genetically encoded diversity in droplets can be easily generated by encapsulating an existing library of cells (e.g. a yeast library) into droplets and running the same assay on all of them (Agresti et al., 2010). Positive samples – i.e. the ones showing the queried phenotype - can then be sorted and their contents sequenced. However, a practical approach to generating large chemical diversity in droplets is still missing in the field.

1.4 Combinatorial small molecule mixtures

Small molecule-based screens often rely on the generation of chemical diversity in samples. Small-scale screens with very limited chemical diversity (six antibiotics) have been performed with manually produced droplets. Boedicker et al. screened for antibiotic sensitivity of methicillin-resistant *Staphylococcus aureus* (MRSA) (Boedicker et al., 2008). A different study performed a model screen of 2-phenylethyl β-D-thiogalactoside (PETG) at different dilutions for its ability to inhibit β-galactosidase activity (Clausell-Tormos et al., 2010). A modified autosampler that can aspirate aqueous samples from 96-well microtiter plates was used to produce trains of large water-in-oil plugs with distinct chemical composition. Even though this system potentially allows the automated generation of diverse compound libraries in the form of plugs, its low throughput of ~1 sample/min is not very amenable to high-throughput screening endeavors. The throughput can be slightly increased by splitting the plugs into many copies which can be used in individual experiments.

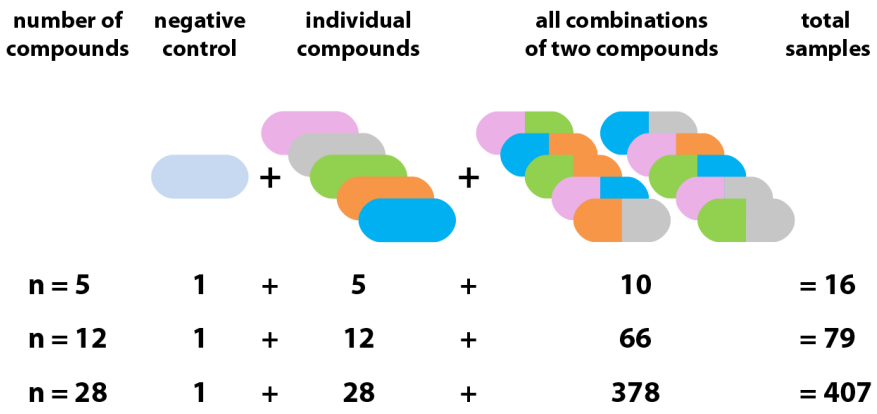

Figure 1.6 Combinatorial mixtures. Combinatorial mixtures allow the generation of large sample diversity as illustrated by these examples.

Combinatorial mixtures allow the generation of a large number of samples with distinct chemical compositions from a limited set of chemical species as depicted in **Figure 1.6.** The number of distinct sample compositions can be calculated using the following equation;

$$m = \frac{n!}{(n-r)!(r)!} \qquad \textbf{Eq. 4}$$

Here, n is the number of drugs in the library, r is the number of compounds in every mixture and m is the resulting number of unique mixtures. As an example, all possible pairwise combinations of twelve compounds yield 66 unique mixtures. If mixtures are made up of always three compounds, the resulting number of unique mixtures already reaches 220. Accordingly, screening even quite limited libraries of compounds quickly yields very high numbers of combinations and with that high sample diversity for screening purposes.

Combinatorial mixtures have been used widely in *in situ* click chemistry applications, where a few very basic starting molecules are used combinatorially in simple reactions with a "high thermodynamic driving force" to form new molecules that can be functionally tested (Kolb et al., 2001). Such approaches are used to create highly diverse compounds from existing building blocks to be used in early-stage drug screening. Combinatorial click chemistry reactions have been successfully performed on dedicated microfluidic devices. Wang et al. developed a microfluidic chip – utilizing pressurized air-controlled valves – that allows the combinatorial screening of 128 reaction conditions (eight acetylenes × 16 azides) and a total of 1024 individual reactions in total, 39 of which resulted in hits (Wang et al., 2006; Wang et al., 2009). However, since compressible air was used to separate plugs the length of the produced plug train was inherently short. In fact only eight samples could be produced per sample tube, which then had to be replaced by a fresh one, due to the limitations of downstream processing in a mass spectrometer and therefore resulted in a very low throughput.

Combinatorial mixtures of small molecules are also omnipresent in biology and medicine. In their natural tissue environment, cells are barely ever exposed to a single species of chemical compounds. Instead, they constantly integrate a multitude of signaling cues provided by the extracellular environment. For instance, cell fate in the developing *Drosophila* eye is decided by the combinatorial effects of epidermal growth factor receptor (EGFR) and Notch signaling acting on pluripotent stem cells (Flores et al., 2000). Chatterjee et al. showed that combinatorial effects elicited by pairwise ligand addition play an important role in the Ca^{2+} signaling cascade leading to the activation of platelets during blood clotting (Chatterjee et al., 2010). In medicine, combination therapies have been proposed almost a century ago and are nowadays used to treat

many types of cancer and infectious disease such as HIV/AIDS (Al-Lazikani et al., 2012; Bliss, 1939; Darbyshire, 1996; Loewe, 1928). Here, the goal is to find synergistic drug pairs, i.e. drugs that show a beneficial effect at lower individual concentrations. In this way the side effects for patients elicited by high doses of individual drugs can be lowered, while at the same time improving their efficacy.

A further application of combinatorial mixtures and the main focus of this thesis is in the field of chemical genetics, where pairs of drugs are investigated for their combined effects.

1.5 Chemical genetics

Chemical genetics is defined by the use of small molecules to interrogate cellular functions instead of traditional genetic tools such as randomized mutation screens (forward genetics) and gene knockout or siRNA screens (reverse genetics) (Alaimo et al., 2001; Schreiber, 1998). This definition of chemical genetics should not be confused with an identical term coined in the kinase field where it describes the use of "genetic engineering to create a specific interaction between a protein and bio-orthogonal small molecule" (Carlson and White, 2011). Many chemical genetic screens are carried out with the purpose of drug discovery. Here, large libraries of compounds are screened until the desired phenotype is elicited and then identifying the target of the compound. Target identification can be achieved by affinity purification methods or synthetic lethal yeast screens (Schenone et al., 2013). This forward chemical genetics approach can be seen as analogous to randomized mutation screens in traditional genetic screens. But libraries of chemical compounds can also be used in reverse chemical genetic screens analogous to RNA interference screening (Schreiber, 2003). Here compounds with known biological targets are used to interrogate the connectivity of cellular pathways by perturbing individual components of these pathways (i.e. the drug targets). This approach greatly benefits from the use of compound combinations, which increase the resolution of the screen when hitting multiple targets within the same signaling pathway (Lehar et al., 2007).

The theoretical background and the classification of effects of drug interactions have been published nearly a century ago by Loewe and Bliss (Bliss, 1939; Loewe, 1928). Modern approaches – mostly in the context of antibiotic resistance – use their terminology to describe the phenotypes observed upon perturbation with combinations of drugs, namely additivity ("no interaction"), synergy ("larger-than-additive effect") and antagonism ("smaller-than-additive effect"; (Yeh et al., 2006; Yeh et al., 2009)). Drug synergy allows the use of lower doses to achieve the same therapeutic effect and can be achieved when drug targets are part of parallel pathways

("specific synergy") or if one drug facilitates cellular entry of the other ("promiscuous synergy") (Cokol et al., 2011). This indicates that systematic screens of drug interactions could be used to infer information about signaling pathway structures by looking at target profiles for all drugs in the screen (**Figure 1.7**).

Microtiter plate-based large-scale phenotypic screens represent the gold standard of chemical genetic methods. Recently, a screen was carried out in the 1536-well plate format to find drugs useful in combination therapy with the Bruton's tyrosine kinase (BTK) inhibitor ibrutinib used in the treatment of B-cell malignancies (Mathews Griner et al., 2014). A total of 459 drugs and drug candidates were evaluated at six different concentrations versus six different concentrations of ibrutinib and multiple favorable interactions potentially useful in combination therapy were discovered. The study shows the value and feasibility of a chemical genetics approach. However, this microtiter plate-based screen relied on large-scale liquid handling robots and the libraries prepared had to be used within 8-12 hours from production.

Chemical genetics screens would benefit greatly from a droplet-based microfluidics approach in order to reduce sample consumption (of compounds and cells) and the cost associated with the large robotics required to carry out the screen. In this work we present such an approach and apply it to investigate the regulation of matrix metalloproteinases, which are introduced in the next section.

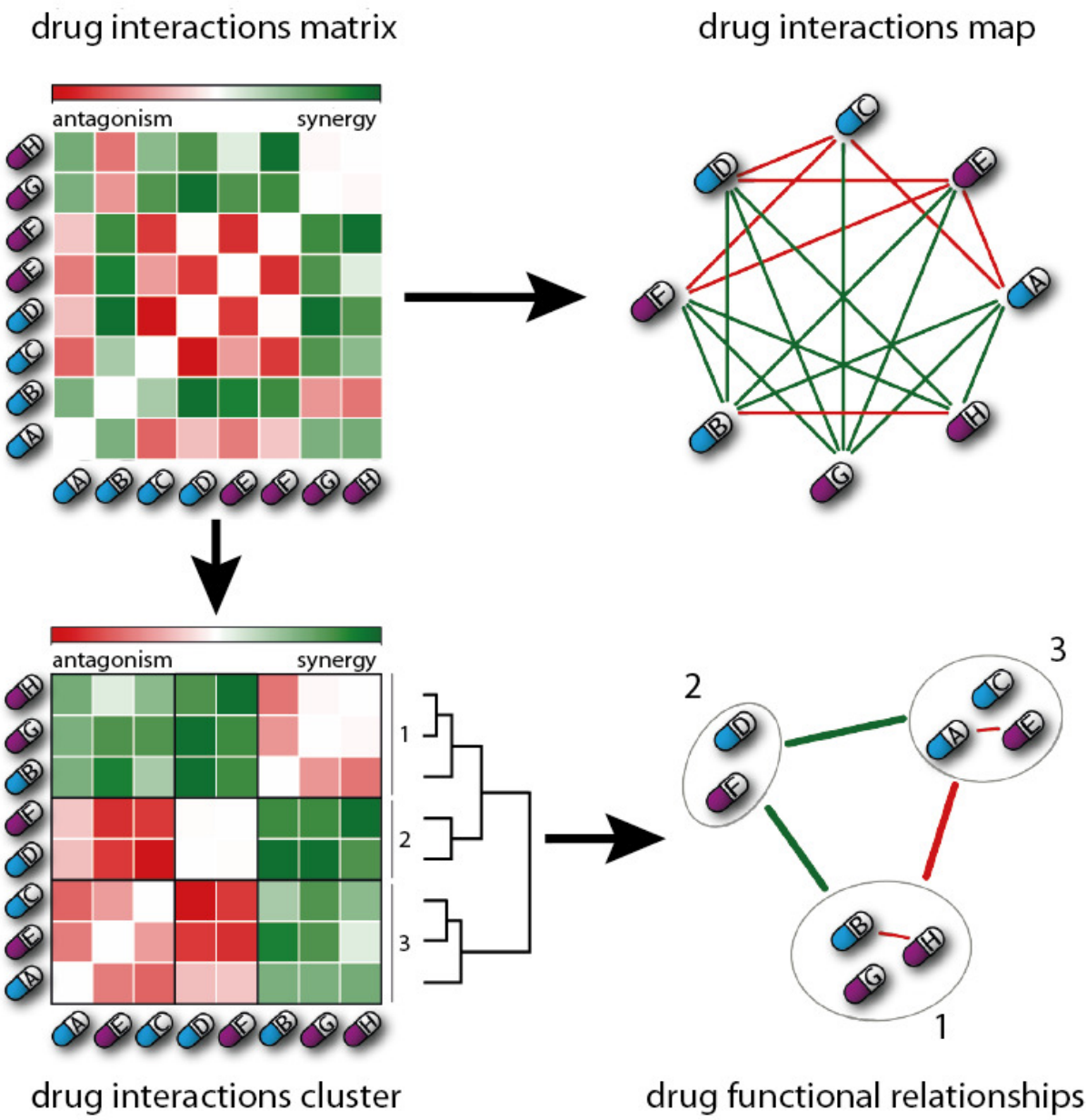

Figure 1.7 Connectivity inference with chemical genetics. Drug interactions are characterized individually into antagonistic, neutral or synergistic interactions (top) and can be clustered into similar groups which allow their classification into functional drug relationships (bottom). (Image adapted from and courtesy of Federica Eduati)

1.6 Matrix metalloproteinases

Matrix metalloproteinases (MMPs) make up a large protein family with more than 20 members in humans, consisting of secreted gelatinases, collagenases, stromelysins as well as matrilysins and the membrane-anchored MT-MMPs (Vandooren et al., 2013). Originally MMPs were named after the substrates they were able to cleave, i.e. gelatinases cleave gelatin. However, gelatinase B was found to be identical to 92-kDa collagenase IV and thus the nomenclature had to be modified and simplified. This has to be taken into consideration especially when considering older publications in the field (Huhtala et al., 1991; Okada et al., 1992). All MMPs share a conserved domain architecture, consisting of a signal peptide for localization, a cleavable pro-peptide keeping the enzyme in an inactive (or zymogenic) state, the catalytic domain and a Zn^{2+}-binding domain. Most also contain a hemopexin domain whose function is linked to substrate interaction, surface receptor binding, inhibitor binding and auto-activation. The two gelatinases (A = MMP-2, B = MMP-9) additionally contain fibronectin repeats which allow them to interact with and degrade long gelatinous substrates.

1.6.1 Physiological roles of MMPs

MMPs are produced by many cell types of the immune system, such as neutrophils and macrophages, cells of the central nervous system and stem cells but also endothelial cells and fibroblasts (Barkho et al., 2008; Kessenbrock et al., 2010). For instance immune cells secrete MMPs to digest focal adhesion between blood vessel endothelial cells to leave the blood stream and enter tissues often tightly regulated by cytokines and growth factors, which in turn are regulated via MMPs. In situations where this delicate regulation is perturbed, chronic inflammation and autoimmune disease ensue. The physiological roles of MMPs are diverse. As expected, many MMPs function in the degradation of their target substrates, which are found in the extracellular matrix (ECM) and in cell-to-cell contacts at focal adhesions, e.g. at the basal membrane. Cells employ MMPs to change their immediate surrounding by either directly cutting ECM components or by releasing or degrading growth factors sequestered there (Mott and Werb, 2004). Therefore, MMPs play important roles in tissue development, remodeling and maintenance, wound healing, cell migration, tissue invasion and extravasation, basal membrane degradation, regulation of inflammation, angiogenesis, synaptic plasticity and skeletal development (Kessenbrock et al., 2010; Vu et al., 1998). It becomes ever clearer that MMPs have additional functions that are not related to the ECM or their primary substrates for proteolysis (Vandooren et al., 2013).

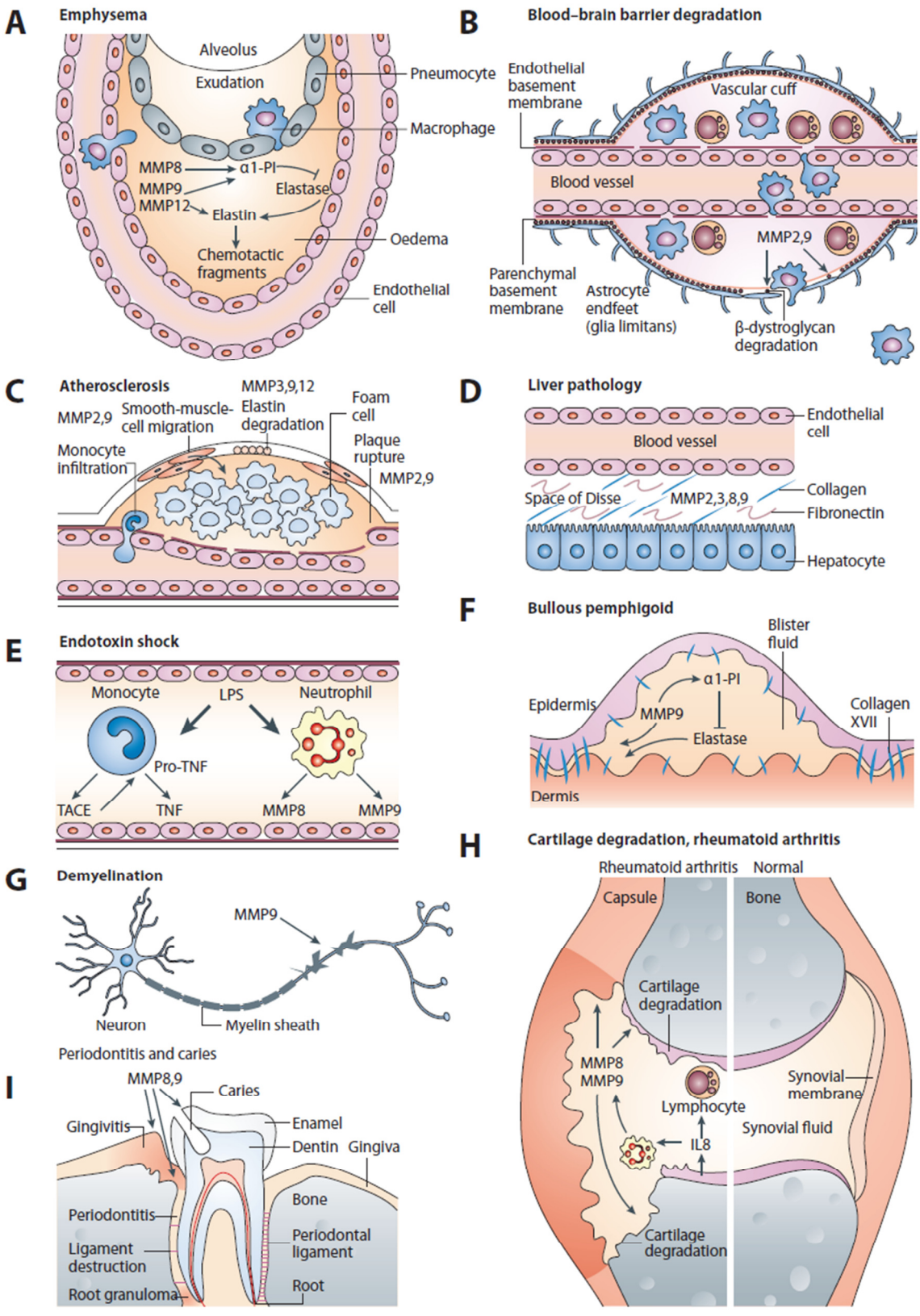

Figure 1.8 Pathological roles of MMPs. MMPs are involved in many tissue pathologies: emphysema (**A**), blood-brain barrier degradation (**B**), atherosclerosis (**C**), liver pathologies (**D**), endotoxin shock (**E**), bullous pemphigoid (**F**), multiple sclerosis (**G**), rheumatoid arthritis (**H**), gingivitis (I) Reproduced with permission from (Hu et al., 2007) © Nature Publishing Group

1.6.2 MMPs in disease

Since MMPs are involved in so many physiological processes, they also play roles in a plethora of malignancies. They are considered important regulatory molecules in both (chronic) inflammation and cancer. An overview over their role in inflammation is depicted in **Figure 1.8** (Hu et al., 2007): as illustrated, MMPs are involved in pathological (connective) tissue and ECM degradation (e.g. in liver pathologies **D**, bullous pemphigoid **F**, multiple sclerosis **G**, rheumatoid arthritis **H**, gingivitis **I**,) and unwanted invasion of cells and secretion of MMPs into tissues (e.g. in emphysema **A**, blood-brain barrier degradation **B**, atherosclerosis **C**, endotoxin shock **E**).

Their essential roles in tissue remodeling and angiogenesis make MMPs very prone to misuse by tumor cells. Tumors grow within existing tissues and thus need room to grow which they can achieve by digesting parts of the extracellular matrix (ECM) that surrounds them. 3D-growth studies and a mouse model have shown how different types of tumor cells rely on MT1-MMP function to grow into the surrounding ECM (Hotary et al., 2003). At the same time growing tumor cells rely on vascularization or angiogenesis in order to prevent hypoxic conditions at the center of the tumor, which prevent further growth. MMPs have been shown to play an essential role in this process by the use of an MMP-9 mouse null model and for MT1-MMP and MMP-2 in rat muscles (Haas et al., 2000; Vu et al., 1998). Importantly, MMPs allow cells in later stage tumors to excise themselves from the tumor tissue and form metastases elsewhere in the body. MMPs actually play a role at both ends of this process by allowing tumor cells to leave their original tumor and by aiding in the tissue invasion and remodeling required to form a new tumor at a target site mediated by MT1-MMP and MMP-14, i.e. in metastatic niche formation (Shuman Moss et al., 2012; Wolf et al., 2007).

1.6.3 The need for selective inhibitors of individual MMPs

Because of their eminent roles in metastasis and inflammation, MMPs have been considered as drug targets for a long time. But even though a lot of research has been directed at finding selective inhibitors for individual MMPs for four decades, only very little progress has been made (Coussens et al., 2002; Overall and Lopez-Otin, 2002). In fact, Doxycycline (Periostat) is the only FDA-approved MMP inhibitor used in the clinic for the treatment of periodontitis and is not specific to one MMP. One of the reasons for this is that MMP family members all depend on very similar mechanisms of action. Inhibitors that act on the active site of MMPs often inhibit many or all MMP family members (many are Zn^{2+} chelators) leading to many unwanted side effects (e.g. join and muscle pain for marimastat (Steward, 1999)) or even more severe relapses in the case of cancer therapy. This is exemplified in a study by Fukuda et al., which showed that

MMP-13 knock-out mice suffered from a 5.7-fold increase in metastases (Fukuda et al., 2011). I some tumor tissues it is not the tumor cells but rather recruited reactive stromal cells that secrete MMPs, which could necessitate another shift in cell targeted therapies (Zucker and Cao, 2009). In the context of inflammation, it has been discovered that MMP-8 is actually involved in the down-regulation of immune responses during allergic asthma (Gueders et al., 2005). Seeing that many of them serve dual roles, MMPs have to be segregated into targets and anti-targets for drug development (Overall and Kleifeld, 2006). This clearly shows that there is a great need for inhibitors of individual MMPs to make therapies more specific and reduce the risk of severe side effects during treatment.

1.6.4 MMP regulation

Existing broadband MMP inhibitors chelate Zn^{2+} ions and thereby down-regulate MMP activity. In order to find targets for selective MMP regulation, inhibitors must be developed that target functions of specific MMPs. As an alternative one could imagine inhibitors targeting the molecular players leading to the dysregulation of MMPs in the first place. This however requires a detailed understanding of the regulation of individual MMPs in different tissues and cell types, which is not yet fully available: The regulation of MMPs is complex and happens at many levels in parallel. There is regulation at the level of gene expression (through various signaling pathways), mRNA degradation, post-translational modification (glycosylation) and through enzymatic activity (required to cleave the protein from its preproenzyme and proenzyme form) as depicted in **Figure 1.9** (Kessenbrock et al., 2010; Vandooren et al., 2013). The processing from inactive to active form can be performed by other MMPs or even other classes of proteinases such as plasmin (which in turn is regulated by MMPs), all of which adds another level of complexity to the regulatory network governing MMP function.

At the transcription level MMP expression is governed by different sets of promoter sequences and transcription factors. Many of them share target sequences such as the one for the cytokine and growth factor responsive activator protein-1 (AP-1) transcription factor and are therefore co-regulated in part (Yan and Boyd, 2007). Several transcription factor binding sites identified for MMPs indicate that they are targeted by signaling pathways triggered by growth factors and cytokines (e.g. EGF, VEGF, TNF-α) and other global signaling pathways such as the NFκB, MAPK, Wnt and p53 pathways amongst others. In light of the complexity of MMP regulation we conclude that the investigation of MMP regulation would profit from a combinatorial chemical genetics approach including drugs targeting signaling pathways in addition to cytokines and growth factors.

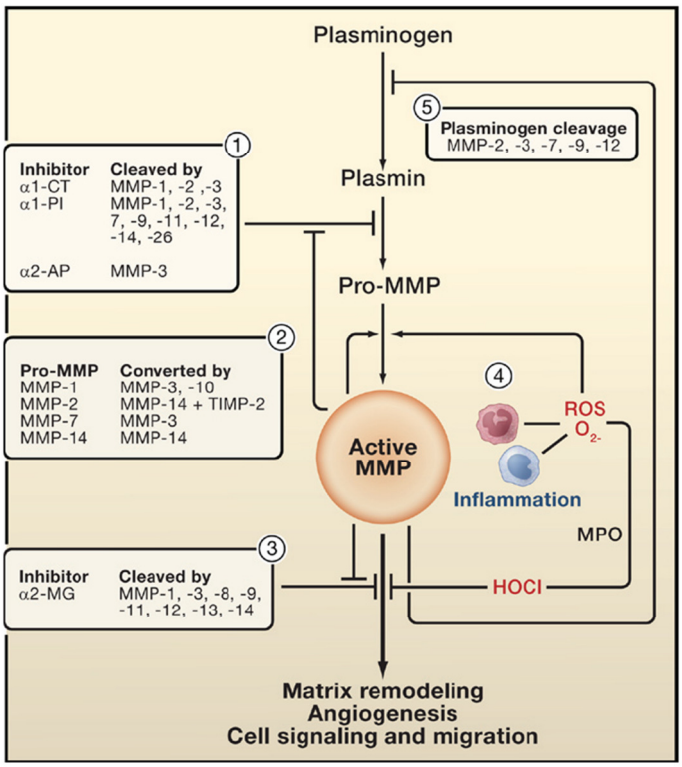

Figure 1.9 Enzymatic regulation of MMP activity. ROS: reactive oxygen species; MPO: myeloperoxidase; TIMP: tissue inhibitor of metalloproteinase. Reproduced with permission from (Kessenbrock et al., 2010) © Elsevier

2 AIM & OUTLINE

The main aim of this thesis was the establishment of a new microfluidic system that allows the generation of chemically distinct plug populations for cell-based assays.

This required the development of two new microfluidic modules, the first of which permits valve-controlled plug production from multiple sample inlets in a fully-combinatorial fashion, while the second allows the addition of assay components after incubation through fusion. Both are explained in chapter **Chapter 3**

Chapter 4 describes a first biological application of the new microfluidic chip designs. Here, combinatorial mixtures of drugs and cytokines are applied in a chemical genetics approach, in which MMP activity is perturbed as a first step towards understanding the regulation of individual MMPs.

A new way to combine chemically distinct plugs with standard cell culture techniques is described in **Chapter 5**. The so-called semi-compartmentalization approach allows the culturing of cells outside of plugs, which makes them fully-accessible to medium change and washing steps and thereby enables long-term cell culture experiments.

Chapter 6 comprises a general discussion and an outlook on future developments.

3 CREATING CHEMICAL DIVERSITY IN DROPLETS

3.1 Introduction

Various microfluidic solutions have been developed to screen diverse biological samples in droplets (section **1.4**), most of which are based on genetically encoded libraries (Agresti et al., 2010). Conversely, there is a lack of devices that can provide similar diversity for small molecules in droplet-based microfluidics. We set out to overcome both of these issues by exerting full control over both (1) sample composition and (2) sample order throughout the course of the complete experimental workflow. Control of sample composition can be achieved by using valves to regulate the injection of samples into a droplet production module. We use a Braille display to control such valves. Control over the sample sequence can be guaranteed by producing plugs that cannot change positions during the course of the experiment and by interspersing them with fluorescent labels to encode their identities within the sequence of plugs. In this chapter we describe a novel microfluidic platform that uses Braille display-controlled valves in the production of chemically distinct plugs.

In order to make this technology compatible with cell-based assays that require long incubation times (e.g. for protein expression to occur) and addition of assay components at a later time point, we developed an improved design of a fusion module. Many fusion modules for droplet coalescence have been developed in the past (section **1.3.2**) but the fusion of droplets with plugs containing incubated cells has not been shown. The reason for this is strong wetting of the channel surface by the aqueous phase containing the cells, which is most likely induced by organic compounds found in the culture medium. Here, we present a simple solution to prevent the occurrence of this phenomenon. We employ additional side channels for the injection of surfactant-laden carrier oil to prevent wetting and use electrodes to aid in droplet coalescence.

3.2 Braille displays can be used to control microfluidic valves and produce plugs

Braille displays were originally developed as a computer display for the blind. Each Braille display unit used in this work consists of eight groups of eight individually controlled and programmable pins (**Figure 3.1**). Pins of Braille displays have previously been used to actuate valves and pumps in microfluidic devices (Futai et al., 2006; Gu et al., 2004; Heo et al., 2006; Tung et al., 2007). The design of a new microfluidic chip that uses such Braille display-controlled valves to control the aqueous phase for combinatorial plug production is described in detail in the following sections.

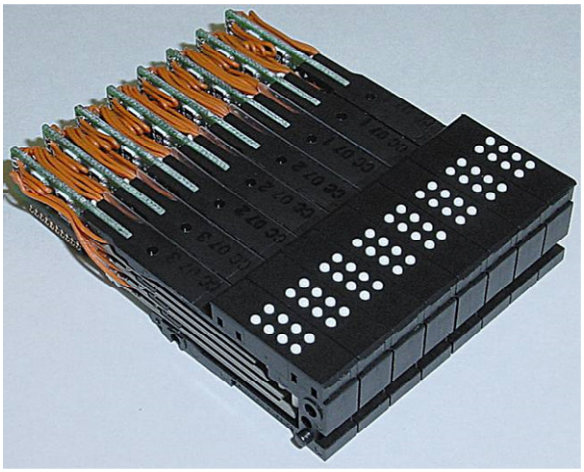

Figure 3.1 Braille display. Photo showing a Braille display unit routinely used in this work. The 64 white pins in the front section are individually addressable and can be controlled by LabView software.

3.2.1 Design and layout

We designed a new microfluidic chip that uses 32 pins of a Braille display unit to control the flow of aqueous solutions in microfluidic channels. Actuation of an individual pin stops the flow in the channel directly above each pin. Such valves control the injection of liquid into the microfluidic channel network from up to 16 individual inlets. Sample flow can either be directed towards plug generation or to a waste outlet, i.e. always two valves control the injection of one sample (**Figure 3.2 A**). The controlled channels converge on a single collection chamber which in turn is connected to a single T junction with a perpendicular oil channel via a short channel. At the T junction plugs are formed by shearing of the aqueous phase by the oil phase. The valves can be used to regulate the chemical composition of the plugs formed at the T junction. They control the flow of aqueous solutions with different chemical compositions injected into the chip inlets from syringes connected to the chip via tubing.

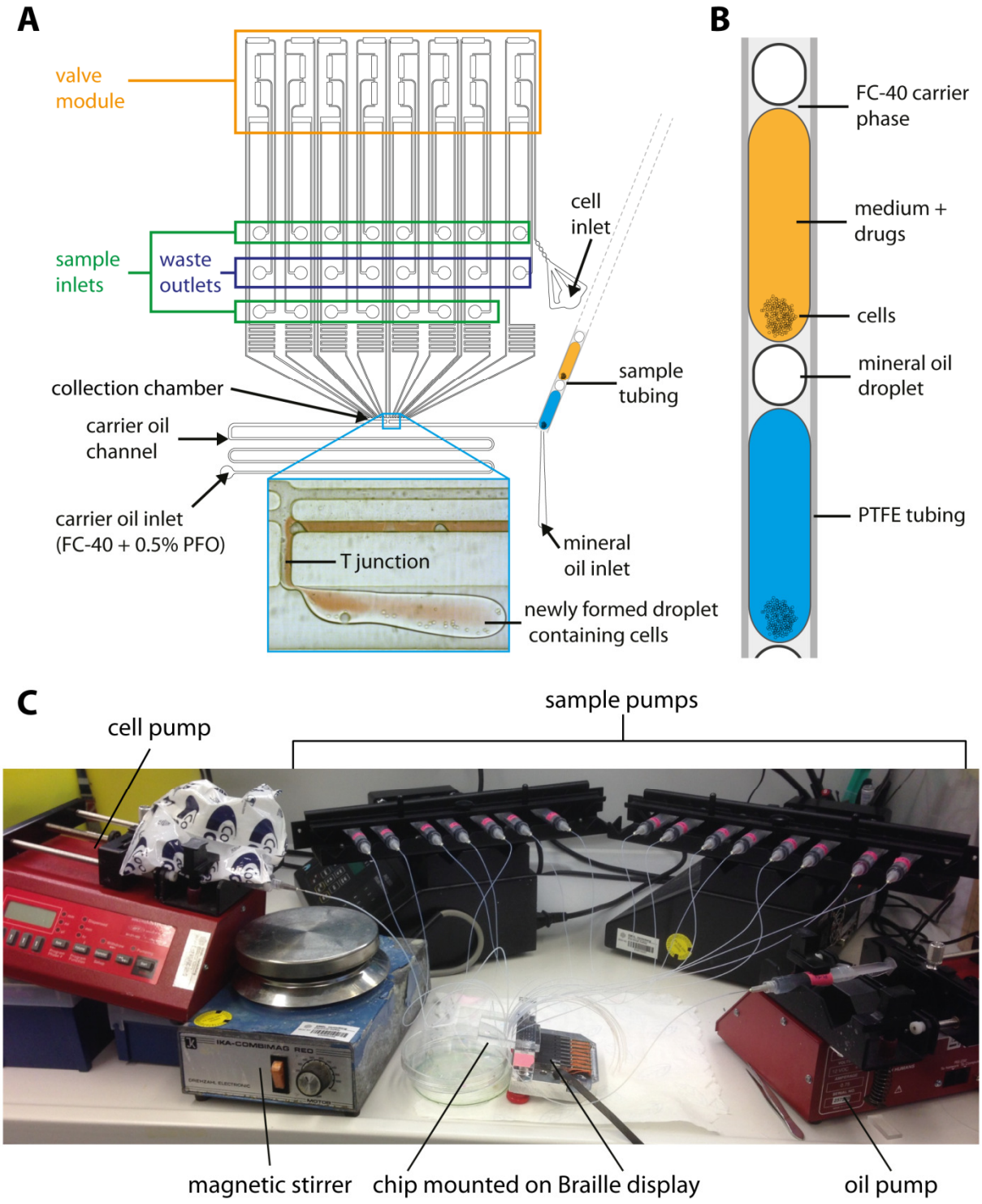

Figure 3.2 Braille chip layout. A) Design of the microfluidic chip consisting of a valve module (mountable onto the Braille display pins), various inlets for aqueous (screening compounds, labels and cells) and oil phases (FC-40 + 0.5% perfluorooctanol (PFO), mineral oil), and a connection port for sample tubing. Plugs are generated at the T junction formed by the carrier oil channel and the sample inlets. The channels have a depth of 60 µm. **B)** Close-up representation of sample tubing filled with sample plugs which are separated from each other by mineral oil plugs. **C)** Photograph of the complete setup in use. Syringes containing screening compounds, cells and oil are mounted to syringe pumps. The Braille display with mounted Braille chip can be seen in the center.

3.2.1.1 Sample & cell infusion

Our chip features a total of 16 inlets for aqueous solutions. Twelve inlets can generally be used for drugs or other small molecules used in the individual experiments, three are used to connect cell medium and fluorescent dyes for the production of control and label plugs and one inlet is dedicated to cell injection. The specific design of the cell inlet reduces cell clumping through accumulation of cells in the dead volume of the inlet (Clausell-Tormos et al., 2008). Samples are injected from syringes mounted onto syringe pumps and connected to the chip through tubing that can be inserted into the inlets on the PDMS chip. The complete setup is shown in **Figure 3.2 C**. The inlets are connected to the valve unit via channels with a width of 100 μm.

3.2.1.2 Valve unit

The valve unit consists of 16 individually addressable valves. Each valve consists of two rectangular channel widenings (490 μm × 2000 μm) that can be manually aligned to the pins of a Braille display when mounting the chip on the control unit. They are 60 μm deep and have a rounded cross-section. The rounded shape is required for complete stopping of liquid flow in the controlled channel (**Figure 3.3**), since a square profile permits flow in the top corners of the channel when a Braille pin is actuated (Unger et al., 2000). Two valves control the flow from every sample inlet and can be used in two configurations: 1) an active configuration in which the flow is diverted to the T junction for plug production and 2) a waste configuration in which all flow is diverted towards a waste outlet. The latter configuration is required to prevent pressure build-up in the system which would eventually lead to leakage due to membrane rupture. To save space in the design, two valves share one waste outlet.

From the valve unit, channels transport the sample reagents to a chamber where all inlet channels merge. One half of the channels have additional serpentine delay lines to compensate for differences in channel lengths. The delay lines compensate differences in back pressure and thereby ensure identical plug volumes. The collection chamber, where all inlets come together, allows the production of plugs simultaneously from multiple sample inlets and is connected to the carrier oil channel via a T junction, which leads to plug formation.

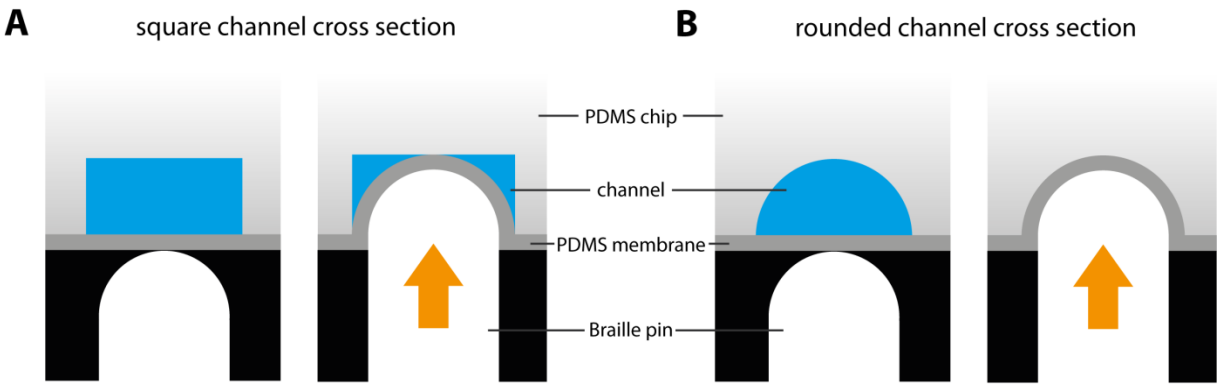

Figure 3.3 Square vs. rounded channel cross section. Cross section of a microfluidic channel aligned to a Braille pin below. A square cross section allows some residual flow through the channel because channel is not completely blocked (**A**), while a rounded cross section allows complete blockage (**B**).

3.2.1.3 Sample plug generation at the T junction

Sample plugs are produced at the T junction, which is formed by the carrier oil channel and the short channel connecting it to the collection chamber (**Figure 3.2 A**). Carrier oil (FC-40 + 0.5% perfluorooctanol (PFO)) is injected from a separate syringe connected via the oil inlet and the carrier oil channel. A delay line leads from the carrier oil inlet to the T junction. This delay line increases the back pressure in the channel to prevent back flow against the flow direction of the carrier oil upon valve opening and plug formation. Ultimate sample plug formation occurs at the junction of the carrier oil channel with the sample tubing at the sample outlet. Here, droplets initially formed at the T junction fuse into larger plugs that span the whole width of the sample tubing into which they are collected. The filled sample tubing is eventually detached from the chip, sealed and placed in an incubator for sample incubation.

3.2.1.4 Mineral oil can be used to prevent fusion of consecutive plugs during incubation

When producing plugs with a very short oil spacer between individual sample plugs, fusion between consecutive plugs can occur. Optionally, mineral oil from a dedicated syringe pump can be injected into a separate inlet merging with the carrier oil channel. By using a low flow rate for the mineral oil (75-175 µL/h) compared to that of the aqueous phase, short plugs of mineral oil are formed and inserted passively in the gaps between the aqueous plugs that are formed by the carrier oil. During plug production, all valves are in the waste-configuration, i.e. all samples flow to the waste and not towards the T junction. Since mineral oil is immiscible with the carrier oil and the aqueous phase, fusion between sample plugs can be prevented throughout the course of a complete experiment (**Figure 3.2 C** and **Figure 3.4**).

Previous attempts to achieve sample isolation have employed gas bubbles instead of mineral oil droplets (Adamson et al., 2006). Air, however, is compressible, which during the course of the experiment leads to differences in valve response times, which in turn lead to differences in plug size and in the worst case to discontinuation of plug production altogether. Using mineral oil plugs to separate sample plugs from each other has the added benefit of allowing higher throughput in sample plug production. Without mineral oil, plugs have to be spaced out significantly to prevent unwanted plug fusion, i.e. the time interval between consecutive plugs can be up to 20 s. With mineral oil plugs this interval can be reduced to times as short as 1 second. In other words, the production time for each sample plug is reduced from 21.5 s to just 2.5 s (cf. section **3.3.1.5**).

Figure 3.4 Mineral oil plugs can be used to separate aqueous plugs from each other. Individual sample plugs containing blue dye, water or red dye are separated from each other by smaller mineral oil plugs, which prevent spontaneous plug fusion when plugs come into close proximity.

3.2.2 Combinatorial mixtures and droplet formation with the Braille chip

One of the aims of this work was to produce plugs containing combinatorial mixtures of compounds and to co-encapsulate cells for biological assays. In our setup, the size of plugs produced on the Braille chip depends on two parameters: 1) the combined flow rates of the aqueous phase and 2) the valve opening times. The first parameter is controlled by the syringe pumps directly and remains constant over the course of the experiment. The latter is controlled by user input in a custom LabView program developed within the lab (Ramesh Utharala, Merten Group).

3.2.2.1 A custom software to control the Braille chip

Newly developed Braille chip control software was used to control the individual pins of the Braille display unit that actuate the valves in our chip. The software allows the user to specifiy which of the 64 pins are actuated simultaneously and for how long. In this way we control which samples are to be produced, i.e. which compound composition they should have and what their size should be. The initial position for all pins is the "all waste" configuration. Here, the valves are used in a configuration that diverts all sample flow to the waste so that no sample plugs are

produced. To explain how the program works, a screenshot of the user interface is shown in **Figure 3.5**.

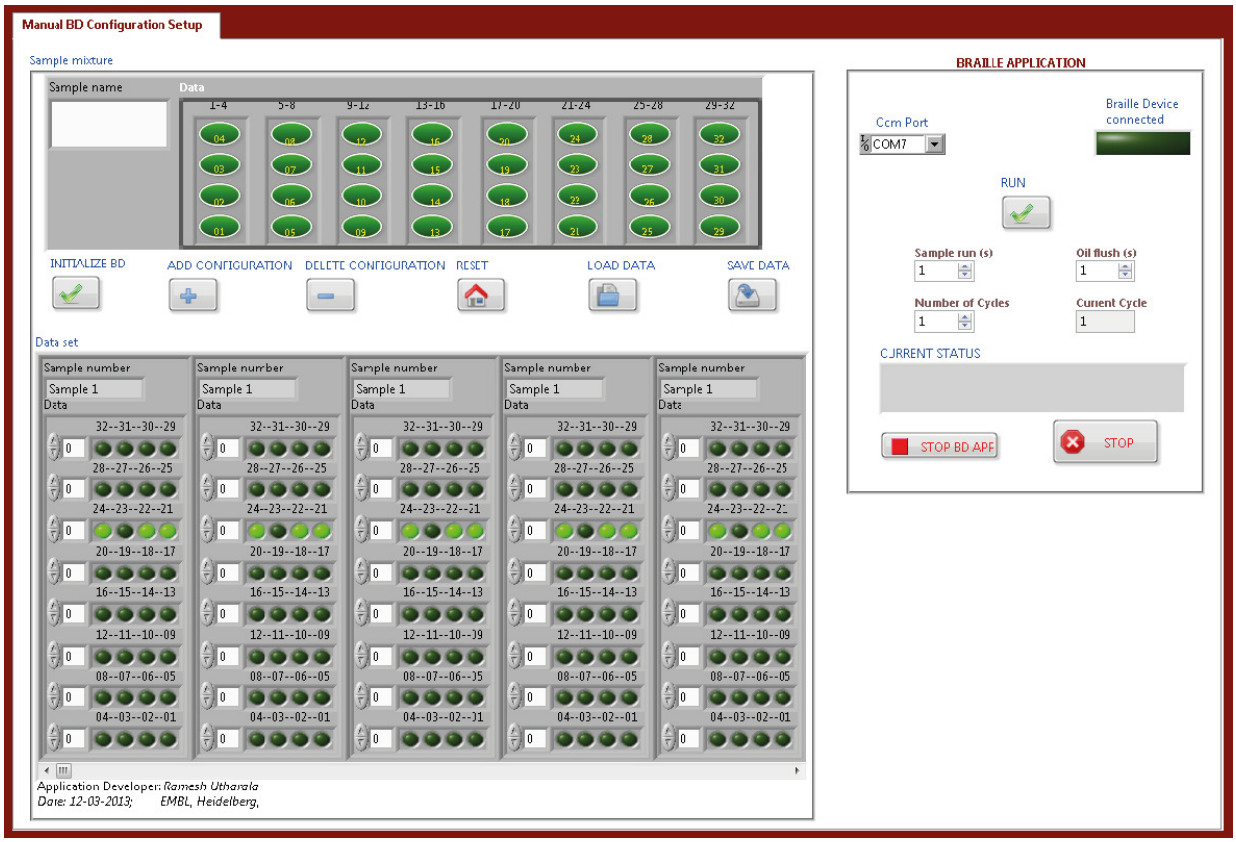

Figure 3.5 Braille chip control software. This screenshot shows the user interface of the software that controls the Braille chip. Individual valves can be actuated in different combinations and for different durations to give control over sample composition and plug size.

In brief, the user interface enables the connection of a Braille display to a computer (Com Port, Initialize BD). Once initialization is complete, the software allows the user to address all pins of the Braille display individually via the panel on the top left of the screen. Here, one can manually choose the individual valves, which should be opened/closed to produce individual samples (indicated by numbers) and give each sample a name. Alternatively saved configurations from previous experiments can be loaded from the tab below. For configurations involving many (hundreds) of samples, configuration files can also be generated in an Excel file and loaded into the program (s. below). The "data set" panel shows the complete sequence including all selected pins (highlighted in bright green).

The right-hand panel can be used to control the size of plugs by setting the time during which the valve configuration is switched to "open" and sample is injected. The user simply specifies the time in seconds in the "Sample run" box. The duration for which all valves are

switched to the waste configuration has to be specified by the user ("Oil flush"). During this time only the two oil phases will flow towards the sample outlet, thereby introducing a gap in between consecutive plugs. Lastly, the user can select the number of cycles for which the specified sample sequence is to be repeated. By controlling the Braille display unit in this way, a sequence of hundreds of plugs can be produced on-chip in a fully automated fashion.

3.2.2.2 Automated plug production

We used the software described in the previous section to optimize the for automated plug production on the Braille chip. We therefore set up a configuration, in which the aqueous phase is "injected" at high flow rates into the carrier oil stream, which flows at a much lower rate. The different flow rates were necessary to produce large plugs, since otherwise only small spaced out droplets would be formed at the T junction, which might result in incomplete sample mixing before plug formation. High aqueous flow rates are further required for fast valve response times, since enough pressure has to build up in the microfluidic channel to push down the thin PDMS membrane and open the valve. We determined the minimal flow rate for reliable plug formation to be at around 650 µL/h for the aqueous phase. Higher rates might be preferable, but also lead to higher reagent consumption. The maximum flow rate for the oil carrier phase was determined to be 200 µL/h. A higher oil flow rate leads to the formation of fragmented plugs and increases the pressure towards the sample inlets, thereby further increasing the need for high aqueous flow rates.

An additional important source of back pressure stems from the type of tubing used to collect the sample plugs. In initial experiments we used a 10 m long tubing of 300 µm inner diameter and 100 µm wall strength. We noticed a significant decrease in plug size over the course of the experiment, which in some instances led to a complete stop of plug formation from some valves. We therefore decided to switch to tubing with an inner diameter of 600 µm, 100 µm wall strength and only 6 m in length. This markedly decreased the effect, but did not completely eliminate it. The pressure difference ΔP in tubes of different diameter can be calculated using the equation of Hagen-Poiseuille, where R is the flow resistance, η is the fluid viscosity, ℓ is the length of the tube, r is the radius of the tube and I_V is the volumetric flow:

$$\Delta P = R I_V = \frac{8\eta\ell}{\pi r^4} I_V \qquad \textbf{Eq. 5}$$

Assuming the tube material is inflexible, we can calculate the back pressure exerted by tubing of different diameters. FC-40 oil (η = 4.1 mPa*s) flowing at 1000 µL/h through a 6 m long tube of 300 µm inner diameter exerts a back pressure of 34.37 MPa, while doubling the inner

diameter to 600 μm reduces back pressure 16-fold to 2.15 MPa, which should have no significant effect on plug production. We hypothesize that the remaining reduction in plug size over time was due to the plugs already filled into the tubing, because segmented flow further increases the back pressure as the surface tension at the water-oil interphase prevents the formation of a parabolic flow profile. This effect can be eliminated by simply filling the tubing with buffer plugs before starting sample plug production (unpublished data by Federica Eduati and Ramesh Utharala).

3.2.3 Cells in plugs

Cell encapsulation in water-in-oil emulsions poses some inherent challenges. In order to keep them alive in plugs, cells must remain in their growth medium throughout the course of the experiment. Complete growth medium, however, contains fetal bovine serum and thus many compounds such as sugars and proteins that can interfere with plug formation and stability by changing the surface tension and viscosity of plugs. An additional effect – termed "wetting" – can be induced by the same factors. Here, the aqueous phase wets the surface of the microfluidic channel, whereby a part of each plug remains on this wetting spot thereby contaminating the following plugs (**Figure 3.6**). Moreover, whilst incubating, the cells themselves produce a plethora of secreted molecules that can have similar effects on plugs. In order to counteract some of these effects, we decided to use the serum-free and defined FreeStyle™ (FS) medium.

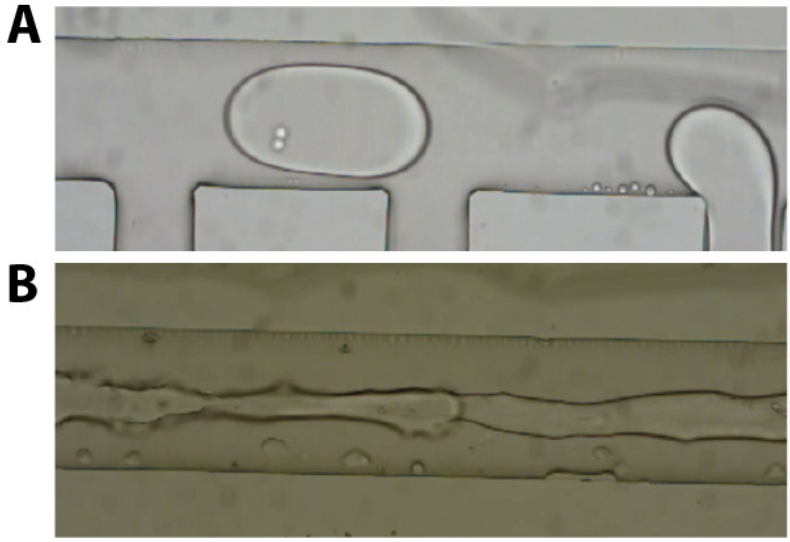

Figure 3.6 Wetting caused by cell culture medium. Initially, separated plugs are formed (**A**). After some time they fuse into one long stream of aqueous phase due to wetting on the channel surface (**B**).

Indeed, the use of FS medium greatly reduced the effects of wetting and allowed the encapsulation of cells with high fidelity. However, when incubating cells at high densities within

nanoliter droplets (200 cells in a 1 µL plug correspond to 20,000 cells in a 96-well plate filled with 100 µL of medium), the many proteins and secondary metabolites that mammalian cells secrete reach toxic concentrations and thus reduce cell viability (Clausell-Tormos et al., 2008). To decrease the effect of such cytotoxicity by dilution and at the same time to supply sufficient nutrients to the cells, we decided to produce large plugs (up to 1 µL in volume).

3.2.3.1 Cells can be co-encapsulated with mixtures of compounds

In a proof-of-principle experiment we wanted to see if we can encapsulate HeLa in FS medium cells together with water, red dye or blue dye. We created repeated cycles of three different mixtures: cells + blue dye, cells + water and cells + red dye. For plug production FC-40 carrier oil was injected at 150 µL/h and all aqueous phases were injected at 600 µL/h. Images of the plug formation from multiple inlets were taken on a standard light microscope (**Figure 3.7 A**). Additional images of the resulting plugs in the sample tubing were acquired at high and low magnification (**Figure 3.7 B**). Multiple cells can be seen in all three plug types, showing that cells can be encapsulated into plugs of different compositions. Thus, our device fulfilled a fundamental requirement for combinatorial sample preparation. It also becomes evident from these images, that cross-contamination is minimal, since no red color is visible in the water plug.

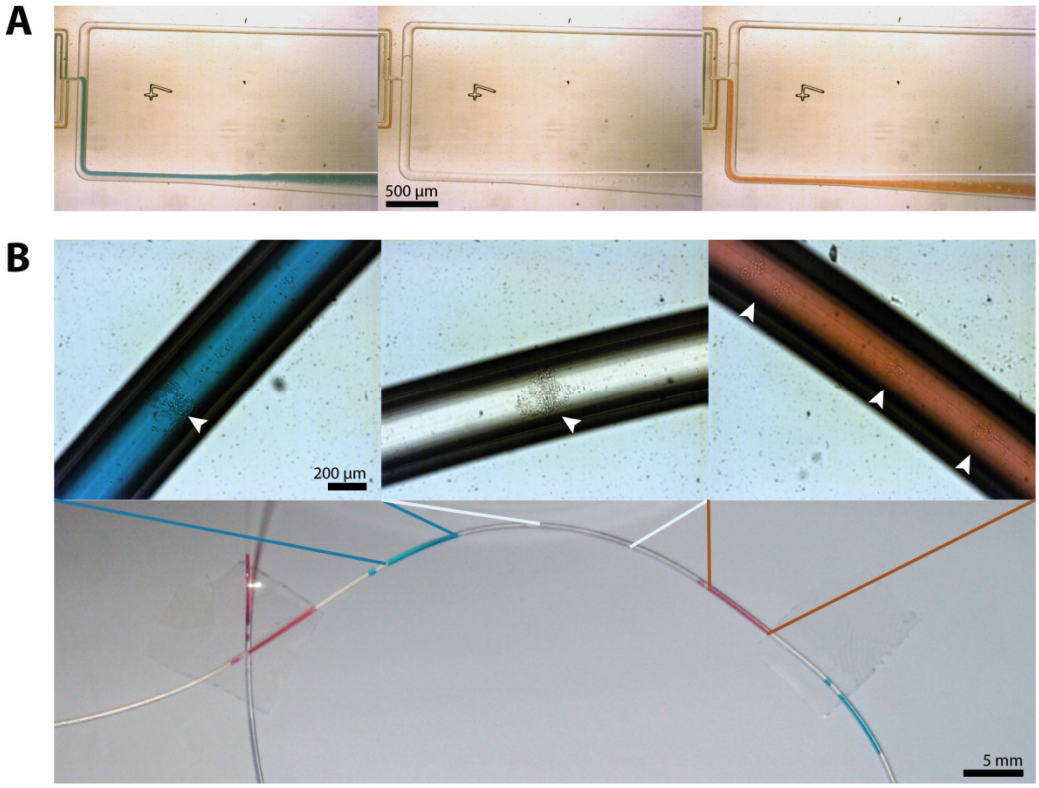

Figure 3.7 Cells can be co-encapsulated with different compounds. A) A Micrograph showing plug production at the T junction of a 6-inlet Braille chip. Plugs are produced containing mixtures of cells and blue dye, red dye or

water. **B)** Resulting plugs imaged different magnifications. Cells are present in all mixtures (indicated by white arrows).

3.3 Fusion module – adding reagents to plugs

A consequence of encapsulating cells in plugs is the loss of direct access to the cells. One cannot simply use a pipette to add reagents to the cells once they are inside a plug, as is possible in open reaction vessels such as microtiter plates. However, many biological experiments require the sequential addition of assay reagents and intermittent incubation periods. Accordingly, we set out to develop a module that allows reliable addition of enzymatic substrates to cell-occupied plugs after their incubation with mixtures of small molecules. As described in the introduction, a variety of microfluidic devices have been previously developed to allow the fusion of droplets and plugs with each other (cf. section **1.3.2**). Nevertheless, this has never been achieved for large plugs containing cells, which pose their own suite of problems. In the following, we describe in detail a new fusion module, which we designed to overcome these previous limitations:

3.3.1 Chip layout

We designed a very simple microfluidic chip for the specific purpose of adding reagents for cell biological assays to pre-formed cell-occupied plugs, which were stored in sample tubing (**Figure 3.8**). Plugs are loaded from a port allowing the connection of tubing from the side to prevent plug breakup upon loading. Furthermore, the chip consists of a drop maker to produce substrate droplets, which in turn is connected to a straight channel leading to an outlet to connect additional tubing for sample incubation. Additional side channels allow the infusion of surfactant-containing oil to reduce wetting. All of these parts are discussed in detail below.

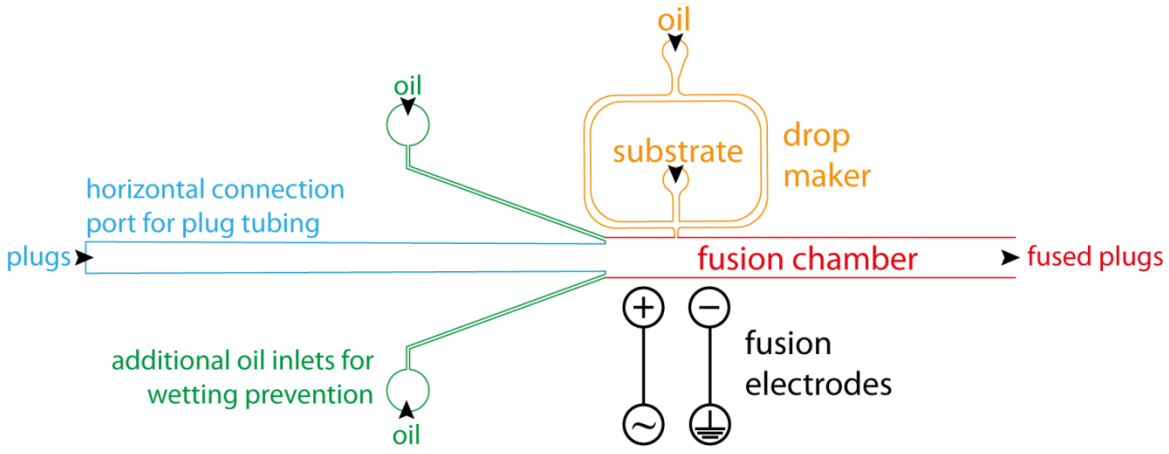

Figure 3.8 Schematic of the fusion chip. The fusion chip consists of different modules (indicated by colors). The channel depth of this device is 500 µm.

3.3.1.1 Plug re-injection requires connection of tubing from the side

A train of pre-formed plugs with volumes of hundreds of nanoliters produced on the Braille chip and stored for incubation in sample tubing cannot be loaded onto a microfluidic chip in the same way as droplet emulsions The dead volume of conventional (vertical) connection ports leads to plug break-up upon re-injection. Accordingly, we decided to use an inlet allowing horizontal tubing connection and sample loading (Clausell-Tormos et al., 2010). The sample loading channel has a depth of about 500 μm and – like the Braille chip – is not bonded to a glass slide but to a thin and flexible PDMS membrane about 150 μm thick. Membrane flexibility is achieved by using a curing agent to elastomer ratio of 1:20 compared to the 1:10 ratio used to cast the rest of the chip. Such a combination of deep channel and membrane flexibility allows a smooth connection to into the side of the fusion chip. Plugs can thus be loaded with no plug break-up or fusion of consecutive plugs with each other.

3.3.1.2 Additional oil inlets reduce wetting of injected plugs

When loading plugs containing many cells into microfluidic chips, a few additional problems arise, which are caused by the following phenomena:

- The production of plugs does not permit the use of stabilizing surfactants (e.g. perfluoropolyether-polyethylene glycol (PFPE-PEG)) in the carrier phase. Even when used at low concentration, surfactants cause plug breakup by lowering their surface tension.
- Cell incubation leads to the accumulation of proteins and complex carbohydrates within the plug.

The lack of surfactant and the presence of cells, proteins and carbohydrates in the plugs after incubation lead to wetting. This can cause coalescence of consecutive plugs at the plug inlet and thus in the best case to cross-contamination between plugs and in the worst case in a continuous flow rather than distinct plugs (**Figure 3.9 A**). To reduce wetting after plug re-injection, our newly developed fusion module includes additional side channels for the addition of surfactant-laden stabilizing carrier oil (FC-40 + 0.1% PFPE-PEG; Sigma-Aldrich, Germany). The use of these side channels reduces wetting in the following ways:

1) added surfactant reduces the propensity of cell plugs to stick to the channel surface by reducing wetting
2) the geometry of the additional oil channels leads to a flow profile in the fusion chamber that keeps the incoming plugs away from the vertical channel walls

3) the additional oil also increases the spacing between consecutive plugs, further reducing the probability of coalescence between consecutive plugs

To test the improved plug loading properties, we loaded pre-incubated plugs containing cells and mixtures of small molecules onto microfluidic fusion devices with or without additional stabilizing oil inlets. Without the use of additional inlets, plugs routinely got retained at the channel wall just after leaving the tubing. Over time the wetting got worse and the train of incoming plugs turned into a single big plug (**Figure 3.9 A**). This was not observed in devices which included the additional oil inlets. Here, the plugs were kept away from the channel walls and consecutive plugs never got close enough to each other for coalescence to occur (**Figure 3.9 B**).

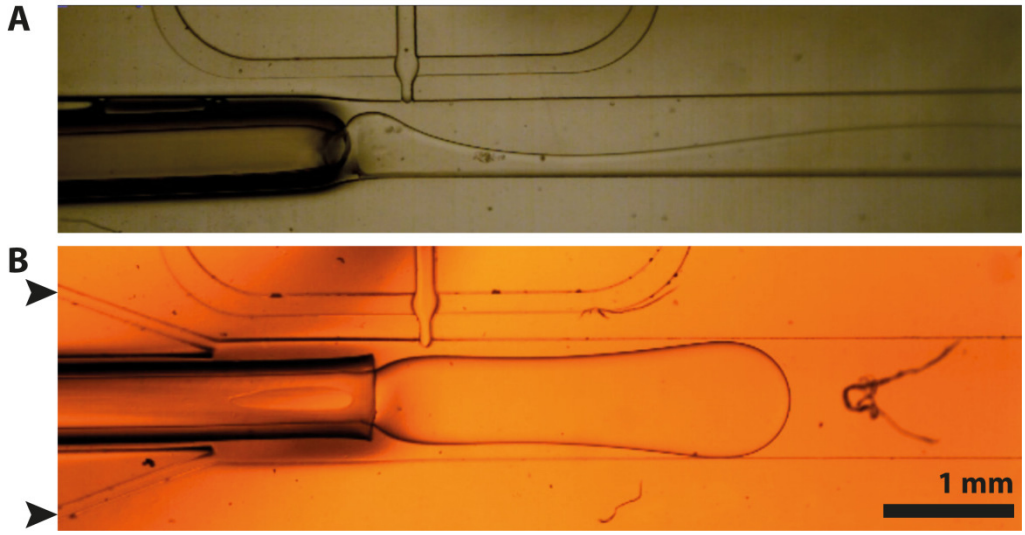

Figure 3.9 Additional oil inlets reduce wetting in the fusion chamber. A) Without additional oil inlets, wetting occurs in the fusion chamber. **B)** Additional oil inlets keep incoming plugs away from the vertical channel walls during fusion and eliminate wetting.

3.3.1.3 Direct injection of substrate droplets into preformed plugs

Substrate droplets are freshly formed in a drop maker, which is located just downstream of the junction formed by the plug inlet and the additional oil inlets. Plug coalescence with substrate droplets therefore occurs while the plug is emerging from the end of the sample tubing at which point it has not had the time to stabilize. We use carrier oil containing 1% PFPE-PEG surfactant in the formation of substrate droplets. The addition of the surfactant fulfills two purposes:

1) It reduces wetting problems that could occur further downstream in the fusion chamber.
2) It stabilizes unfused substrate droplets so that they do not fuse with each other or sample plugs further downstream (unfused substrate droplets can be easily distinguished from

sample plugs by their length in any successive fluorescence readout and can therefore be excluded from data analysis).

When injected from the sample tubing, the sample plugs fill the fusion channel almost completely. Fusion occurs by injecting the substrate droplets directly into the non-stabilized sample plug even before droplet formation is completed (**Figure 3.10**).

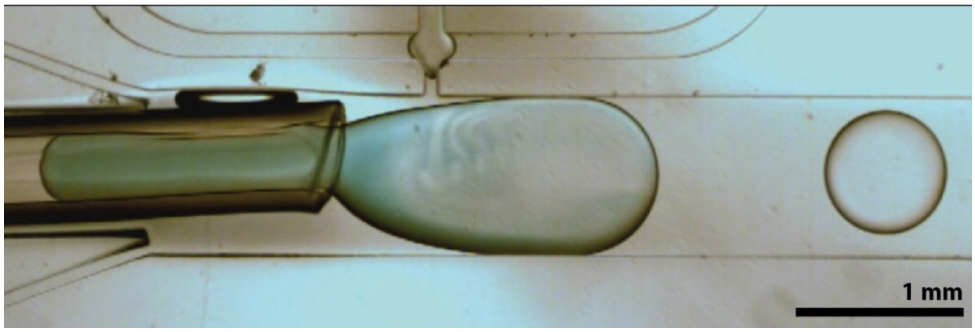

Figure 3.10 Fusion of plugs with substrate droplets. A plug containing blue dye fuses with droplets of substrate. An unfused substrate droplet can be seen on the right hand side of the image.

By keeping all flow rates constant, the same amount of substrate can be added to each plug. However, since there are always minor fluctuations in the size of the plugs a one-to-one fusion of substrate droplets to sample plugs would be ill-advised since the substrate would be diluted to different extents. Therefore, we produced substrate droplets at a much higher frequency than the incoming plugs. As an arbitrary example, if a plug of length ℓ would fuse with 20 substrate droplets, a second plug of length $\ell/2$ would fuse with 10 substrate plugs. In this way we ensured that the total substrate concentration of the resulting fused plugs is constant and independent of the initial sample plug size. This precludes a 1:1 synchronization of plugs to droplets, which is hard to achieve.

3.3.1.4 Inducing a dielectric field improves the reliability of the fusion process

After fusion with substrate droplets, sample plugs are collected in a stretch of tubing for further incubation with the substrate and consecutive assay readout. While performing fusion experiments, we observed irregularities in fusion efficiency when attaching long collection tubing. We attributed the irregularities to an increase of pressure in the microfluidic system that makes fusion unreliable. Often, sample droplets did not fuse with the sample plugs, but rather "bounced" off the plug surface (**Figure 3.11**). This observation prompted us to include two electrodes in our design, which induce a dielectric field across the fusion chamber to ensure droplet fusion (cf. section **1.3.2**). For this purpose, two wires were brought into close proximity of the

fusion chamber; one was connected to a high voltage amplifier (Trek Model 623B, TREK Inc., Lockport NY), while the other acted as a grounding electrode.

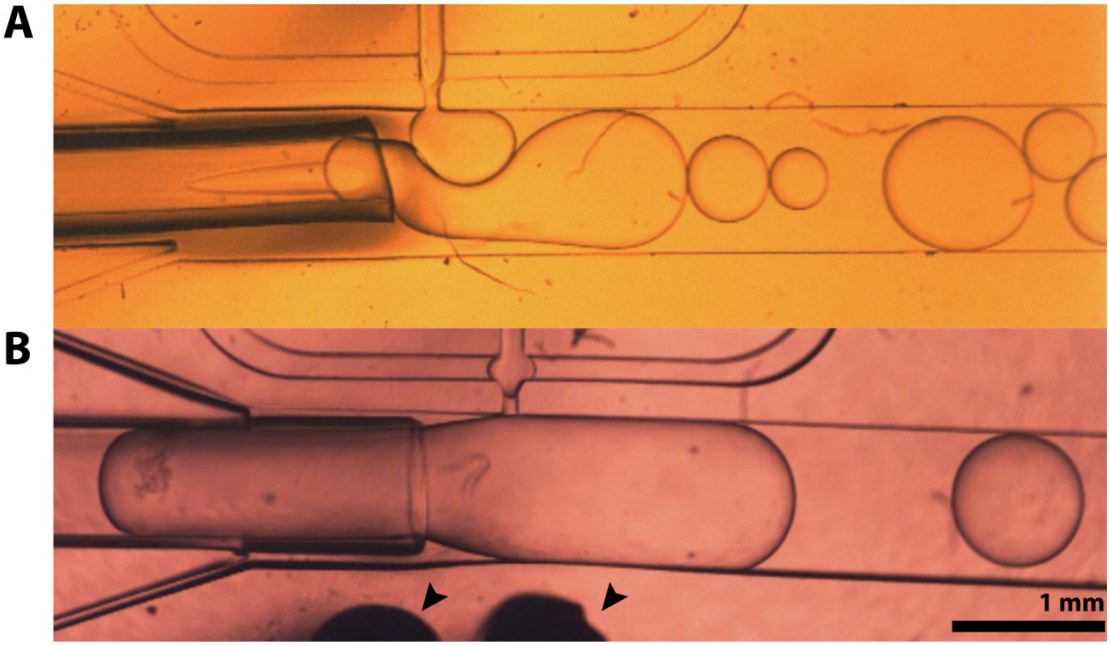

Figure 3.11 Electrodes aide in fusion. A) Fusion of substrate droplets to incoming plugs is not reliable with changing pressure regimes. **B)** The addition of electrodes (indicated by arrows) close to the fusion chamber reliably stabilizes fusion.

A function generator (PCGU1000, Velleman NV, Belgium) was used to control the AC output of the high voltage amplifier, including the frequency, amplitude and shape of the wave function. We performed trial experiments with test plugs containing cells and a long piece of tubing attached to the fusion chip. The trials allowed us to determine optimal settings for droplet coalescence at a frequency of 64 kHz, an amplitude of 1 Vpp and with a square wave shape. With these settings, droplet fusion could be worked reliably over the complete course of a typical fusion experiment (up to 4 hours).

3.3.1.5 The use of mineral oil in sample plug spacing

During the storage and transport of long trains of plugs in tubing, the distance between the plugs can change over time (based on draining of the oil), which in turn can lead to unwanted fusion of consecutive plugs (cf. section **3.2.1.4**). This can be avoided by additional spacing with mineral oil plugs which does not interfere with the fusion process since the substrate solution is completely immiscible with the mineral oil and therefore only fuses with the sample plugs (**Figure 3.12**).

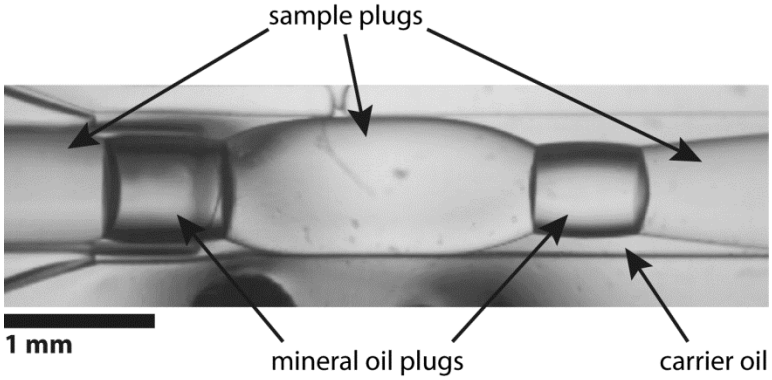

Figure 3.12 Separation of consecutive sample plugs by mineral oil plugs. Mineral oil separates sample plugs from each other even during fusion.

3.4 Discussion

We have developed a new microfluidic technology that allows combinatorial plug production controlled by Braille display. In order to do so, we have built on the pioneering work of the Takayama lab and expanded the use of Braille displays to enable more complex droplet-based microfluidic applications (Gu et al., 2004). Our device allows the production of plugs containing combinatorial mixtures of up to 16 compounds and cells. This enables the production of plugs with highly diverse chemical composition. The plugs can be used as miniaturized reaction vessels to screen the effect of compound mixtures on cells (**Figure 3.7**).Previous work by Wang et al. reported combinatorial plug production for combinatorial click chemistry (Wang et al., 2006; Wang et al., 2009) but relied on the manual exchange of sample tubing after only eight samples and did not contain any cells (cf. **General discussion**). Our setup allows the automated production of trains of thousands of densely spaced plugs. We achieve this by using tubing with a large inner diameter of 600 μm to reduce the back pressure in the system and by pre-filling the tube with buffer plugs to ensure that the back pressure remains constant throughout plug production (cf. section **3.2.2.2**). Instead of the pressurized air used in the aforementioned publications, we used mineral oil plugs to prevent the fusion of consecutive sample plugs, which would lead to cross-contamination between samples (**Figure 3.4 & Figure 3.12**). This allows us to create trains of plugs that are very closely spaced and thus increases the throughput of sample production by reducing the injection time of carrier oil, which is used to space out the plugs. This is not possible when using pressurized air since it is compressible.

Our fusion module combines several components to enable the coalescence of droplets containing assay components with a train of plugs containing cells, which were incubated in the presence of drugs. Wetting of channel walls by the plug contents presented the main challenge to

overcome. In the past it has prevented plug loading onto microfluidic chips after incubation and thereby prohibited any downstream operations such as the addition of reagents. We tackled this problem by including additional channels for carrier oil infusion in order to prevent incoming plugs from touching the channel walls. We additionally added low amounts of surfactant to the additional carrier oil, which further reduced wetting (**Figure 3.9**). Since the addition of surfactant from the side channels as well as from the assay reagent droplet maker stabilizes the droplets and thus prevents droplet coalescence, our setup required the use of electrodes for reliable plug-to-droplet coalescence (**Figure 3.11**). Finally, the use of mineral oil plugs in combination with the fusion module allowed fusion to be carried out at higher throughput since even closely spaced plugs could not fuse with consecutive plugs (**Figure 3.12**). In this way plug production time could be reduced from 22 s/plug to 3 s/plug or 163 plugs/h and 1200 plugs/h respectively. Therefore, our design provides a useful addition to the collection of existing fusion modules presented in the introduction (section **1.3.2**) by enabling cell-based assays, which require long incubation times to be carried out in droplet-based microfluidic devices.

Both microfluidic modules described above were used in combination for a first application to investigate the regulation of matrix metalloproteinases, which is described in detail in the next chapter. Generally, our technology is compatible with any assay that produces a fluorescent compound, which is released from the cell into culture medium, since we measure the overall fluorescence of the plug and not the individual cells contained within the plug. The lower sample consumption compared to the one of the gold standard of high-throughput drug screening - microtiter plate-based screens - allows the use of rare samples such as primary cells or dissociated cells from tumor biopsies (cf. **General Discussion**).

4 INVESTIGATING THE REGULATION OF MATRIX METALLOPROTEINASES

4.1 Introduction

One field of application for our newly developed Braille display-based method is chemical genetic screening (cf. section **1.5**). Briefly, in such a screen combinatorial mixtures of drugs with defined molecular targets are used to elucidate cellular pathway topologies (Lehar et al., 2007). The phenotypes of cells perturbed with individual drugs are compared to the phenotypes of those perturbed with combinations of the same drugs. Resulting combination phenotype strengths are caused by different types of interactions between drug targets and can be categorized into three distinct groups: additive, synergistic or antagonistic interactions. By identifying the interaction type for many different drug combinations, we can hence deduce protein network architectures at high resolution.

Studies of the regulation of matrix metalloproteinases (MMPs) could benefit greatly from such an approach (cf. section **1.6.3**). We chose HT1080 fibrosarcoma cells as a model system to investigate MMP regulation, since they constitutively express MMP-9 at high levels compared to other cell lines (e.g. HeLa) (Gervasi et al., 1996; Giambernardi et al., 1998; Moll et al., 1990). Our goal was to encapsulate freshly harvested HT1080 fibrosarcoma cells in plugs together with combinations of effectors of MMP expression on the Braille chip, then incubate the plugs with the effectors, add a fluorogenic MMP substrate on the fusion module and read out the fluorescence signal using our optical setup. The experiment was designed to enable chemical genetic screens at high throughput and low sample consumption.

In addition, the experiments described in the chapter below permitted us to further characterize and optimize our new microfluidic setup while using biological test samples and to develop the tools necessary to analyze the collected data.

4.2 Dynamics of 520 MMP FRET substrate XIV conversion

We used a broad-spectrum fluorogenic FRET substrate (520 MMP FRET substrate XIV; AnaSpec, Freemont CA) to measure MMP activity in our samples. The FRET substrate consists of two fluorophores separated by an MMP-cleavable peptide substrate. The two fluorophores (5-FAM & QXL™520) act as FRET pair, i.e. QXL™520 quenches the fluorescence of the donor 5-FAM via Förster resonance energy transfer (FRET; **Figure 4.1 A**). Upon peptide cleavage, the two fluorophores are separated in space and 5-FAM fluorescence becomes visible when excited at 488 nm. In initial experiments, we tested the dynamics of substrate cleavage by HT1080 and HeLa cells (as negative control). We seeded 22,500 cells/well of each cell line in FS medium in a

96-well microtiter plate, added 2.5 µM of fluorogenic substrate and incubated at 37 °C for 3.5 h while measuring fluorescence at 521 nm in 10 min intervals (**Figure 4.1 B**). As expected, the two cell types showed significantly different substrate conversion dynamics. HT1080 cells convert the substrate at high rates, while conversion by the HeLa cells is very limited.

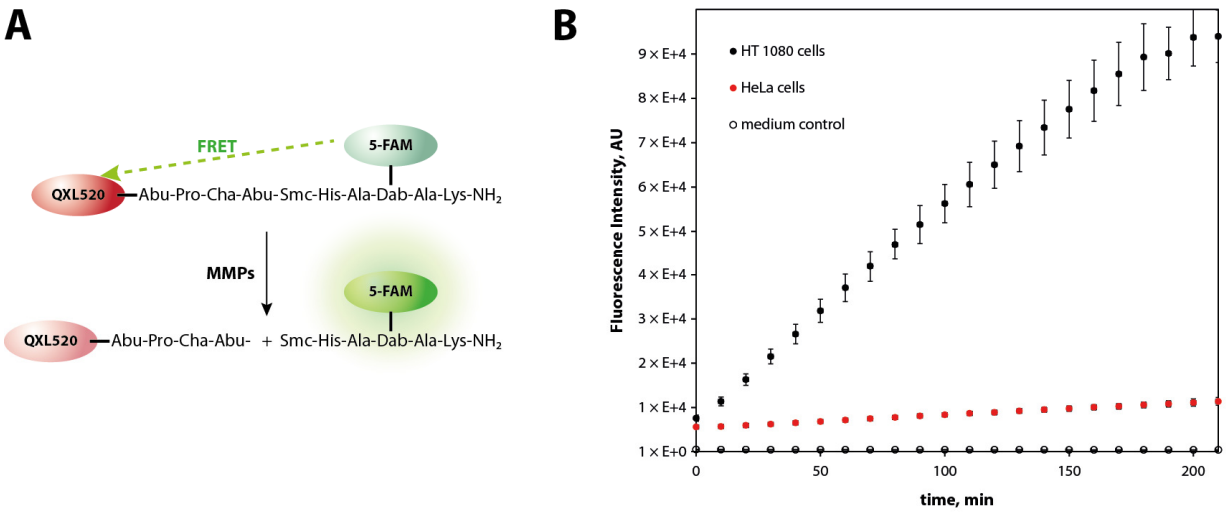

Figure 4.1 Fluorogenic MMP FRET substrate conversion. A) Cleavage of the peptide substrate by MMP enzymatic activity, separates donor (5-FAM) from quencher (QXL520) fluorophore. 5-FAM fluorescence can then be measured at 521 nm (adapted from manufacturer website: www.anaspec.com). **B)** MMP FRET substrate conversion by HT1080 (●) and HeLa cells (●) as measured in a microtiter plate reader.

Based on this data, we decided to use incubation times of at least one hour for further experiments employing this substrate. As a consequence of this, it was also necessary to add the substrate after the incubation of cells and effectors using our newly developed fusion chip (cf. **3.3**), since long-term incubation with the fluorogenic substrate would just lead to complete substrate conversion and thus equal fluorescence signals for all conditions.

4.3 Substrate conversion in plugs measured by PMTs

To show that we could also measure MMP FRET substrate conversion in plugs, we used a 6-inlet Braille chip to encapsulate HT1080 cells together with alternating concentrations of fluorogenic substrate (0.5 µM & 2.5 µM) to simulate two different MMP expression/activity levels. We incubated for one hour and measured fluorescence at 520 nm with our photo multiplier tube (PMT) setup (**Figure 4.2**; cf. section **7.3**). The fluorescence intensity is given by the amplitude in volts measured by the PMTs and scales nicely with the fluorogenic substrate

concentrations of the plugs as indicated by the scale bars on the left. These results show that we can indeed measure the enzymatic activity of a group of cells directly in large plugs.

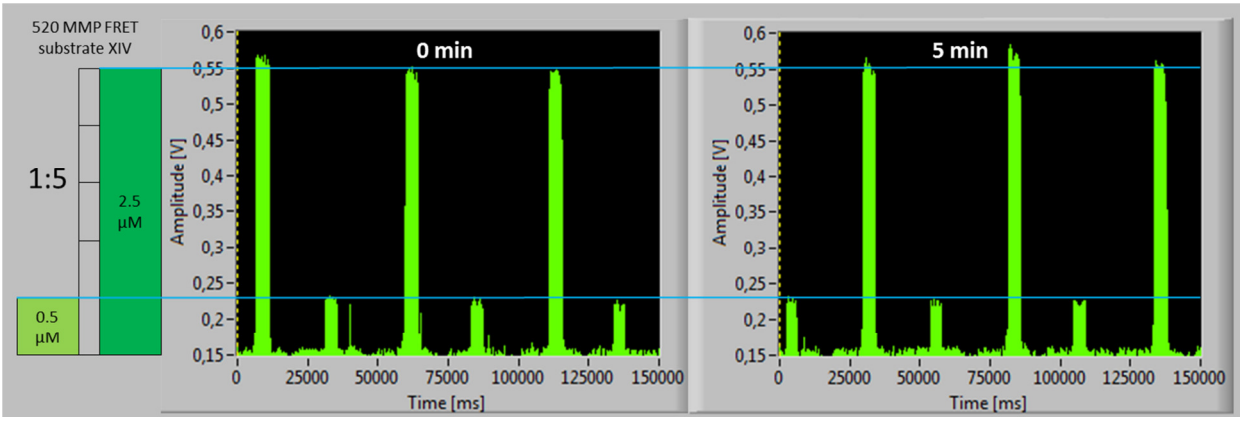

Figure 4.2 PMT measurements of MMP FRET substrate conversion in plugs. HT1080 cells were co-encapsulated with 0.5 µM or 2.5 µM 520 MMP FRET substrate XIV, incubated for 60 min and plug fluorescence was measured with a PMT at 520 nm. The left panel shows peak intensities at the start of the fluorescence measurements and the right panel 5 minutes later.

4.4 Monitoring MMP inhibition in plugs

So far, we showed how to detect different substrate concentrations as a proxy for different enzymatic activity. Because we needed to be able to measure alterations in MMP enzymatic activity directly, we tested the broad spectrum catalytic inhibitor of MMPs marimastat for its use as positive control for inhibition in our setup. In an initial experiment, we seeded 22,500 HT1080 cells/well in a 96-well microtiter plate. We then added marimastat to resulting concentrations of 10 µM and 100 µM and incubated for 22 hours at 37 °C and 5% CO_2. Fluorogenic substrate was freshly added immediately before measuring fluorescence at 520 nm in a microtiter plate reader for 4 h at intervals of 5 min (**Figure 4.3 A**). At 100 µM the activity of cell-derived MMPs is significantly lowered (**Figure 4.3 B**). The effect is clearly visible after one hour of incubation with the fluorogenic substrate and marimastat was therefore used as an inhibition control in all further experiments (cf. below).

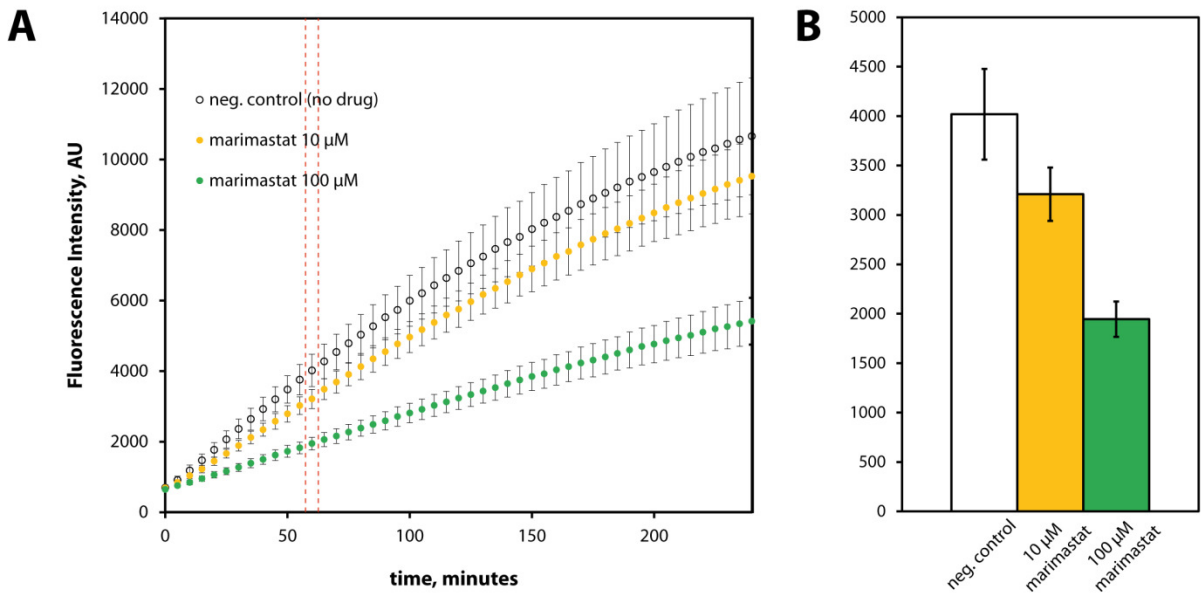

Figure 4.3 Marimastat inhibits MMP activity. A) 22,500 HT1080 cells per well were seeded in quadruplicates in a 96-well microtiter plate and incubated with marimastat at 10 µM (●), 100 µM (●) or no drug (○) for 22 h. Substrate fluorescence was measured at 520 nm every 5 min during 4 h. The red dashed lines indicate the samples shown as boxplot on the right in **B).**

4.5 Plug fluorescence measurements with a CCD camera

When a PMT setup is not available and measurements in only one fluorescence channel are required, a charge-coupled device (CCD) camera can be used as an alternative to measure plug fluorescence. Here, we excited fluorescence with a fluorescence lamp instead of a laser and imaged the whole width of the tubing containing the plugs at intervals of 300 ms in both the green fluorescent (FL) and bright field channels (BF). Exposure times were adjusted for every experiment to prevent over exposed images, which would preclude any quantitative image analysis. We acquired time lapse movies that spanned the complete duration of an experiment. This way, data similar to that measured by PMTs could be analyzed, i.e. there were multiple fluorescence and bright field images per plug (**Figure 4.4 B**). However, this approach is at the same time limited to only one fluorescence channel and the bright field channel. If more than one fluorescence wavelength should be measured, PMTs are the method of choice.

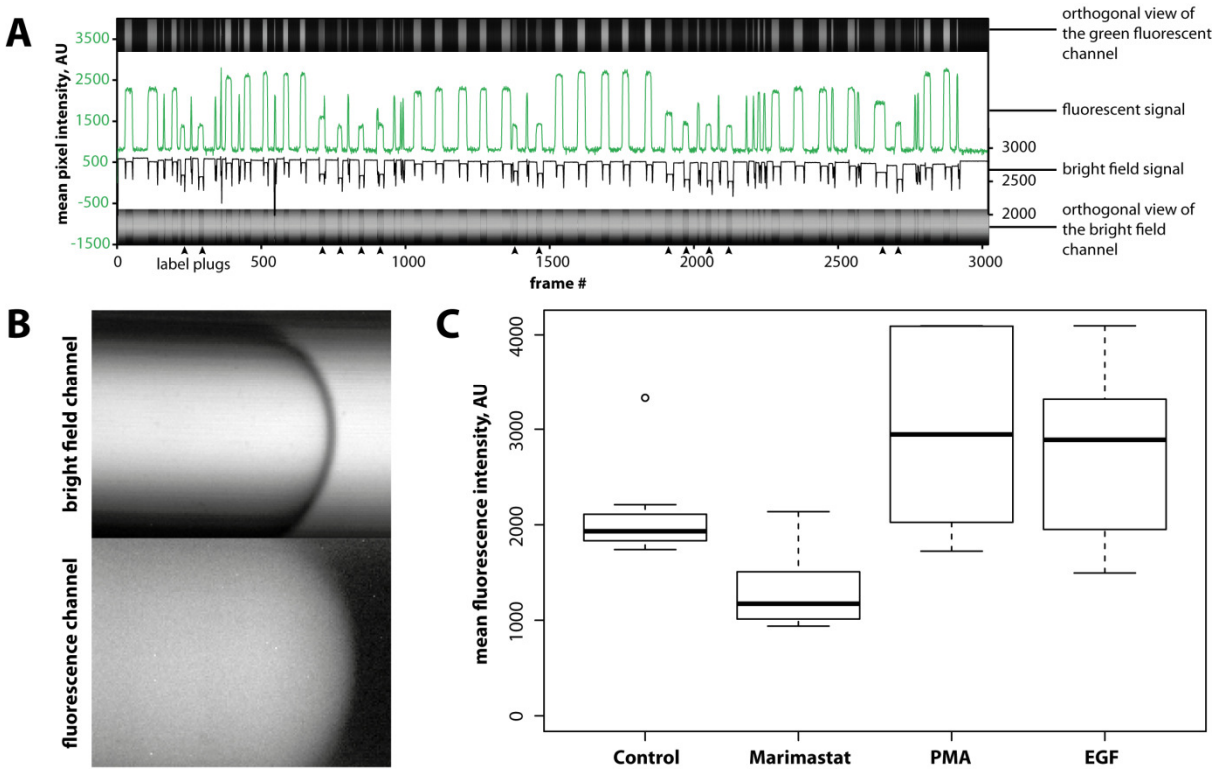

Figure 4.4 Fluorescence measurements in plugs using a CCD camera. A) Orthogonal view of a series of images taken at 300 ms intervals in the green fluorescent channel (top) and in bright field (bottom) and a plot of the light intensity measured for green fluorescence (green line) and bright field (black line). **B)** Micrographs of an example plug in the tubing (600 µm diameter) in BF (above) and FL (below). **C)** Boxplot of the mean fluorescence intensity produced by the conversion of 520 MMP FRET substrate XIV in plugs with FS medium only (control; n=8), marimastat (50 µM; n=8), PMA (80 nM; n=8) and EGF plugs (100 ng/mL; n=9).

An easy way to generate a visual overview of the whole data set is by using the "orthogonal views" function found in the image analysis software FIJI (Fiji is just ImageJ) (**Figure 4.4 A**). The function integrates the pixel intensity values of each frame in a movie and plots the values as a column in a new image. The "plot profile" command then generates a plot of the fluorescence in the tubing over time. The sequence was encoded by labeling plugs between samples with dark blue dye, which results in lower bright field light intensity values. To test if we could measure differences in MMP FRET substrate conversion in plugs, we produced plugs containing mixtures of HT1080 cells in 1:1 mixtures with FS medium (control), the broadband MMP inhibitor marimastat, activator of MMP phorbol-12-myristate 12-acetate (PMA) or epidermal growth factor (EGF), which is known to activate MMP-9. **Figure 4.4 C** shows that we can indeed measure differences in MMP activity when incubating cells in plugs with different compounds for 20 hours. MMP activity is reduced in the presence of marimastat, while PMA or EGF exposure increases the detected fluorescence signal.

4.6 Drugs affecting MMP activity

In order to perform model screens for combinatorial effectors of MMP activity, we chose drugs according to two criteria: 1) they should have known effects on MMP-2/-9 activity (cf. section **4.6.2**) or 2) they should be inhibitors or activators of important signaling pathways in the cell. Identified drugs are listed in **Table 4.1** & **Table 4.2** together with their targets/effects.

Table 4.1 Known effectors of MMP activity

Name	MMP	Function	Reference
Phorbol-12-myristate 12-acetate (PMA)	MMP-2/MMP-9	Activator	(Lohi et al., 1996)
5-methyl-2-(4-methylphenyl)-1H-benzimidazole (MPBD)	MMP-9	Inhibitor	(Nair et al., 2008)
Simvastatin	MMP-9	Inhibitor	(Vandooren et al., 2013)
Marimastat	MMPs (broad band)	Inhibitor	(Steward, 1999)

Table 4.2 Inhibitor/activator of important cellular pathways

Name	Target & effect	Reference
ACHP	IKK inhibitor	(Sanda et al., 2005)
AZ 10417808	Casp-3 inhibitor	(Scott et al., 2003)
Cyt387	Jak inhibitor	(Pardanani et al., 2009)
IKK-16	IKK inhibitor	(Waelchli et al., 2006)
Ivachtin	Casp-3 inhibitor	(Kravchenko et al., 2005)
IWR-1	Wnt inhibitor	(Chen et al., 2009)
L-779,450	Raf inhibitor - also inhibits p38 and GSK3	(Takle et al., 2006)
MK-2206	Akt inhibitor	(Hirai et al., 2010)
Nutlin-3	p53 pathway activator	(Vassilev et al., 2004)
NVP-BSK805	Jak inhibitor	(Baffert et al., 2010)
PHT-427	Akt inhibitor	(Meuillet et al., 2010)
Pifithrin alpha	p53 inhibitor	(Komarov et al., 1999)
Roscovitine	p53 expression inducer	(Meijer et al., 1997)
SB590885	Raf inhibitor	(Takle et al., 2006)
Tunicamycin	p53 expression inducer (via ER stress)	(Lin et al., 2012)
ZM306416	KDR (=VEGFR-2) inhibitor	(Hennequin et al., 1999)

4.6.1 Model screen for MMP activity (six versus six compounds)

For an initial small scale screen, we selected twelve compounds from the list (**Table 4.2**) above and created two groups of six compounds each to be tested in combinations of two (**Figure 4.5**). This resulted in a total of 49 individual drug mixes (1 FS medium control + 12 individual compound + 36 combinations). Five replicates of each sample were generated using the Braille chip with the following sequence:

6 × (FS + FS + cells) → label → 5 × (Cyt387 + FS + cells) → label → 5 × (EGF + FS + cells) → … → 5 × (Cyt387 + EGF + cells) → label → 5 × (Cyt387 + Ivachtin + cells)…

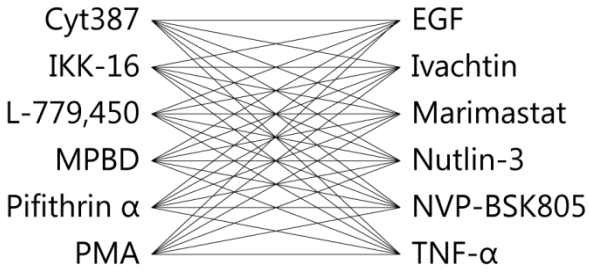

Figure 4.5 Mixtures of 6 vs 6 drugs. All 36 possible combinations of six versus six drugs are shown (left side versus right side).

In order to separate the samples from each other, to reduce cross-contamination and to keep track of the sequence, we produced blue fluorescent Cascade® Blue (CB) label samples in between all drug samples. These blue labels were detected by PMT in the blue fluorescence channel and were used to segregate and identify samples. For this purpose, we defined a fluorescence threshold in the blue fluorescence channel to detect all label plugs above background levels (red circles **Figure 4.6**). By additionally setting a minimal distance threshold in between detected label plugs, we divided all detected peaks into "label" (sequence of closely spaced blue peaks) and "sample" (all signal in between the blue peaks). The division of the blue fluorescence signal allowed us to identify all samples in the green fluorescence channel (orange boxes in **Figure 4.6**). The resulting overview was generally used as a first glance at the complete dataset to estimate data quality and sample detection fidelity (e.g. input sequence = output sequence?). By also setting a minimal length for each sample plug, unfused substrate droplets could be easily filtered out from the collected data set and did not interfere in the analysis. Rather, unfused substrate droplets could be used as an internal control for the optical setup, i.e. if their signal suddenly dropped, something must have been wrong with the optical setup or the fusion unit.

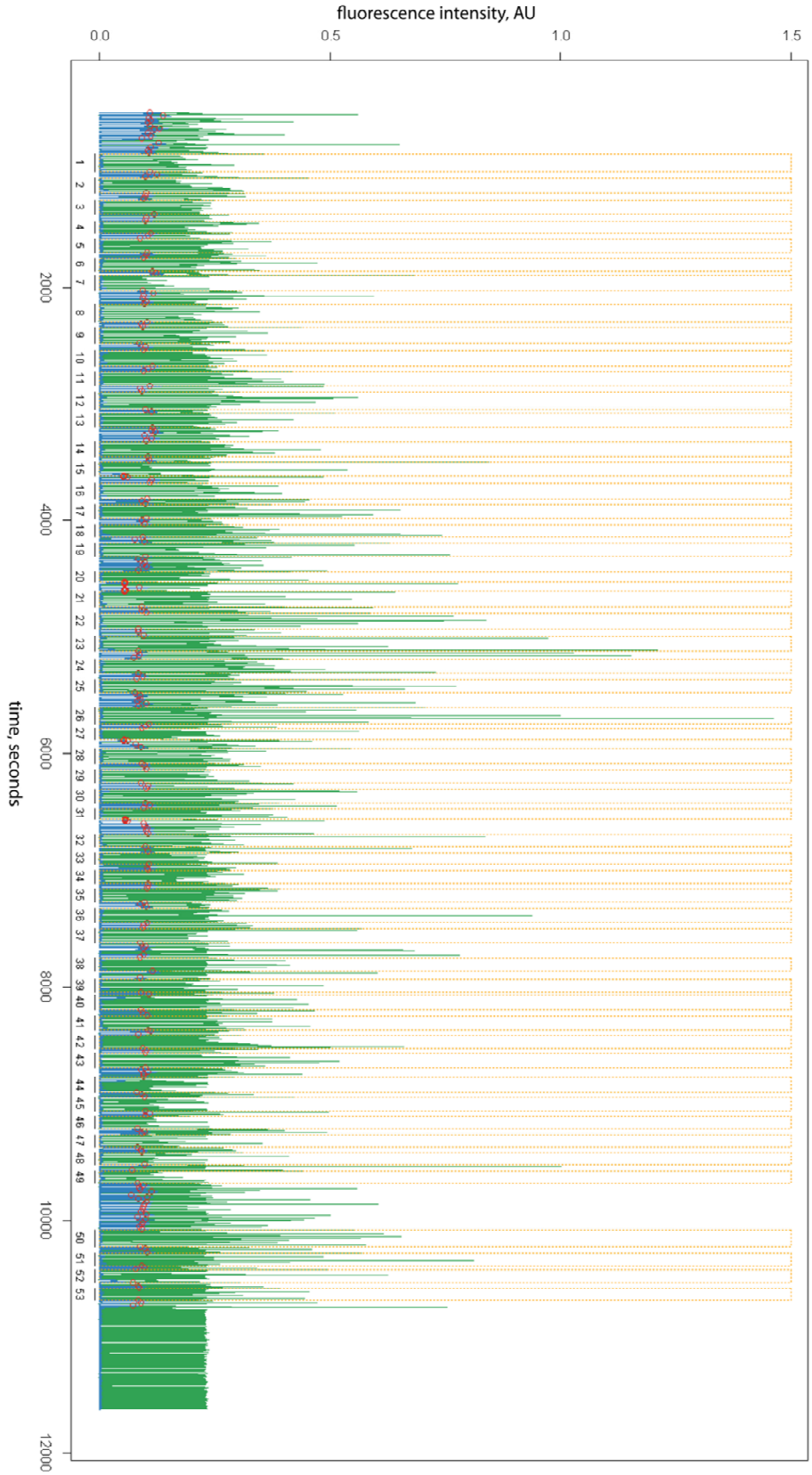

Figure 4.6 Overview for collected fluorescence data. The graph depicts the total acquired signal in a six vs six drug screen, where MMP FRET substrate fluorescence is shown in green and Cascade blue® label fluorescence in blue. Detected label peaks for sample segregation are indicated with red circles and orange boxes indicate detected sample plugs.

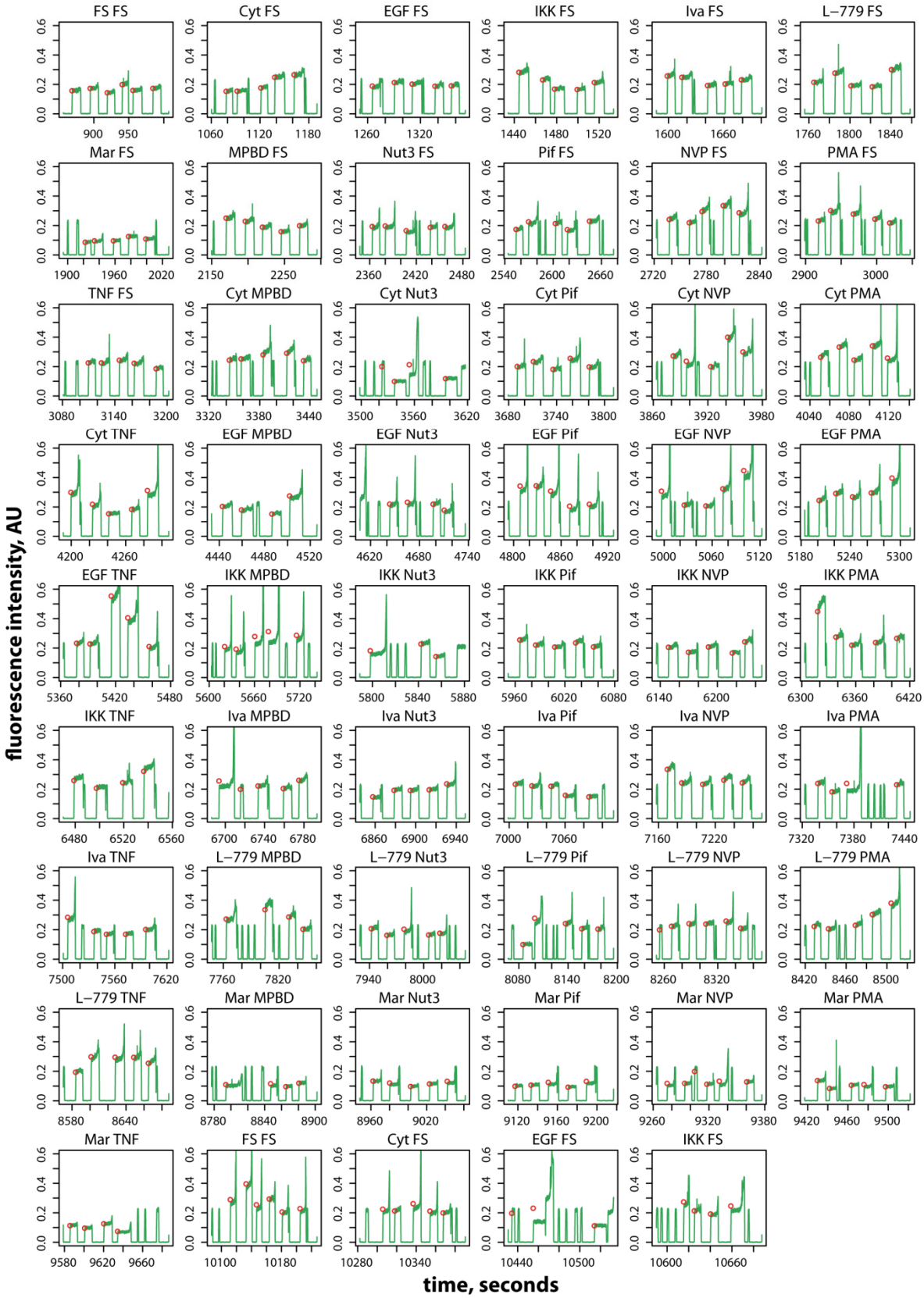

Figure 4.7 Individual plots for all detected drug combination samples in a six vs six drug screen. Each combination is indicated above every individual plot. Green lines show MMP FRET substrate fluorescence and red circles indicate individual detected plug signals. FS medium control samples were produced in six replicates, while all other samples were produced in five replicates.

The plots in **Figure 4.7** show all individual peaks of a measured sample sequence. Red circles indicate all detected sample peaks and their mean intensity values. Short peaks correspond to unfused substrate droplets and are excluded from analysis. By looking at the number of detected peaks one can detect samples, where plug fusion occurred, i.e. less peaks are detected and one or more of the peaks are wider than average (e.g. sample Mar MPBD). This representation of the data was therefore used to exclude certain samples from analysis, for instance sample EGF FS which shows only three detected peaks and very heterogeneous signals compared to most other samples (cf. the difference between the two EGF FS samples in **Figure 4.8**).

Some of the peaks showed a steep increase in fluorescence signal on one side. This can occur when the laser directly hits cells, which accumulate at the end of each plug. Not all cell clumps pass exactly through the center of the laser spot however, leading to significant differences between supposedly identical peaks. However, since we obtain several hundred data points per plug, we decided to only use the middle section of each peak in the data analysis, so that data points stemming from cell clumps are excluded.

In order to compare different samples and to eventually identify inhibitors or activators of MMP activity, we plotted all samples as boxplots (**Figure 4.8**). Markedly, all samples containing marimastat (orange box) showed low fluorescence and narrow variability. Most other samples however, showed quite large error bars overlapping with those of unperturbed samples. This made it difficult to identify possible effects elicited by the drugs and their combinations. However, this was not specific to our newly established method, as demonstrated in an experiment carried out in parallel in a 96-well microtiter plate (**Figure 4.9 B**). Here, sample variability amongst replicates is lower, but the overall trends are very similar (e.g. EGF mixtures). Most samples with the marked exception of marimastat (in orange) did not elicit a strong phenotype. Nutlin 3 – an activator of the p53 pathway – could be another exception, since it seems to negatively affect MMP activity in both approaches (indicated by arrowheads).

The marked difference between the two FS medium control samples measured here, indicated however, that the cell number per plug could vary and could therefore be responsible for the large variability within replicates of the same sample. On the other hand, we were not able to completely reproduce data obtained in a microtiter plate experiment. Also, in both, the plug and the plate reader experiments, very few samples (with the exception of marimastat) showed significant activation or inhibition of MMP activity. We therefore searched for more effective concentrations for our compounds.

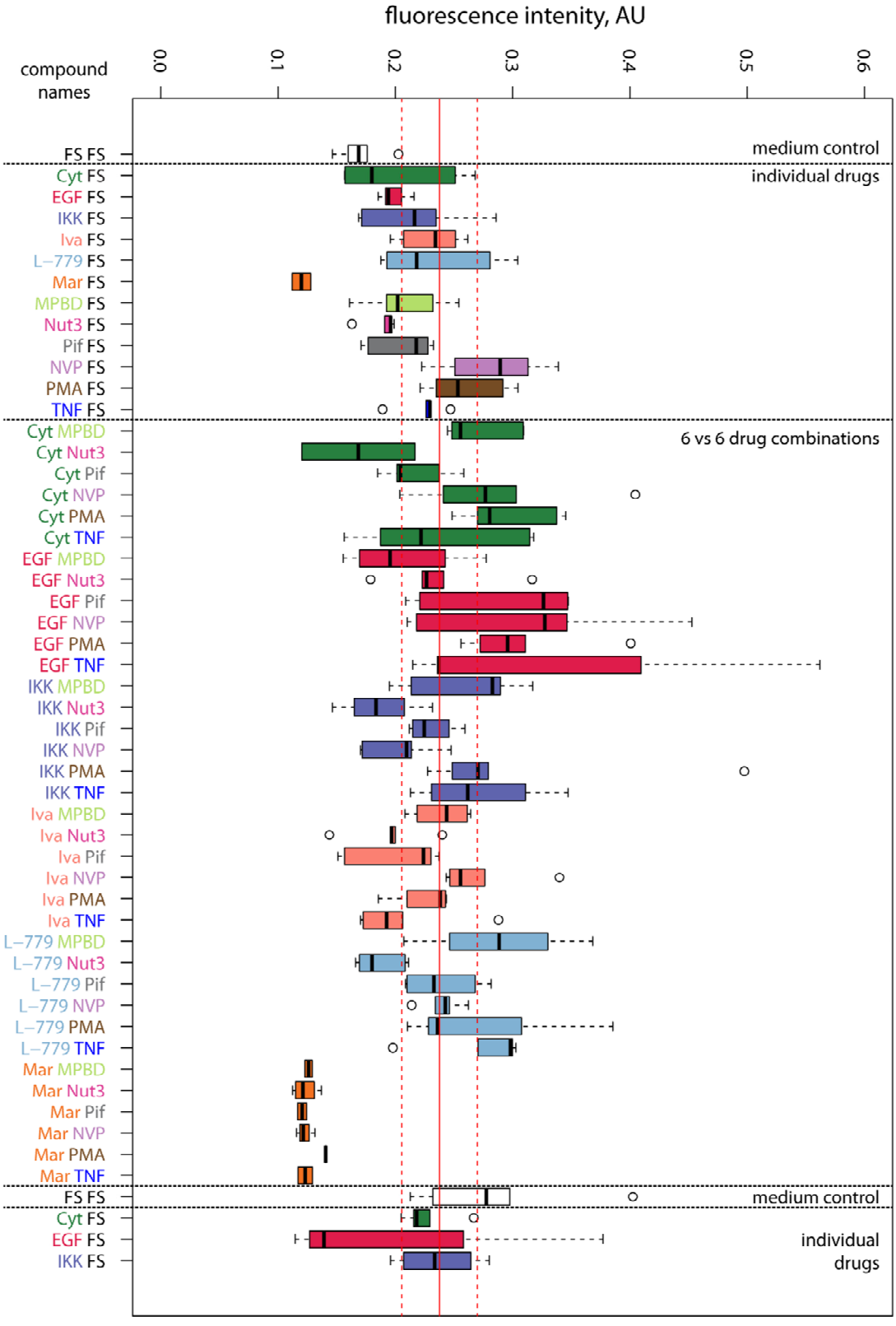

Figure 4.8 Fluorescence intensity distribution of each sample in a six vs six drug screen. Every boxplot in this graph represents the green fluorescence distribution of five individual plugs for each sample (six plugs for the medium control (FSFS) samples); open circles indicate outliers. The solid and dashed red lines indicate the mean fluorescence intensity and standard deviation of all cell-containing label plugs that were used as an unperturbed control. The colors indicate always the first component of every compound mixture.

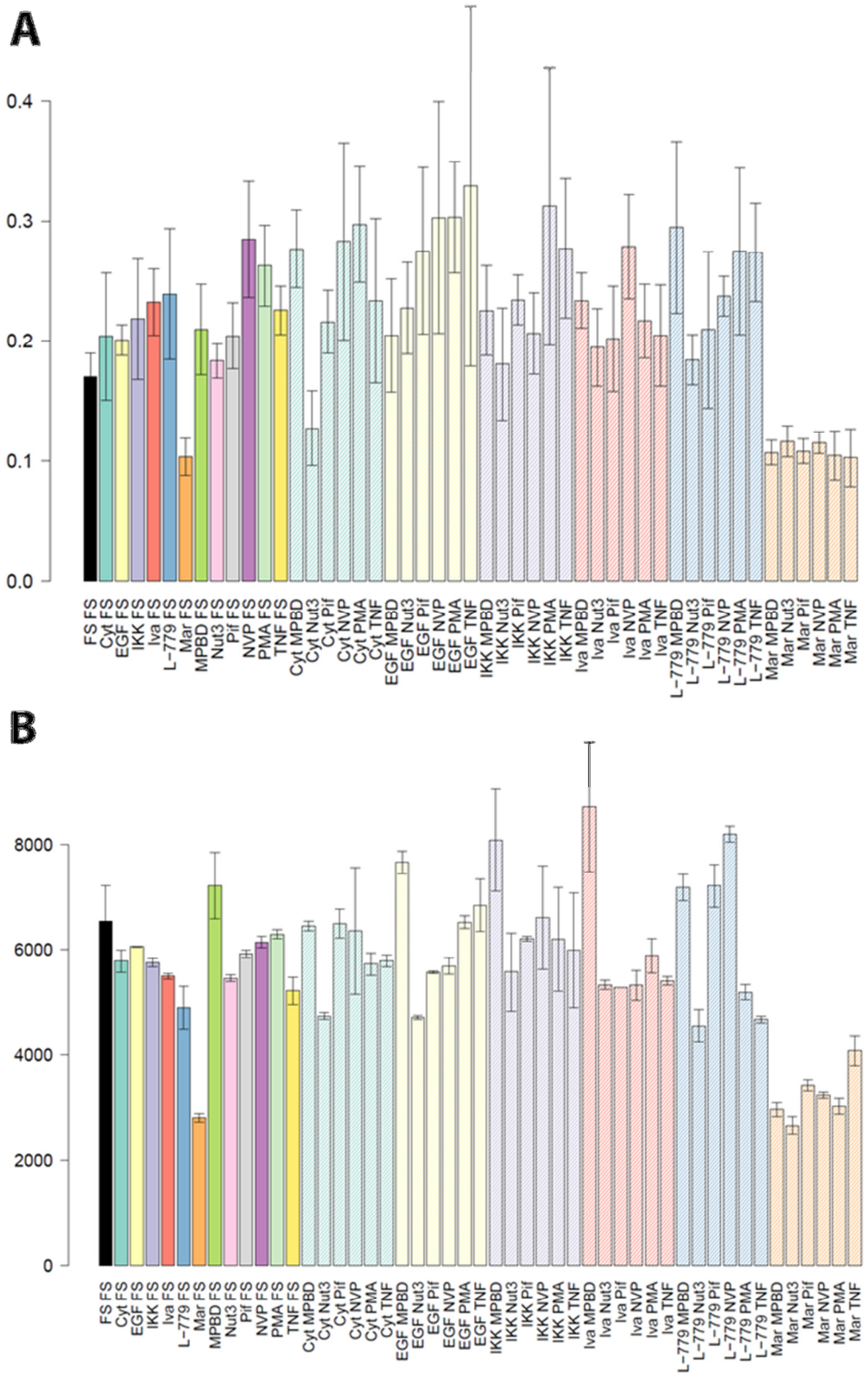

Figure 4.9 Comparison of microtiter plate reader data with data from plugs in a 6 vs 6 drug screen. HT1080 cells were exposed to twelve compounds (Cyt387, EGF, IKK-16, Ivachtin, L-779,450, marimastat, MPBD, Nutlin-3, Pifithrin-α, NVP-BSK805, PMA and TNF-α) and mixtures of the first six versus the last six compounds. The same experiment was carried out in plugs and measured by PMTs (**A**) and in a microtiter plate measured in a microtiter plate reader (**B**).

4.6.2 Evaluating the effective concentration for all drugs

Since no significant effect on MMP activity was observed in the plug screen, we conducted a small 96-well microtiter plate screen with the purpose of finding the appropriate working concentrations for all drugs. We wanted to identify drug concentrations, at which we could see an effect on MMP substrate conversion, while at the same time checking for any cytotoxic effects. To assess cytotoxicity we used the fluorescent cell viability dye alamarBlue®, whose fluorescence signal scales proportionally with the number of live cells (**Figure 4.10**). All 22 compounds listed in **Table 4.1** and **Table 4.2** with the addition of epidermal growth factor (EGF) and tumor necrosis factor alpha (TNF-α) were tested in this screen.

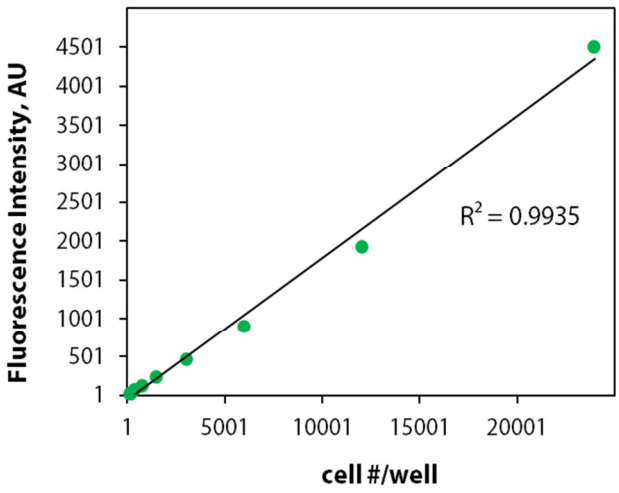

Figure 4.10 alamarBlue® fluorescence scales proportionally to cell number. HT1080 cells were seeded in triplicates at different densities (0; 49; 97; 195; 390; 781; 1,562; 3,125; 6,250; 12,500; 25,000 cells /well) and incubated for 4 h with alamarBlue®. Fluorescence was excited at 560 nm and measured at 590 nm in a microtiter plate reader. Individual measurements are depicted as green points, while the black line represents a linear fit of the data.

Compounds were prepared in 2-fold serial dilutions including and significantly exceeding the spectrum of values for working concentrations found in literature (**Table 4.1/Table 4.2**). Additionally, wells containing no compound (DMSO control) and with 10% DMSO (kills all cells) were included to act as positive and negative controls respectively for both cell viability and MMP activity. All samples were prepared in triplicate and HT1080 cells were seeded in two different densities (5,000 & 10,000 cells/well), which resulted in a total of 18 96-well microtiter plates. Cells were left to attach for 24 h before compounds were added with the help of a liquid handling robot and were incubated for 48 hours at 37 °C and 5% CO_2. MMP FRET substrate and alamarBlue® were pre-mixed and added to each well and incubated for 90 minutes before measuring fluorescence at 520 nm and 590 nm in a microtiter plate reader.

Figure 4.11 depicts MMP FRET substrate conversion and cell viability data for all compounds at all concentrations after 90 min of incubation with both substrates. Both, the MMP enzymatic activity and cell viability, were normalized by using the normalized percent inhibition (NPI) method (Malo et al., 2006). Instead of the means of the positive and negative controls we used the median values to account for variability in the controls, since the median is less sensitive to extreme outliers in the data. Strong outliers could be attributed to pipetting errors (empty wells) or bacterial contamination (as confirmed by microscopy) leading to strong negative or positive outliers in fluorescence intensity respectively. Consistent with measurements in the six vs six screen in plugs, not many significant differences could be observed for any of the different drug concentrations. Most compounds elicited similar responses for both cell densities (plot for 5,000 cells in the Appendix). Two of three p53 effectors (pifithrin α and nutlin-3) showed significant positive cell proliferative effects, which make it hard to judge their effect on MMPs. PMA, which is used in many studies to promote MMP expression, indeed showed higher MMP activity at both cell densities and was included in further experiments at a concentration of 80 nM. Not surprisingly, marimastat could also be confirmed as a useful negative control.

Tunicamycin showed some increase in MMP activity, but also effectively killed cells. However, this could be interpreted as higher MMP activity or expression before cytotoxic effects took over. Similar things can be said about Simvastatin (a reported inhibitor of MMP-9), which showed increased cytotoxicity with decreasing MMP activity. Others, like ACHP and Roscovitine showed quite different phenotypes for the two cell densities and large differences within one cell density, again making it hard to draw any meaningful conclusions. EGF showed some positive effects on MMP activity. Thus, in order to identify more model compounds with measureable effects on MMP activity, we decided to test additional growth factors and cytokines. With this class of compounds, cytotoxic effects were considered to be less likely, since they are produced naturally in the body and actually represent the physiological signals used to modulate the activity of many MMPs (Yan and Boyd, 2007). For these reasons, we expected stronger phenotypes in screens conducted with growth factors and cytokines. The following sections will describe these experiments in detail.

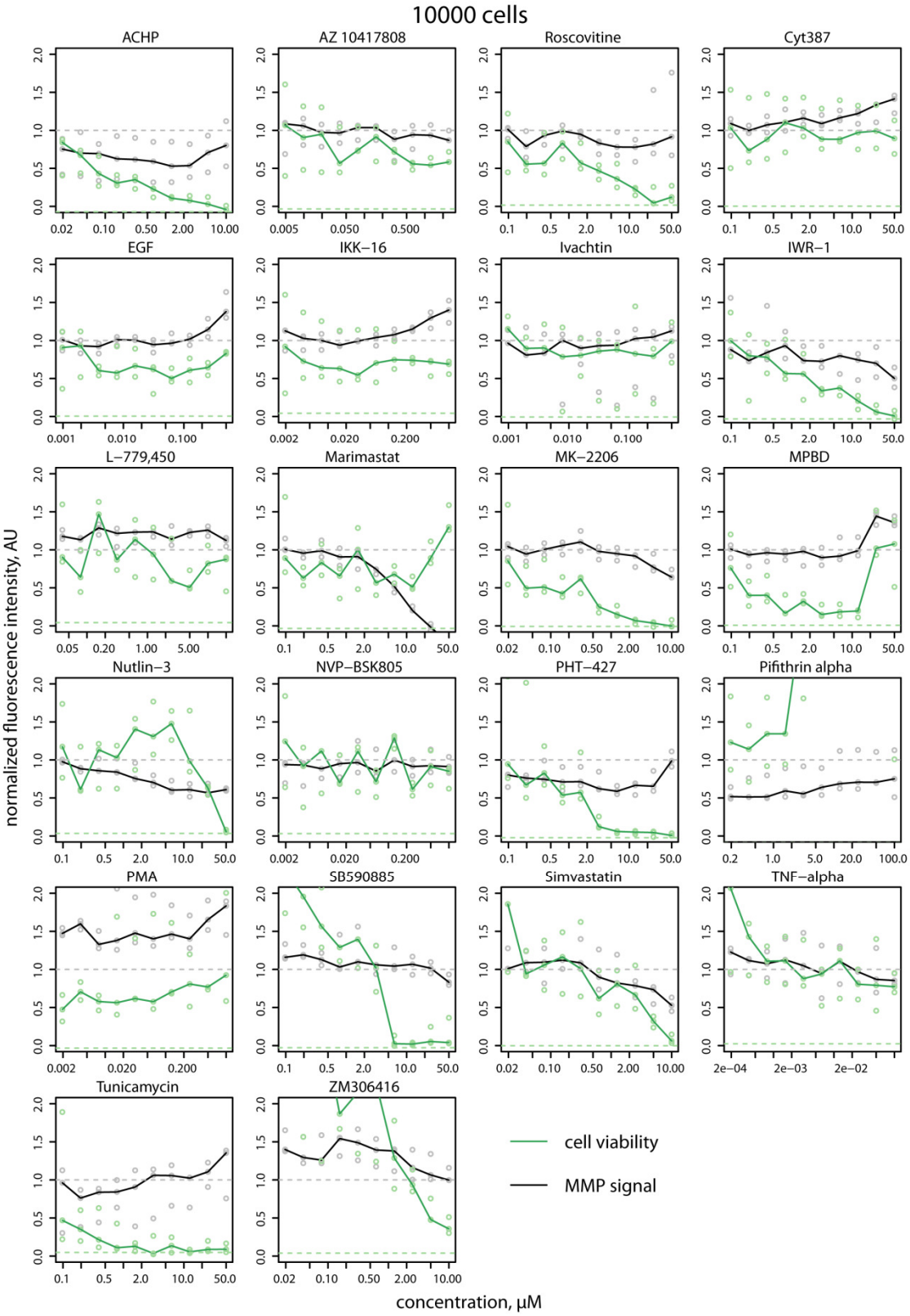

Figure 4.11 Cell viability and MMP activity at different drug concentrations. 10,000 HT1080 cells/well were incubated in 96-well microtiter plates together with different concentrations of MMP effectors for 48 hours. Cell viability was measured via the conversion of alamarBlue® as measured at 590 nm in a microtiter plate reader after 90 min of incubation (⊖). MMP activity was monitored via the conversion of 520 MMP FRET substrate XIV as measured at 520 nm (⊖). Dashed lines indicate the MMP activity of unperturbed cells (gray) and the alamarBlue® signal detected for cells grown in a lethal 10% DMSO solution (green).

4.6.3 Growth factors & cytokines as effectors of MMP activity

Many growth factors and cytokines have been described to have synergistic effects on MMP expression and/or activity (cf. reference list below). More specifically, MMP-9 is known to be regulated by growth factors and cytokines through the AP-1 element in the promoter region, which it shares with many MMPs but not MMP-2. Therefore, we expected to get more specific effects on MMP-9 activity compared to the drugs described in the previous section (Nagase et al., 2006; Van den Steen et al., 2002; Vandooren et al., 2013; Yan and Boyd, 2007). Some findings indicate that MMPs are also directly involved in the enzymatic release of growth factors residing in the extracellular matrix, opening the possibility for potential feedback loops in the activation of MMPs (Mott and Werb, 2004). **Table 4.3** lists the results of a literature search for growth factors and cytokines reported to elicit individual or combinatorial effects on MMP expression and/or activity in different cellular systems, as well as their targets and effects:

Table 4.3 Growth factors and cytokines. Reported individual and combinatorial effects

Name	MMP	Function	Reference
EGF	MMP-9	Activator/Inhibitor?	(Uttamsingh et al., 2008; Vandooren et al., 2013)
Bradykinin (BK) & TNF-α	MMP-3	Synergistic increase (in 18co cells)	(Yoo et al., 2011)
EGF & TGF-β1	MMP-1/-3/-9/-10 mRNA levels	Synergistic increase (RIE cells)	(Uttamsingh et al., 2008)
IFN- β	MMP-9	Inhibition (T cells)	(Stuve et al., 1996)
IFN-γ & IL-1 β	MMP-9	Synergistic increase (in CoMTB)	(Harris et al., 2007)
IGF-1	multiple MMPs	Activity increase (MCF-7 cells)	(Walsh and Damjanovski, 2011)
IL-10	MMP-9	Expression inhibition (cytotrophoblasts)	(Roth and Fisher, 1999)
IL-17	MMP-1	Expression increase (HCF cells)	(Cortez et al., 2007)
IL-1α & TNF- α	MMP-13	Synergistic increase with PMA (in SW 1353 cells)	(Shi et al., 2004)
IL-1β & angiotensin II	MMP-9	Increase (synergy?; in rat cardiac fibroblasts)	(Okada et al., 2010)
IL-8	MMP-2/-9	Expression increase (HMEC/HUVEC cells)	(Li et al., 2003)
TNF-α	MMP-2/MMP-9	Activator	(Han et al., 2001; Vandooren et al., 2013)

4.6.4 Full combinatorial screen of twelve compounds

We performed a full combinatorial of the effects of twelve compounds (marimastat (Mar), IGF-1, EGF, TNF-α, bradykinin (BK), TGF-β, IFN-β, IFN-γ, IL-1 α, IL-1β, PMA, IL-10) on HT1080 cells (**Table 4.3**). We included the combinations found in literature as controls, but added further compounds in order to identify interactions previously not described. We produced 79 individual sample combinations (medium control + twelve individual compounds + 66 combinations of two each, cf. **Figure 1.6**). Every sample combination was set up in five replicates and label plugs (FS medium + Cascade® blue + cells) were used to separate one sample from the next (three or six label plugs each). In other words, a pairwise combinatorial screen consisting of 686 plugs/cycle was performed. The plugs were produced on the 16-inlet Braille chip connected to a 5 m polytetrafluoroethylene (PTFE) tubing wrapped around a bottle for stability (**Figure 3.2 A**). Aqueous samples were each injected for 1.5 s at 1000 μL/h and with a 4 s interval between each plug, while the carrier oil FC-40 + 0.5% PFO was injected continuously at 200 μL/h. Individual plugs were further separated from each other by additional infusion of mineral oil at the sample outlet at 100 μL/h. To evaluate the reproducibility of our approach, we continued producing combinations after one cycle was completed. The tubing was long enough to accommodate 1.5 cycles or over 1000 individual plugs. Sample plugs stored in tubing were incubated at 37 °C and 5% CO_2 for 42 h.

In order to measure MMP activity in each sample, fluorogenic substrate was added to each plug by fusing substrate droplets with incoming plugs on our newly developed fusion device (cf. section **3.3**). To assess how much substrate was added into each plug, we added a red fluorescent dye (Alexa Fluor® 596) into the substrate solution. We visually inspected the sample plugs during the fusion process using a light microscope and noticed a fungal contamination of the sample plugs. This might have led to unwanted effects on the growth of cells and MMP activity within the plugs, due to competition for nutrients and potential cytotoxic effects from compounds of fungal origin. Nevertheless, we proceeded with the experiment and used the measurements as a test set for our newly developed data analysis package.

After their fusion with assay substrates, sample plugs were collected once more in tubing for 1 h of incubation with assay reagents. After this additional incubation, green, blue and orange plug fluorescence was measured simultaneously with PMTs. An overview of all fluorescence signals recorded during the whole experiment is shown in **Figure 10.2** in the appendix. Each measured peak corresponds to a sample plug or unfused substrate droplets, which can be distinguished by their length (= number of recorded data points). Label plugs were identified by their blue fluorescent signal and were used to segregate the data into individual samples (**Figure 10.3** in

the appendix). Since all plugs were measured in the sequence they were produced in, sample identity could be determined by identifying the first sample and then following the list of inputs used in the sample generation. As an internal control to preclude any missing samples or a frame shift, we used the easily identifiable inhibitor (marimastat) samples.

All samples are depicted in **Figure 10.4** in the appendix. To evaluate the quality of our data, we plotted each sample as a boxplot (**Figure 4.12**). Every cycle starts with a medium control sample (FS1FS2, green), which indicates the unperturbed state. We included marimastat as a positive control, since it can be easily distinguished from the other samples. In order to have a measure for the variability of the data, we further plotted the mean green fluorescence signal detected for the label plugs (blue line) and its standard deviation (blue shaded area). Because the label plugs also contain cells, but no drugs, they serve as an additional unperturbed control throughout the course of the experiment. Consequently, only a sample outside the blue shaded area can be considered a hit. Below the boxplots, we depict the mean orange fluorescence signal for every plug (red line) and its standard deviation (orange area). This control indicates how much substrate was added to each plug during the fusion. We have developed a new approach to analyze data from full combinatorial screens measured in plugs, which allows us to easily monitor sample variance throughout the experiment. It allows the identification of samples with significant changes in MMP activity and will therefore be a very useful tool in future plug screening endeavors.

As mentioned above, the data set presented here was based on contaminated samples and therefore, any conclusions drawn from the data analysis will not be valid. Notwithstanding, the experiment presented here allowed us to draw conclusions about the possible throughput of our newly established system and make estimates about the reproducibility of the sample using this method, which is discussed in detail in the following section and the **General discussion** section.

Figure 4.12 Fluorescence intensity distribution of each sample in a six vs six drug screen. Every boxplot in this graph represents the green fluorescence distribution generated by MMP FRET substrate conversion by HT1080 cells in five individual plugs for each sample (six plugs for the FS1FS2 medium control samples; indicated in green). Cycle 1 contained 79 individual sample compositions and 79 Cascade® blue labels to encode the sequence in a total of 686 plugs. Cycle 2 reproduced the first half of cycle 1. The red line represents mean orange Alexa Fluor® 596 fluorescence and the orange shaded are its standard deviation. It indicates the amount of substrate added to each sample. The blue line and shaded area represents the green fluorescence generated by MMP FRET substrate conversion in all label plugs, which also contained cells as an internal control.

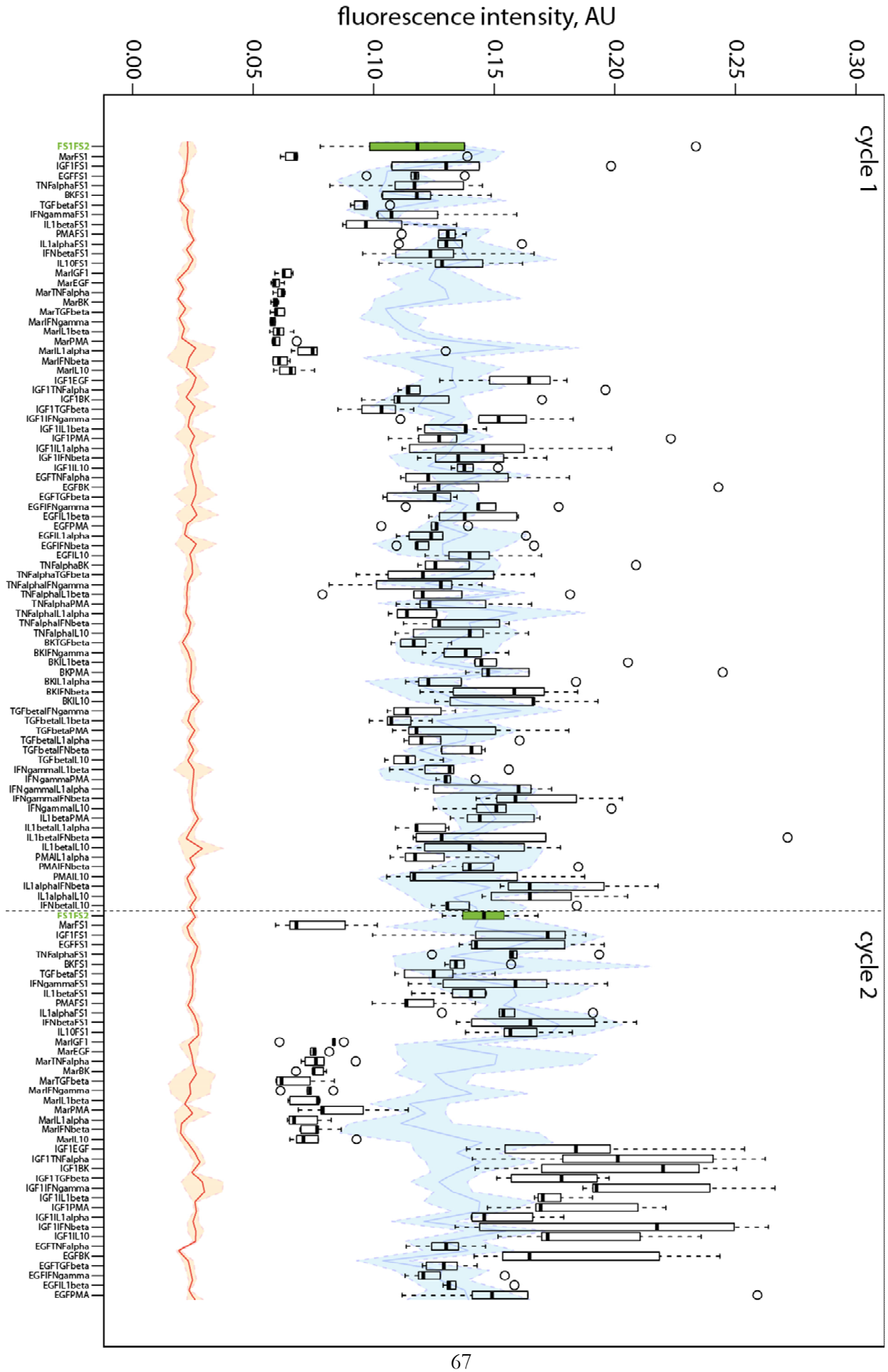
fluorescence intensity, AU
0.00
0.05
0.10
0.15
0.20
0.25
0.30
cycle 1
cycle 2
FS1FS2
MarFS1
IGF1FS1
EGFFS1
TNFalphaFS1
BKFS1
TGFbetaFS1
IFNgammaFS1
IL1betaFS1
PMAFS1
IL1alphaFS1
IFNbetaFS1
IL10FS1
MarIGF1
MarEGF
MarTNFalpha
MarBK
MarTGFbeta
MarIFNgamma
MarIL1beta
MarPMA
MarIL1alpha
MarIFNbeta
MarIL10
IGF1EGF
IGF1TNFalpha
IGF1BK
IGF1TGFbeta
IGF1IFNgamma
IGF1IL1beta
IGF1PMA
IGF1IL1alpha
IGF1IFNbeta
IGF1IL10
EGFTNFalpha
EGFBK
EGFTGFbeta
EGFIFNgamma
EGFIL1beta
EGFPMA
EGFIL1alpha
EGFIFNbeta
EGFIL10
TNFalphaBK
TNFalphaTGFbeta
TNFalphaIFNgamma
TNFalphaIL1beta
TNFalphaPMA
TNFalphaIL1alpha
TNFalphaIFNbeta
TNFalphaIL10
BKTGFbeta
BKIFNgamma
BKIL1beta
BKPMA
BKIL1alpha
BKIFNbeta
BKIL10
TGFbetaIFNgamma
TGFbetaIL1beta
TGFbetaPMA
TGFbetaIL1alpha
TGFbetaIFNbeta
TGFbetaIL10
IFNgammaIL1beta
IFNgammaPMA
IFNgammaIL1alpha
IFNgammaIFNbeta
IFNgammaIL10
IL1betaPMA
IL1betaIL1alpha
IL1betaIFNbeta
IL1betaIL10
PMAIL1alpha
PMAIFNbeta
PMAIL10
IL1alphaIFNbeta
IL1alphaIL10
IFNbetaIL10
FS1FS2
MarFS1
IGF1FS1
EGFFS1
TNFalphaFS1
BKFS1
TGFbetaFS1
IFNgammaFS1
IL1betaFS1
PMAFS1
IL1alphaFS1
IFNbetaFS1
IL10FS1
MarIGF1
MarEGF
MarTNFalpha
MarBK
MarTGFbeta
MarIFNgamma
MarIL1beta
MarPMA
MarIL1alpha
MarIFNbeta
MarIL10
IGF1EGF
IGF1TNFalpha
IGF1BK
IGF1TGFbeta
IGF1IFNgamma
IGF1IL1beta
IGF1PMA
IGF1IL1alpha
IGF1IFNbeta
IGF1IL10
EGFTNFalpha
EGFBK
EGFTGFbeta
EGFIFNgamma
EGFIL1beta
EGFPMA

4.7 Discussion

The HT1080 model system for MMP expression was used as a first application for our new combinatorial screening platform. We could successfully encapsulate HT1080 cells together with a broad band MMP FRET substrate to measure MMP activity within plugs (**Figure 4.2**), recapitulating data measured in a microtiter plate (**Figure 4.1**). The addition of marimastat, a broad spectrum inhibitor of MMPs, resulted in inhibition of MMP activity in those plugs compared to plugs containing only culture medium. Marimastat was therefore used as a positive control in consecutive experiments (**Figure 4.4**, **Figure 4.8** & **Figure 4.12**). For screens using drugs or growth factors and cytokines as effectors of MMP activity, we produced trains of hundreds to thousands of sample plugs that could be individually measured, identified and analyzed (**Figure 4.8** & **Figure 4.12**). However, we were unable to identify reproducible compound combinations with synergistic or antagonistic effects on MMP activity. Two possible reasons for the inconclusive outcome of both these screens are 1) the variability in the number of cells encapsulated into individual plugs and 2) the sensitivity and specificity of the MMP activity assay.

One of the technical challenges of encapsulating mammalian cells into droplets is to control the number of cells present in each plug. An ostensibly easy way to approach this problem would be to include the reagents of a quantitative cell viability assay within each plug. Equal fluorescence intensity values for all plugs in a sequence would mean that the same number of cells was present in each plug. Even if the measured fluorescence intensity should vary greatly, the signal could still be used to normalize MMP activity levels to cell number. Such assays, e.g. commercially available alamarBlue® or calcein blue AM, are based on the conversion of a non-fluorescent substrate into a highly fluorescent compound by live cells (**Figure 4.10**). However, the same chemical properties that allow these compounds to enter cells probably also allow them to exchange between consecutive plugs by crossing the water/oil interface. For instance, the reactive component of alamarBlue® is resazurin, which is converted into strongly fluorescent resorufin. Resorufin has been shown to quickly exchange between droplets through the carrier phase and thus cannot be used as a reliable cell number indicator in our plugs (Skhiri et al., 2012). The fluorescent component of the Calcein blue AM cell viability assay is coumarin, which is also known to show this type of exchange behavior in droplets (Woronoff et al., 2011).

Consequently, to ensure stable numbers of cells per plug, one has to rely on indirect controls. One way to achieve this is the production of control samples with identical composition at defined intervals within the train of sample plugs or by including cells in the barcode plugs in between each sample (**Figure 4.12**). If the fluorescence levels in these plugs are constant over the

course of an experiment, it means that the same is true for the amount of cells, when assuming a linear relationship between MMP substrate conversion and cell number. By using this approach, we could calculate the variability of the medium control in the experiment presented in section **4.6.4** to be 16% as given by the coefficient of variation. This variability could be further reduced by improving the stirring of cells within the syringe used to infuse the cell suspension or using a higher cell density to start with. Furthermore, longer incubation times after substrate fusion might improve the signal-to-noise ratio.

Beyond the reproducibility of the number of cells encapsulated into individual samples, we hypothesize that the unspecific conversion of the MMP FRET substrate by many MMPs was a major cause of the insensitivity of our assay to different compound mixtures. This was true for drugs, which act as specific inhibitors of cellular signaling pathways (**Figure 4.8**) as well as mixtures of growth factors and cytokines (**Figure 4.12**). Since HT1080 cells were reported to secrete MMP-9 at high levels and MMP-9 expression is known to be controlled in part by growth factors and cytokines, we expected significant changes in measured MMP activity when exposing cells to combinations of purified growth factors and cytokines (Gervasi et al., 1996; Moll et al., 1990). However, we were not able to observe such an effect and attribute this to the presence of multiple members of the MMP protein family (cf. **General Discussion**, (Giambernardi et al., 1998)). Indeed, some MMPs are known to regulate other MMP family members, which might lead to very complex readouts that are not easily disentangled, especially when measuring overall MMP activity (Kessenbrock et al., 2010). Thus, a readout of the enzymatic activity of individual MMP family members would be required. Yet, specific substrates for individual MMPs have not been reported for the same reason that no specific inhibitors exist and accordingly further chemical genetic studies will have to rely on alternative readouts, such as measurements of specific MMP expression. This could be achieved via a *lacZ* gene reporter construct, in which β-galactosidase is expressed under the control of specific MMP promoter sequences similar to a luciferase-based system described by Yan et al. and which is outlined in the **General Discussion** section (Yan et al., 2004). Such an assay would allow us to disentangle the contributions of individual MMPs to the overall MMP activity observed in a given sample.

5 SEMI-COMPARTMENTALIZATION

5.1 Introduction

The previous chapters describe a new microfluidic method that allows the reliable generation of high chemical diversity in aqueous droplets containing cells (cf. section **3.2.3.1**). Moreover, a new fusion module allows the addition of assay components to already existing trains of plugs after incubation, thereby further increasing the range of assays that can be carried out (cf. section **3.3**). Nevertheless, conducting cell-based assays in aqueous microcompartments has a number of limitations that considerably limit the variety of biological assays, that can be performed on these cells. For one, cells can be cultured in plugs for only a few days before they run out of nutrients and cytotoxic compounds produced by the cells accumulate (cf. section **1.3.3**, (Clausell-Tormos et al., 2008)). Next, imaging of individual cells within droplets, e.g. to determine intracellular protein localization via fluorescence microscopy, is not feasible because cells continuously float out of the focal plane within the plugs. Lastly, the lack of direct access to cells makes it impossible to remove a specific compound from existing droplets, which can be easily done in conventional tissue culture approaches by simply replacing the culture medium and thereby washing the cells. Such washing steps are required in many immunofluorescence approaches, where superfluous antibodies have to be removed from the medium.

To overcome these limitations, we developed a new microfluidic setup, which exploits the permeability of polydimethylsiloxane (PDMS) to some small molecules and thereby grants access to the contents of plugs in microfluidic channels (cf. section **5.1.1**). In a previous study, Shim et al. showed that a bacterial auto-inducer could be delivered from a reservoir across a membrane to bacteria encapsulated in droplets and thereby activate quorum sensing (Shim et al., 2011). Here, we use the inverse approach to deliver small molecules from trains of plugs produced with our Braille chip to cells cultured across a thin PDMS membrane, thereby combining the advantages of droplet-based microfluidics with full access to cells for washing, imaging and standard cell culturing techniques.

5.1.1 Diffusion of compounds through PDMS

At the nanoscale, PDMS represents a porous meshwork of fibers, through which gasses and to a much smaller extent liquids can permeate while still being completely transparent. These properties make PDMS the material of choice for many microfluidic devices used in biological applications, where good gas permeability is a requirement for cell culture. Two studies first described the phenomenon of analyte diffusion into PDMS by observing rhodamine B and Nile red absorption into the channel walls of a microfluidic channel (**Figure 5.1 a-c** (Roman et al., 2005; Toepke and Beebe, 2006)). In a follow-up study they could show that this was also true for

biologically active compounds, e.g. estrogen (Regehr et al., 2009). Estrogen is hydrophobic and was shown to be absorbed into PDMS as well as released from PDMS without loss of activity on cells.

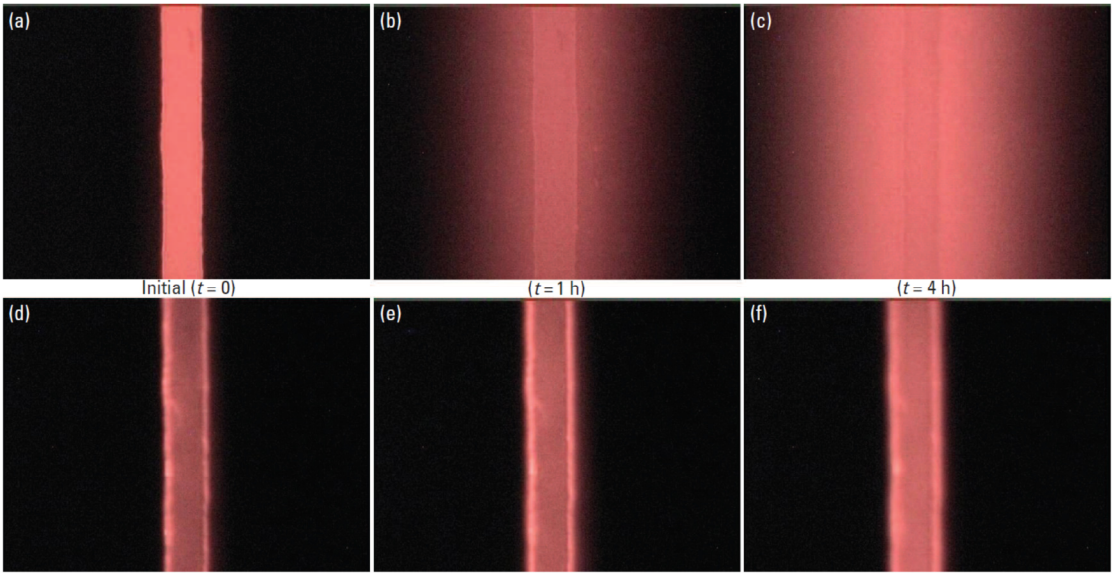

Figure 5.1 Diffusion of Rhodamine B into PDMS. (a-c) Rhodamine B is absorbed into the walls of an untreated PDMS channel. **(d-f)** The same setup when the PDMS channel was treated with a sol-gel (PDMS-SiO_2) Reproduced with permission from (Mukhopadhyay, 2007) © American Chemical Society

In a quantitative analysis of molecular absorption into PDMS, Wang et al. found that the log*P* of a given molecule directly predicts its absorption propensity into PDMS (Wang et al., 2012b). The log*P* of any soluble molecule is its partition ratio between octanol and water, i.e. the lipophilicity of a compound, given by:

$$\log P_{\frac{oct}{dH_2O}} = \log\left(\frac{[solute]_{octanol}}{[solute]_{dH_2O}}\right) \qquad \textbf{Eq. 6}$$

They found that molecules with log*P* values lower than 2.47 show less than 10% absorption into PDMS, while at log*P* values higher than 2.62 more than 90% absorption occurs. Evidently, such absorption during cell culture might interfere strongly with biological assays.

A few studies were therefore performed with the goal of preventing this phenomenon, mostly by caulking the PDMS material with hydrophobic compounds such as parylene C or metal alkoxides (**Figure 5.1 d-f** (Lei et al., 2011; Roman and Culbertson, 2006; Roman et al., 2005)). This successfully prevented diffusion of various compounds into the PDMS of the channel walls. Others however, showed that the permeability of PDMS could be used to transport molecules from a reservoir into droplets within a PDMS microfluidic device (Shim et al., 2011). In this way,

the authors controlled the solubility and crystallization of proteins in droplets and activated quorum sensing in bacterial cells grown in droplets by delivering different amounts of auto inducer.

5.2 Results

5.2.1 Chip design

In this chapter, I describe a new microfluidic approach, which brings cells into close proximity to plugs containing small diffusible compounds such as drugs, without actually encapsulating the cells into the plugs themselves. Since the compounds in the plugs are not fully compartmentalized, we termed the new method "semi-compartmentalization". Rather, the compounds diffuse so that significant concentrations are reached in limited areas around their origin, i.e. the plug. Cells are separated from the plugs by a thin (100-150 μm) layer of PDMS through which the drugs can diffuse and reach the cells. This separation can be achieved in two ways:

1) **Separation in parallel channels (Figure 5.2 A & C):** For the first approach, we designed a microfluidic chip consisting of three microfluidic channels, which run in parallel and are separated from each other by a thin wall of PDMS. The widest channel is the plug channel. Plugs produced on an autosampler and containing assay reagents are loaded via a sideways connection port. Neighboring the plug channel is the cell channel, in which cells can be incubated. The cell channel is separated from the plug channel by a wall of PDMS with a thickness of 100 μm. A PDMS wall of equal thickness separates the cell channel from a third channel through which fresh culture medium can be continuously infused into the chip to feed the cells via diffusion of nutrients through the channel wall. This can be done without creating flow in the cell channel, thus avoiding shear stress on the cells. Since no connections exist between the three channels, they can be individually accessed.
2) **Separation by a thin PDMS membrane (Figure 5.2 B & D):** In the second layout we designed, cells are separated from the plugs through a thin PDMS membrane. This simplified version of the semi-compartmentalization chip consists merely of one long serpentine channel for plug loading and incubation. Cells are seeded onto the membrane from the outside. This setup allows full access to the cells throughout the incubation period just like culturing them in a standard tissue culture dish.

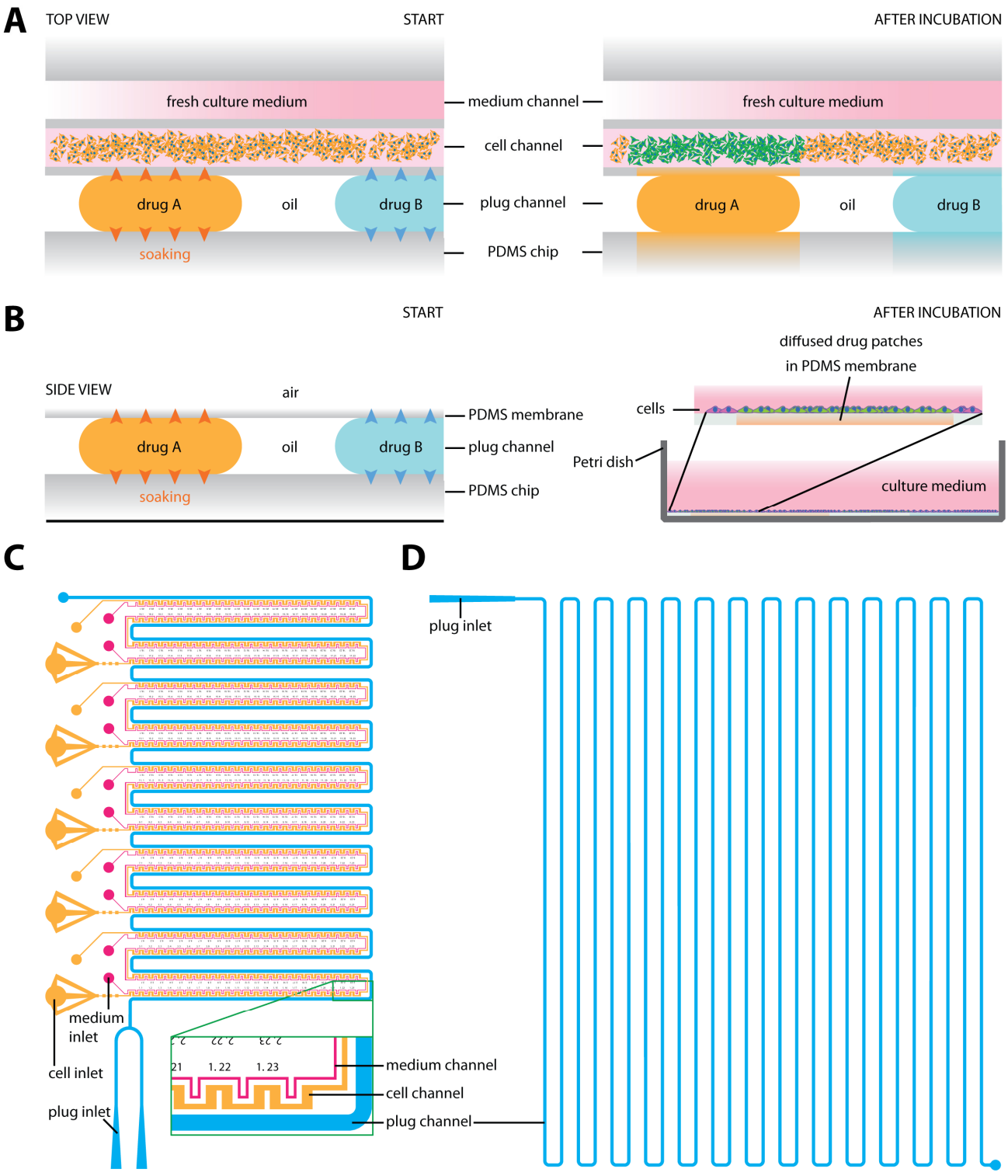

Figure 5.2 Semi-compartmentalization. Drugs can be delivered from pre-formed plugs through PDMS to cells in culture in two ways: from a plug channel to a parallel neighboring cell channel (**A**) or to cells seeded on a thin PDMS membrane comprising the roof of the plug channel (**B**). The designs of both semi-compartmentalization chip variants: parallel setup (**C**) and membrane setup (**D**). The channel depth in both devices is 200 µm.

5.2.2 Fluorescent dyes can be used to study the diffusion of small molecules into PDMS

In order to characterize the extent of diffusion of small molecules through PDMS, we conducted experiments with different fluorescent dyes, since their diffusion patterns can be easily recorded by fluorescent microscopy. Besides the differences in their spectral properties, the dyes also have differences in their physicochemical properties, in particular their log*P* values (partition coefficient between octanol and water, cf. section **5.1.1**). We chose the two fluorescent dyes, fluorescein (log*P* = -0.67) and Nile red (log*P* = 5), as proxies for hydrophilic and hydrophobic drug molecules respectively to conduct our own absorption/diffusion studies.

5.2.2.1 Plasma treatment affects the absorption of molecules into PDMS

Most drugs have log*P* values somewhere in between those of fluorescein and Nile red. The average log*P* value for newly discovered chemical drug entities was determined by Lipinski et al. to be 1.80 (Lipinski et al., 2012), while other studies determined it to be somewhere close to 2.5 for synthetic oral drugs (Proudfoot, 2005) or 3.1-3.4 in industry collections (Macarron et al., 2011). Since fluorescein barely showed any absorption by PDMS and Nile red showed exactly opposite behavior, we set out to find conditions that would increase the fluorescein absorption and decrease that of Nile red. PDMS constitutes a very hydrophobic environment (Bodas and Khan-Malek, 2006) and therefore, we hypothesized that by making the PDMS more hydrophilic, we could achieve our goal.

PDMS can be treated with oxygen plasma to make it more hydrophilic (Bodas and Khan-Malek, 2006). We created a simple setup to test what effect this treatment would have on the diffusion of fluorescent dyes through PDMS (**Figure 5.3 A**). We punched holes of different diameters into a chunk of PDMS to create wells. The central well with a diameter of 5 mm acted as a source and three wells with 4 mm diameters were arranged around the source at a distance of 1 mm and acted as sinks for the fluorescent dyes. This setup was used to test the diffusion of fluorescein (10 μM), Nile red (150 μM) and sulforhodamine B (150 μM) from the central well through PDMS to the sink wells filled with dH_2O. One set of wells was pre-treated in oxygen plasma for 3 hours at full power (100 W), while the other was not treated. Both were then soaked in PBS at 65 °C overnight.

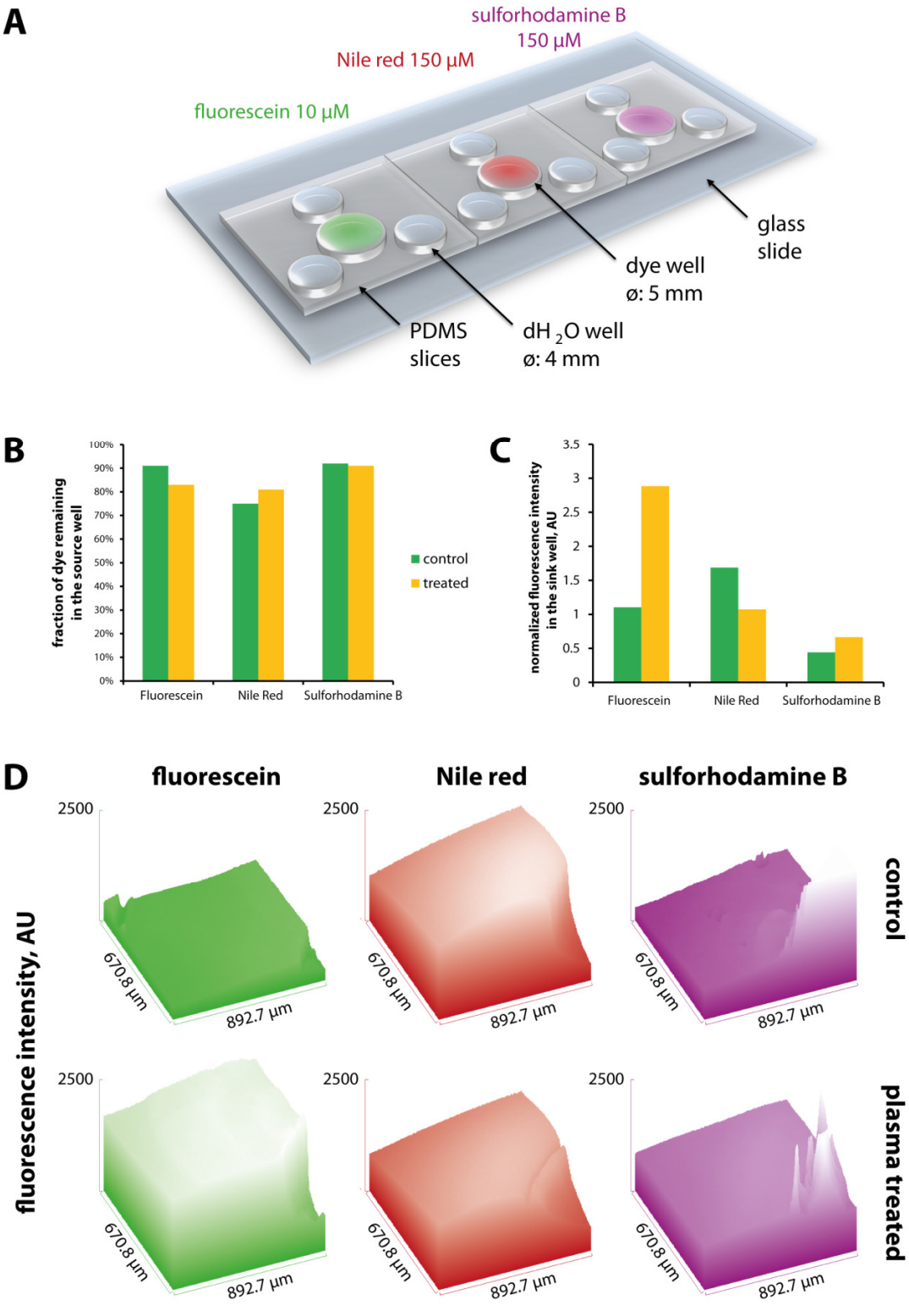

Figure 5.3 The diffusibility of compounds through PDMS can be altered by oxygen plasma treatment. A) Schematic representation of the experimental setup. Fluorescein (10 µM), Nile red (150 µM) and sulforhodamine B (150 µM) were incubated in the central well in an untreated setup and an oxygen plasma treated setup. **B)** Plate reader measurement of remaining fluorescence in the central well after incubation. **C)** Plate reader measurements of fluorescence observed in the outer sink wells after incubation. **D)** Surface plots of micrographs taken of the source well walls facing the sink wells after incubation.

The central wells were then filled with one of the three fluorescent dyes and incubated overnight. We measured the fluorescence of the central well compared to that of the original fluorescent dye solutions to determine the fraction of fluorescent dye left over in both conditions (**Figure 5.3 B**). Indeed, the left over fluorescein concentration was lower in the plasma treated condition, while the Nile red concentration decreased less and the sulforhodamine B concentration did not change much between the two conditions tested. We also measured the fluorescence of all sink wells. As expected, we observed the reverse behavior here, i.e. an increase in fluorescein fluorescence, a slight increase in the sulforhodamine fluorescence and a marked decrease in total Nile red fluorescence (**Figure 5.3 C**).

Figure 5.3 D shows a different representation of the data. Microscopic images were taken at the edges of all source wells facing the sink wells to observe the diffused dyes directly. The figure shows surface plot (Image J function) representations of the images. The top row shows the untreated control samples while the lower row shows plasma treated samples. Again, we show that more hydrophilic PDMS material facilitates fluorescein diffusion and at the same time lowers the mobility of hydrophobic Nile red. We therefore conclude that plasma treatment of microfluidic chips allows a certain degree of control over the diffusibility of compounds through PDMS.

5.2.2.2 Diffusion of Nile red from water-in-oil plugs into PDMS

In order to test if compounds diffuse out of plugs and into the PDMS channel wall, we produced Nile red plugs and loaded them onto the parallel setup semi-compartmentalization chip (**Figure 5.4 A**). The plugs were incubated on-chip over the course of 14 hours. During this time, the Nile red dye contained in the plugs diffused into the surrounding PDMS. **Figure 5.4 B** shows the extent to which Nile red diffused from the plugs. This showed that compounds can indeed diffuse out of plugs into the surrounding PDMS and should easily reach cells in the neighboring cell channel.

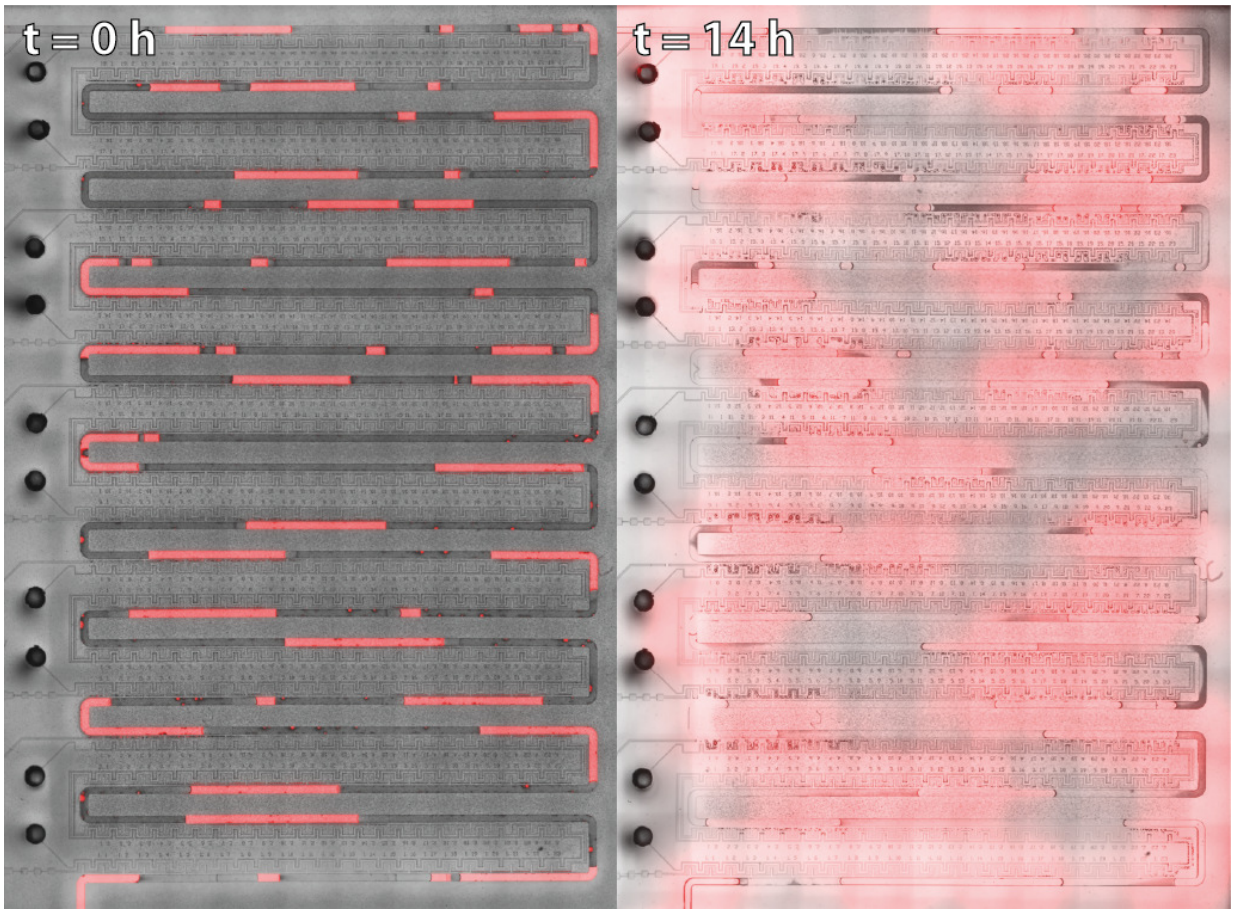

Figure 5.4 Diffusion of Nile red from plugs into PDMS. Nile red plugs loaded into the plug channel of a semi-comp chip at the start of the experiment and after 14 hours of incubation.

5.2.3 Semi-compartmentalized GFP induction in HeLa T-Rex™ cells

5.2.3.1 Induction of HeLa T-Rex™ cells with tetracycline

We used HeLa T-Rex™ cells that express green fluorescent protein (GFP) under the control of a tetracycline (tet)-inducible promoter as a model system to test cross-PDMS induction (Castello et al., 2012). Tetracycline is a water-soluble antibiotic and, when added to T-Rex™ cells, activates GFP expression. The experiment was designed to show that small molecules (such as tetracycline) can diffuse through PDMS and elicit a reaction in their target cells. First, we tested the inducibility of T-Rex™ cells in our hands by incubating them in medium containing 1 µg/mL tetracycline for 24 hours and then imaging them under a fluorescence microscope (**Figure 5.5 A**). As a control, cells were left untreated and imaged in the same way (**Figure 5.5 B**). Almost all cells treated with tetracycline showed GFP expression, whereas only a tiny fraction of the non-treated cells was GFP-positive, probably due to leaky expression of GFP. We concluded that the cells were well suited for induction experiments described below, since fully-induced cells could be easily distinguished from cells showing background promoter activity.

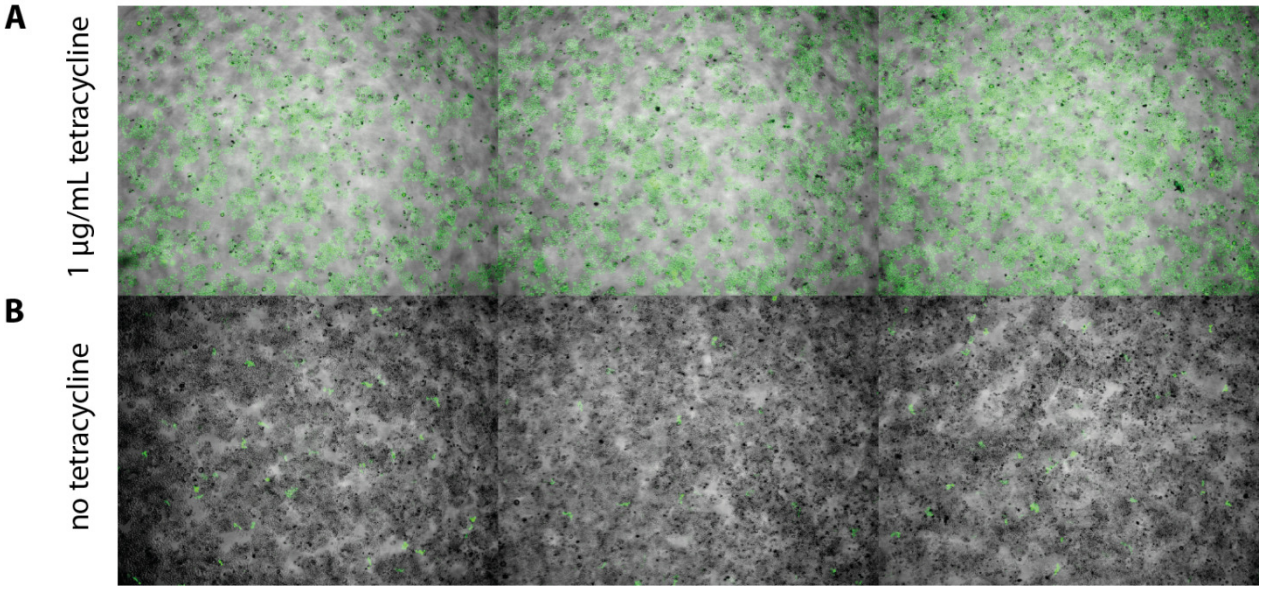

Figure 5.5 Tetracycline-based induction of GFP expression in HeLa T-Rex™ cells. HeLa T-Rex™ cells were seeded at equal densities in a 96-well microtiter plate and grown for 48 hours with 1 µg/mL of tetracycline (**A**) or without any drug (**B**). GFP expression was detected by imaging in the green fluorescence channel.

5.2.3.2 Test experiment with artificial PDMS wells

In a next step, we wanted to test if tetracycline and the related antibiotic minocycline could indeed trigger GFP expression in HeLa T-Rex™ cells after diffusion through PDMS. Minocycline is more hydrophobic (log*P* 2.12; CHEMBL database) than tetracycline (log*P* 0.62), but also binds to the tet promoter. If both small molecules could trigger GFP expression this would indicate that a variety of small molecules, beyond only the most water soluble, could be used in semi-compartmentalization-based screens. We produced a test setup made from PDMS that consisted of two small wells separated by a thin membrane similar to a design published by Evenou et al. (Evenou et al., 2012) (**Figure 5.6 A**). In order to produce the device, we used a 6 mm biopsy punch to stamp out a small well out of a 1 mm thick PDMS membrane. By bonding the 1 mm thick membrane to a thin 150 µm membrane, a small well was formed, which we used for drug incubation. Another 9 mm thick chunk of PDMS was punctured with a 12 mm biopsy punch and bonded to the other side of the thin membrane, thereby forming a larger well for cell incubation. This setup allows sequential incubation, first of antibiotics in the small well and then, after flipping by 180°, of cells in the large well.

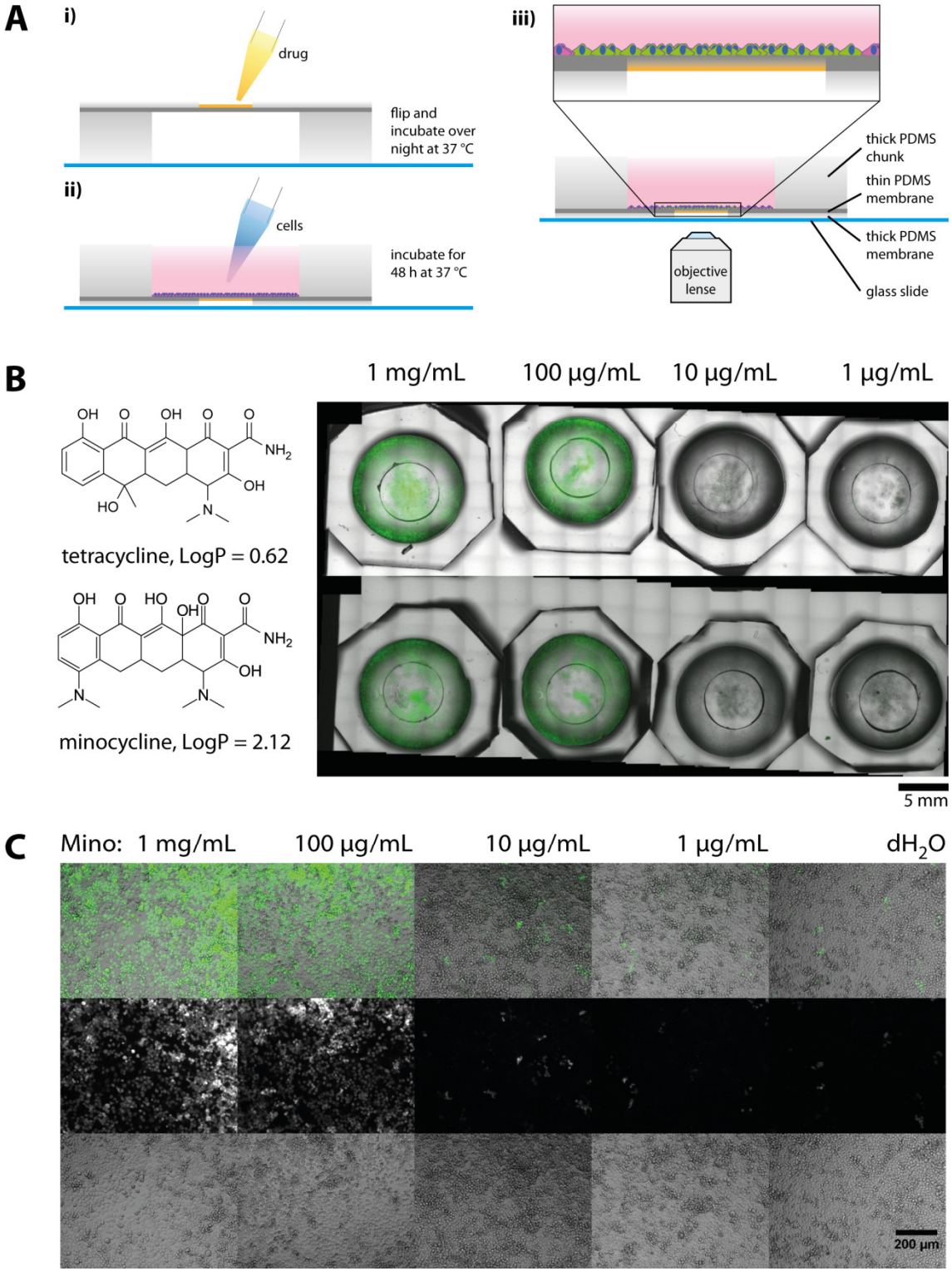

Figure 5.6 Induction of GFP expression in HeLa T-Rex™ cells through a thin PDMS membrane. A) Schematic of the experimental setup. The drug was dispensed into the smaller of two wells separated by a PDMS membrane and incubated overnight at 37 °C (**i**). Cells were seeded in the larger well and incubated for 48 h (**ii**) before imaging with a fluorescence microscope (**iii**). **B)** Cells were incubated with tetracycline or minocycline at drug concentrations of 1 mg/mL, 100 µg/mL, 10 µg/mL and 1 µg/mL. **C)** Micrographs of GFP-expressing cells at different minocycline concentrations in the green fluorescence channel (middle), bright field channel (bottom) and an overlay of both channels (top).

A ten-fold serial dilution in water ranging from 1 mg/mL to 1 μg/mL (the dose used in standard tissue culture experiments) was produced for both tetracycline and minocycline. 10 μL of each solution were pipetted into the smaller of the two wells and incubated over night at 37 °C and 5% CO_2. This way, the compound solution was completely absorbed by the membrane. Next, 200 μL of HeLa T-Rex™ cell suspension were added to the larger well and incubated for another 48 h at 37 °C and 5% CO_2. All wells were imaged over their whole area at low magnification and the resulting images were stitched together to create an overview of each well (**Figure 5.6 B**).

Both tetracycline and minocycline lead to a substantial increase in GFP expression at high concentrations (0.1-1 mg/mL), which is even more evident at higher magnification (**Figure 5.6 C,** images are representative for both compounds). Therefore, sufficient concentrations of both inducers diffuse through the PDMS membrane to activate GFP expression on the opposite side of the membrane. 1-10 μg/mL of minocycline were insufficient to activate GFP expression to high levels. 10 μg/mL of minocycline led to a slight increase in GFP expression, but 1 μg/mL remains at control (dH_2O) level (**Figure 5.5 B**). We decided to use a concentration of 1 mg/mL tetracycline for the plug-based experiments discussed below, since in that setup the compounds have to cross two hydrophobic barriers: the PDMS wall/membrane and the carrier oil phase separating the aqueous phase from the channel wall.

5.2.3.3 Induction of GFP expression in parallel channels

Before loading tetracycline plugs into a plug channel to induce GFP expression, we created a simplified version of the semi-compartmentalization chip with the parallel channel layout (**Figure 5.7 A**). This simplified chip consisted of short cell and medium channels and contained six additional channels, which were designed to simulate tetracycline plugs. We filled only one of the six channels with tetracycline, while the others were filled with water. Cells were then seeded in the cell channel and medium was continuously flushed through the medium channel. We incubated the chip for two days so that tetracycline could reach the cell channel and GFP expression could take place. Next, we imaged cells in the cell channel at increasing distances from the channel containing 1 mg/mL tetracycline (**Figure 5.7 B**). As expected, induction of GFP expression was strongest in the channel section closest to the tetracycline-filled channel and decreased when moving away from that position.

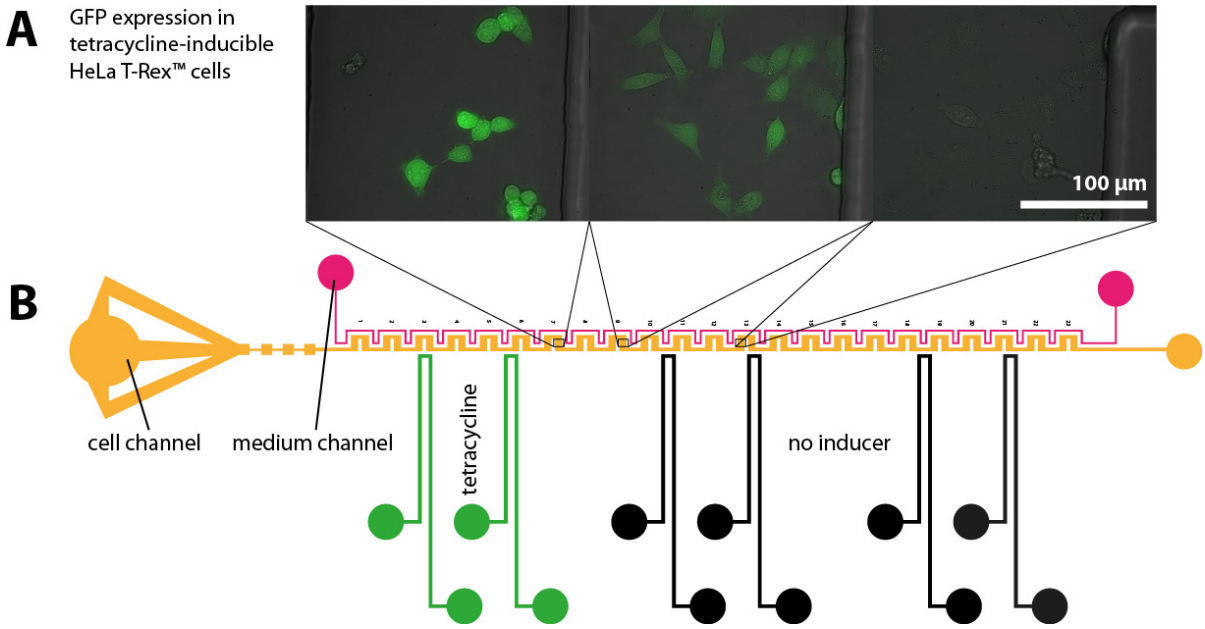

Figure 5.7 Induction of GFP expression in parallel channels. Schematic of the chip design used for this experiment. 1 mg/mL Tetracycline was filled into the microfluidic channel loop indicated with "inducer". Micrographs were taken of tet-inducible HeLa T-Rex™cells seeded into the central cell channel at increasing distances from the "inducer" loop after 60 hours of incubation.

5.2.3.4 Tetracycline can diffuse from the plug channel to the cell channel

Next, we tested the feasibility of GFP induction by tetracycline loaded from plugs in the parallel channel setup of our microfluidic device (**Figure 5.2 A & C**). The three channels of this setup can be accessed individually, so that flow in one channel does not affect the other two channels. However, nutrients and drugs can diffuse through the channel walls into the other channels. The medium channel is used to constantly infuse medium to continuously feed cells in the cell channel and remove potentially accumulating waste products during long incubation times. Small molecules can be delivered to cells from the plug channel, where plugs loaded with these compounds can be "parked" in close vicinity to the cells.

For a typical experiment, HeLa T-Rex™ cells were loaded into the cell channels of a microfluidic device that had been oxygen plasma treated to turn the chip hydrophilic (cf. section **5.2.2.1**) and improve soaking in medium overnight. A sequence of plugs containing tetracycline (1 mg/mL in dH_2O), sulforhodamine B (100 µM in dH_2O) and dH_2O was produced using an autosampler to sequentially aspirate samples from a 96-well microtiter plate (cf. **Materials & Methods**). Sulforhodamine B plugs were included to keep track of the plug sequence by visual inspection during production (pink color) and on-chip by imaging in the green fluorescence channel. Once the channel was completely filled with a sequence of plugs, the flow was stopped,

the inlets and outlets sealed with screws and the whole chip incubated for 65 h at 37 °C and 5% CO_2.

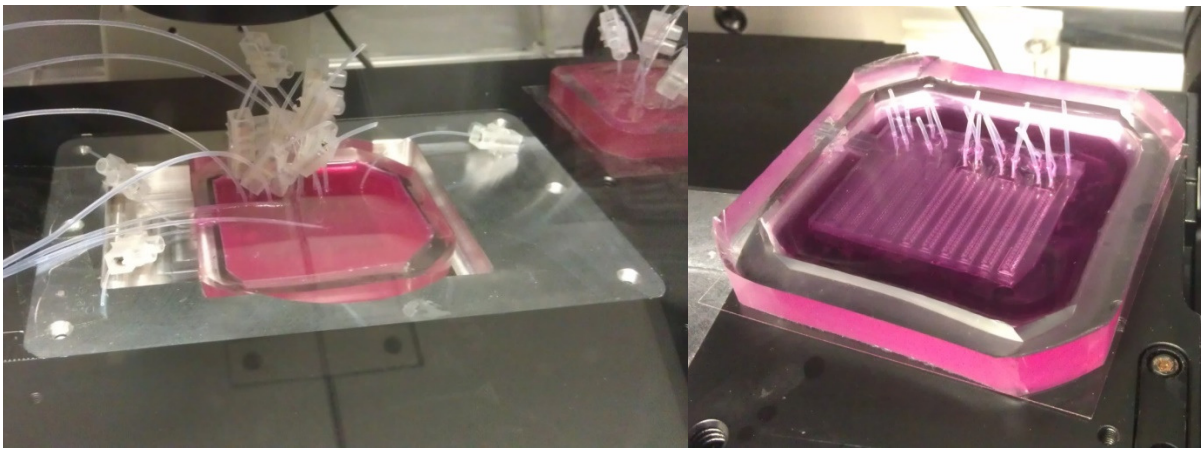

Figure 5.8 Photographs of a semi-compartmentalization chip. Semicomp chip with connected tubing for constant medium supply on a microscope stage (left) and surrounded by a thick PDMS wall after a finished experiment (right).

In order to keep the chip soaked with medium throughout the course of several days, we bonded a thick "wall" of PDMS to the same glass cover slip the chip was attached to. This created a reservoir that was constantly refilled with medium and compensated for evaporation, thereby preventing the chip from drying out (**Figure 5.8**). Medium was also continuously infused through the medium channel to deliver nutrients to the cells in the cell channel. After incubation, cells were imaged next to specific plugs in order to evaluate their GFP expression (**Figure 5.9**). Cells in the vicinity of tetracycline plugs expressed high levels of GFP, while cells in the vicinity of sulforhodamine B or water plugs did not elicit any green fluorescence stemming from GFP expression. In other words, we were able to specifically induce GFP expression in cells via tetracycline diffusing out of water-in-oil plugs and through 100 μm of PDMS.

However, a few drawbacks remained. First, the plugs were not completely halted in their position after loading and kept moving for some time while exposing cells to their content. This could lead to some cross-contamination with compounds from other plugs if plugs are not spaced out enough. However, larger distances between two consecutive plugs lead to lower throughput because an overall smaller number of plugs can be loaded into one channel. Additionally, using the autosampler for plug production is very time consuming and results in very large plugs that have to be split to smaller sizes on-chip. Plus, cell handling on-chip is not straightforward, as fresh medium has to be supplied for days to keep the cells viable and the chip

soaked over time. This process is prone to technical malfunctions such as stalling of the pump controlling growth medium infusion.

In the next sections, I describe an alternative approach to semi-compartmentalization with more space for sample plugs and simplified cell handling.

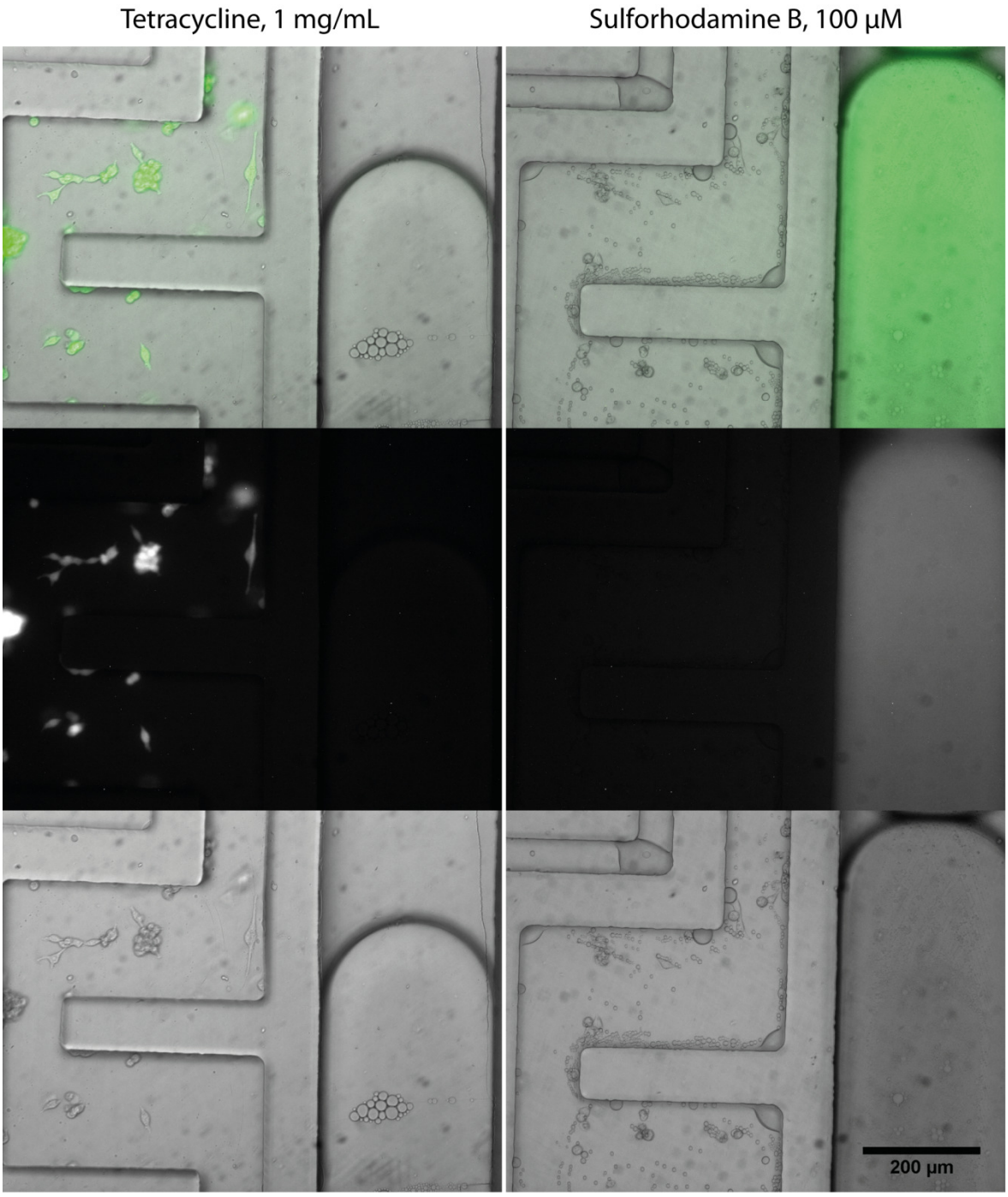

Figure 5.9 GFP expression in HeLa T-Rex™ cells induced by tetracycline in parallel channels. GFP expression of HeLa T-Rex™ cells imaged in the green fluorescence channel in the cell channel next to plugs containing 1 mg/mL tetracycline (left) or 100 µM sulforhodamine B (right).

5.2.3.5 Induction of GFP expression across a PDMS membrane

In the previous section, we could show that GFP expression in HeLa T-Rex™ cells can be induced by tetracycline diffusing out of water-in-oil plugs and through 100 µm of PDMS channel wall. Accordingly, this should also work through a thin PDMS membrane forming the floor of the channel, similar to the PDMS well experiment described above (**Figure 5.6**). In a first trial experiment, we used the semi-compartmentalization chip with parallel channels (**Figure 5.2 C**), but did not bond it to a glass slide and did not soak it in medium. Instead, we intended to soak the thin and dry PDMS membrane used to seal off the microfluidic channels with our compounds. As before, tetracycline, sulforhodamine B and water plugs were loaded sequentially, stopped in the channel by sealing all outlets and incubated overnight at 37 °C. After incubation, the plugs were flushed out of the channel with FC-40 oil. In order to identify all plugs and register their positions, we imaged the whole before and after plug incubation in BF and FL (data not shown). Plug positions changed during the incubation, but their movement was limited to a stretch of channel close to the plug inlet. Further along the channel, plug positions were stable throughout the course of incubation.

The chip was placed in a 100 mm tissue culture dish and submerged in a dense suspension of HeLa T-Rex™ cells. The cells attached to the membrane on the outside of the chip – eventually covering its surface completely – and were incubated for an additional 48 hours at 37 °C and 5% CO_2. Next, the chip was removed from the Petri dish and placed on a thin cover slip for imaging. Green fluorescent cells were visible in only one area of the chip which turned out to be in the location, where a long tetracycline plug had been registered. We imaged the cells in this area of the membrane and stitched the individual images together in order to create an overview (**Figure 5.10 A**). The area occupied by GFP-positive cells was indeed limited to the width of the underlying cell channel (**Figure 5.10 B**).

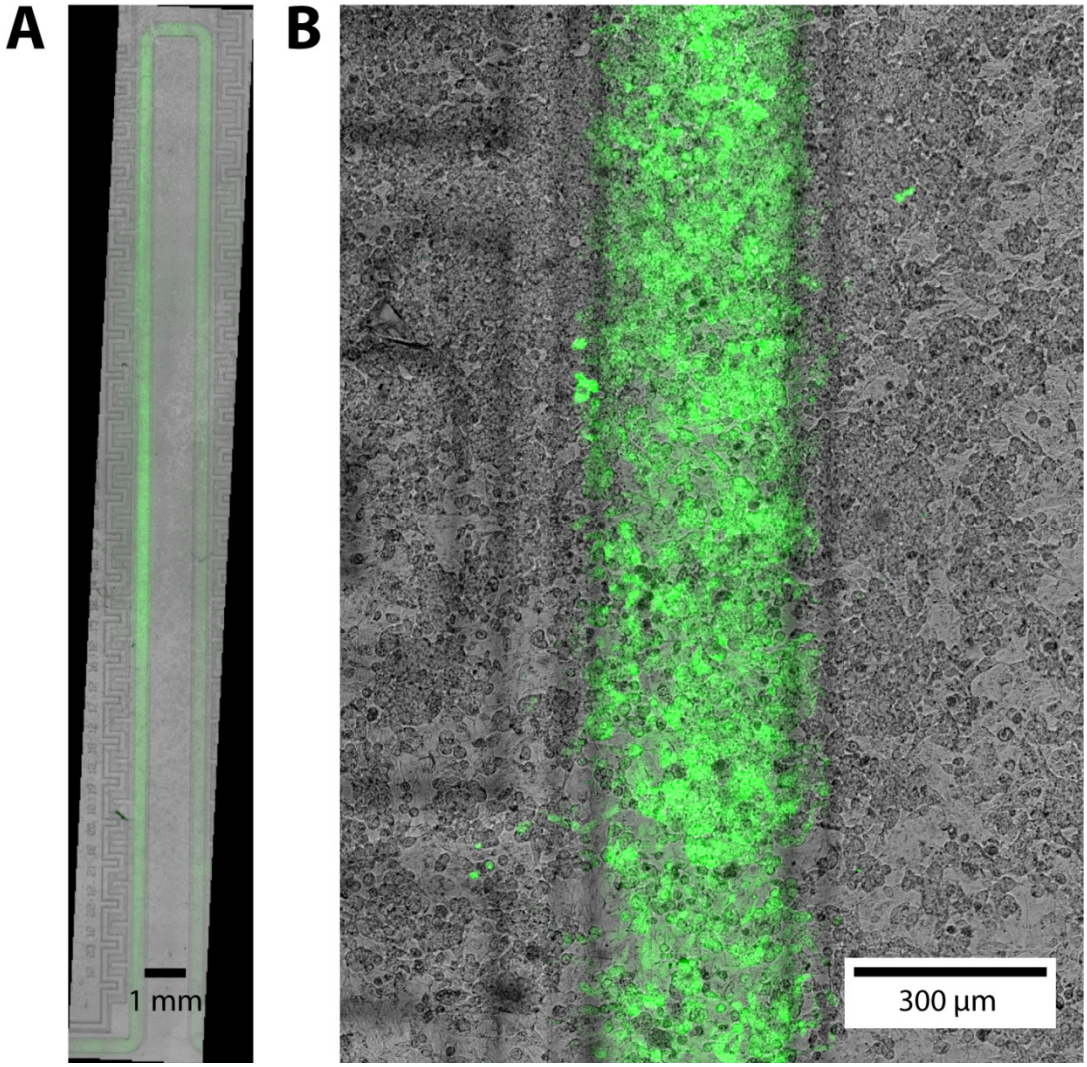

Figure 5.10 GFP expression in HeLa T-Rex™ cells induced by tetracycline from a plug through a PDMS membrane is limited to the position of a tetracycline plug. Micrographs of HeLa T-Rex™ cells on a PDMS membrane in the green fluorescent channel: complete overview over extent of plug location (**A**) and zoomed in (**B**).

5.2.4 A new simplified chip layout to maximize throughput

Having confirmed, that this modified setup (**5.2.3.5**) works even better than experiments performed within the three parallel channels and moreover, it improved cell handling, we redesigned our whole chip. We removed the now obsolete cell and medium channels completely and merely included a long plug channel in the new design (**Figure 5.2 D**). To increase the number of plugs that could be loaded onto the chip, we elongated the plug channel. Furthermore, we decided to use the Braille chip to produce tetracycline plugs (cf. section **3.2**), since it allows more control over plug size and composition and because plug production is faster than on the autosampler.

We produced plugs containing 1 mg/mL tetracycline and loaded them onto the modified semi-compartmentalization chip for incubation. The chip was not plasma treated or soaked in medium, but rather we wanted to soak dry PDMS with plug contents. Once the whole chip was filled, plug flow was stopped by cutting the tubing used to load the plugs and sealing all outlets with liquid PDMS. To reduce evaporation, we additionally covered the whole chip surface with sticky tape and then incubated the chip overnight at 37 °C. Plug positions were imaged before and after plug incubation in order to note any differences in size and position throughout incubation (**Figure 5.11 A**).

Next, the plug channel was cut open and all plugs were flushed out with oil, while making sure that the tetracycline solution did not come into contact with the outside of the chip. Any such contact would have contaminated the culture medium with enough tetracycline to trigger GFP expression in all cells. Then, the chip was flipped upside down and placed in a tissue culture dish. A dense suspension of HeLa T-Rex™ cells in DMEM was dispensed onto the chip, completely submerging the latter. Again, the chip and the cells were incubated for 48 h at 37 °C and 5% CO_2. Following the incubation, the chip was flipped and placed on a 70×70 mm coverslip for imaging in the bright field and fluorescence channels. An image of the whole chip in the green fluorescence channel is displayed in **Figure 5.11 B**. When compared the positions of GFP-positive cells on the PDMS membrane with the positions of tetracycline plugs during pre-incubation (**Figure 5.11 D**). We could show that clusters of GFP-expressing cells were localized strictly to positions previously occupied by plugs. Moreover, the areas of induced cells from neighboring plugs did not overlap, which shows that we can indeed locally induce cells on the PDMS substrate (**Figure 5.11 C**).

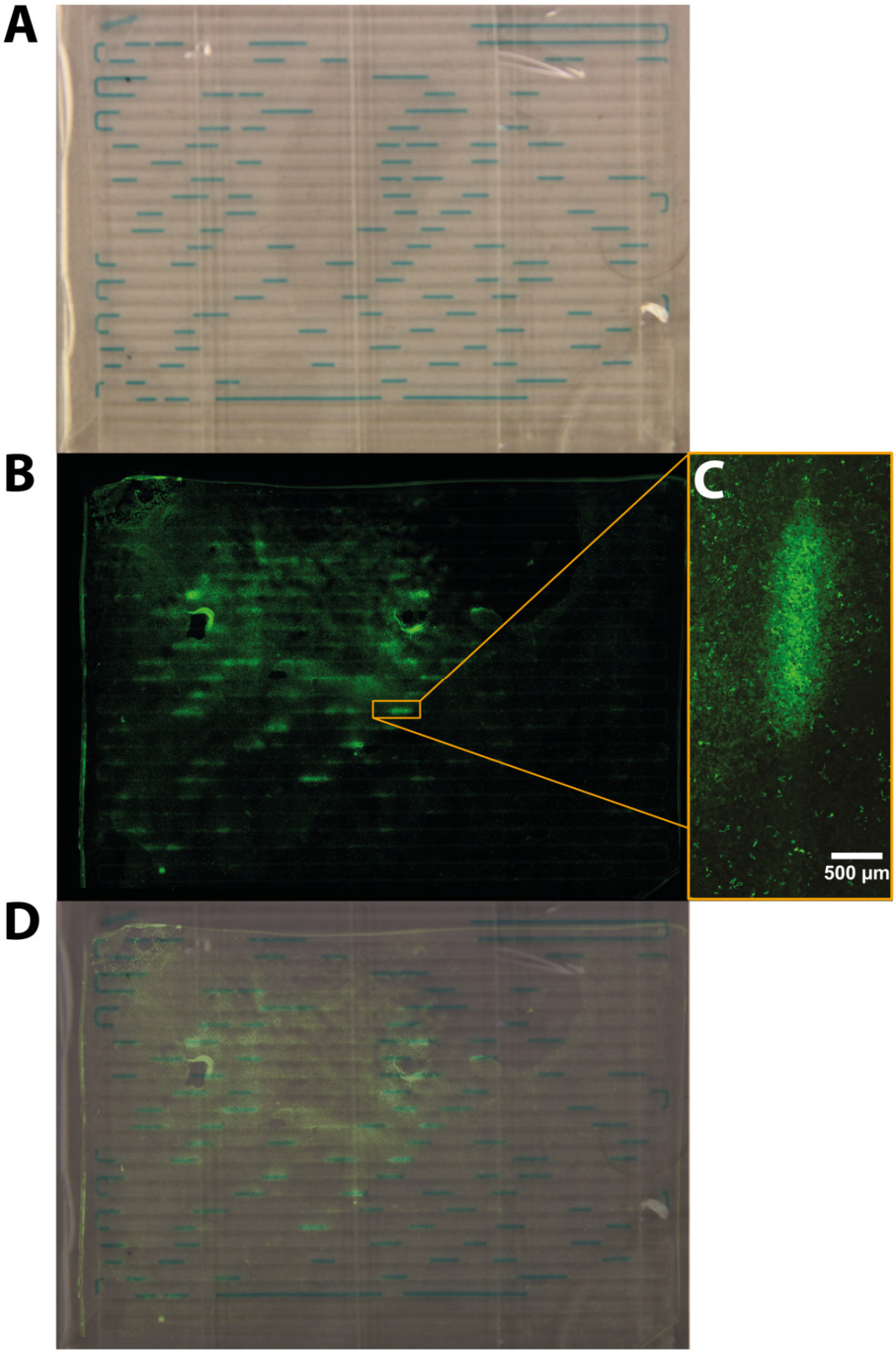

Figure 5.11 GFP expression induced from an array of plugs containing tetracycline. A) Photograph showing the positions of the plug array after soaking the PDMS membrane covering the chip with tetracycline spots. **B)** Composite micrograph of the PDMS membrane surface imaged in the green fluorescence channel. **C)** Close-up view of induced cells on the PDMS membrane surface imaged. **D)** An overlay of the photograph and the fluorescence micrograph showing the position of tetracycline plugs and induced cells.

5.3 Discussion

We have conducted experiments to investigate the diffusion of small molecules through PDMS (cf. section **5.2.2**). As reported earlier, this diffusion depends to a large extent on the log*P* of the compounds investigated, as shown by the distinct diffusion behavior of Nile red (log*P* = 5) compared to that of fluorescein (log*P* = -0.67) (**Figure 5.3**, (Wang et al., 2012b)). In addition, we found that the diffusion behavior of small molecules can be altered by treating the PDMS in oxygen plasma to render it more hydrophilic, a treatment that was described in more detail by Bodas and Khan-Malek (Bodas and Khan-Malek, 2006). Most drug-like compounds have rather hydrophobic log*P* values in the range of 2-3 (Lipinski et al., 2012; Macarron et al., 2011; Proudfoot, 2005). The treatment improved the diffusibility of hydrophilic compounds, while it hindered the diffusibility of hydrophobic compounds (**Figure 5.3**), which increases the range of drugs compatible with our approach. This was further demonstrated by using the two closely related drugs tetracycline and minocycline with different log*P* values of 0.62 and 2.12 in a model experiment of GFP activation in HeLa cells (**Figure 5.6**). Lastly, the plasma treatment has the added benefit of drastically reducing the loss of hydrophobic drugs to the chip material during plug loading, which would lead to cross contamination with other compounds.

Subsequent experiments using tet-inducible GFP expression in HeLa cells as a model system, demonstrated that drug delivery to cells not only worked when the drugs were not infused directly into a microfluidic channel (**Figure 5.7**), but also when they were instead delivered from plugs to cells located in a parallel channel and separated by 100 μm of PDMS (**Figure 5.9**). Localized induction could also be shown using a simplified version of the chip, which consisted merely of a long incubation channel sealed off with a thin PDMS membrane and therefore allowed the storage of more plugs. It also allowed the culturing of cells on the chip surface in the same way as in a standard tissue culture dish, which obviates the use of additional channels (**Figure 5.2 D & Figure 5.11**). Shim et al. had reported similar findings for small compound delivery to bacterial cells encapsulated in plugs through PDMS and carrier oil (Shim et al., 2011). However, since in their approach cells were located within the plugs and the compounds were delivered from a continuous phase, the possibility to expose the cells to many different compounds was strongly limited. Conversely, our approach is compatible with trains of plugs with diverse chemical composition, for instance by combining it with the combinatorial plug production described in **Chapter 3**.

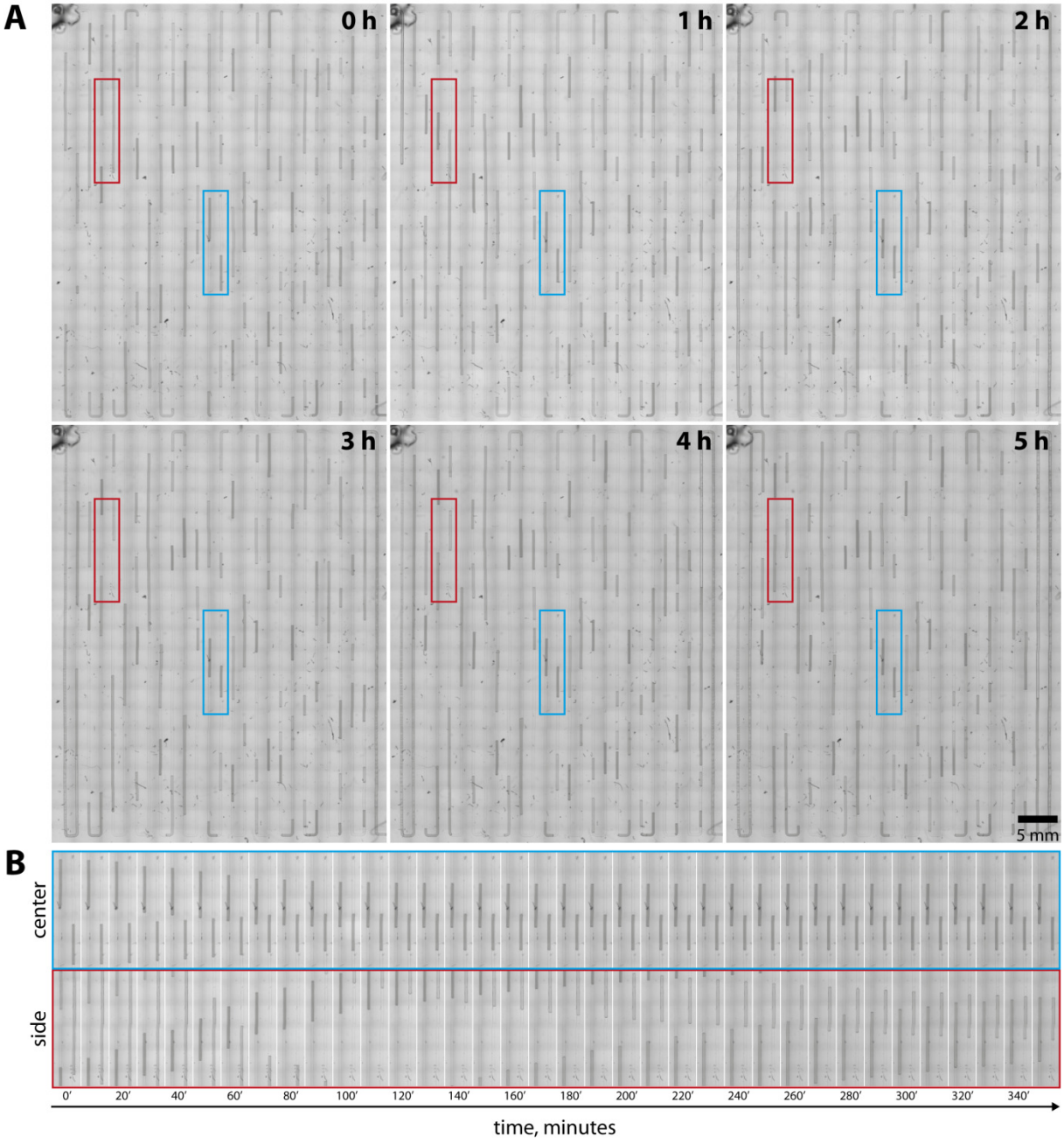

Figure 5.12 Permeation-driven flow causes plugs to move asymmetrically over time. A) Micrographs stitched together into an overview over the whole chip. Red and blue boxes indicate the positions monitored in detail for every time point in **B)** to show the movement of plugs at a central (blue) and side (red) position.

In some experiments we noticed movement of plugs during plug incubation times and a simultaneous appearance of air in the plug channel (**Figure 5.12 A**). We initially hypothesized that this was due to leakage of liquid out of the chip or actual evaporation of the aqueous contents into the air. However, no matter what we tried to limit this evaporation – sealing the chip completely with air-impermeable material or incubation in a completely water-saturated atmosphere – the observation was still the same. Seeing this, it seems more likely that most of this "evaporation" is

actually due to the soaking of the plug contents into the PDMS material of the chip itself. This explanation is supported by the observed shrinking of plugs over time. Randall and Doyle published a detailed study of this "permeation-driven flow" (Randall and Doyle, 2005). In our setup, liquid in the channel is absorbed by the dry and porous PDMS which forms a fairly large evaporation sink. Since the volume of absorbed liquid has to be replaced, air flows in from the areas with least resistance, i.e. the large plug inlet and outlet. This also explains why we observe more plug movement on the chip edges compared to the center of the chip (**Figure 5.12 B**).

In conclusion, we have developed a new microfluidic method that allows the combination of high chemical diversity - offered by combinatorial plug production - with cell-based assays that require washing steps, e.g. immunostaining. Such assays are not feasible when cells are encapsulated within droplets due to a lack of access. In addition, cells seeded onto the chip surface can be imaged at high resolution using standard light microscopy, which is not easily feasible within droplets because cells drift out of focus. The limitation posed by the phenomenon of permeation-driven flow displayed in **Figure 5.12** should be controllable by pre-soaking the chip in water or, if that is not sufficient, by treating the plug channel walls (but not the membrane) with a water-impermeable coating such as parylene C (Lei et al., 2011). This would eliminate the biggest sink for permeation represented by the bulk of the PDMS chip and at the same time concentrate all permeation on the thin membrane. Therefore, plug movement should be drastically reduced and allow reliable patterning of the complete membrane with small compounds for localized drug assays within a single tissue culture, which are discussed in more detail in the **General discussion**.

6 GENERAL DISCUSSION

We have established a new fully integrated microfluidic system allowing the generation of systematic (barcoded) combinatorial mixtures in water-in-oil plugs hosting live cells. It furthermore allows the addition of assay substrates at a later time point (e.g. after incubation) with the use of a newly developed fusion chip and is fully compatible with cell-based assays, overcoming a big hurdle in the field of droplet-based microfluidics. Our system is based on individually actuatable pins of a Braille display, which open and close valves in microfluidic channels and thereby control the generation of mixtures of liquids injected from different inlets. In proof-of-principle experiments, the new device enabled the production and measurement of 686 individual sample and label plugs, which were used to encode the sample sequence and to prevent cross-contamination between samples (cf. section **4.6.4**). The sample plug sequence consisted of five replicates of all possible combinatorial mixtures of twelve compounds, which resulted in 79 unique sample mixtures that were co-encapsulated with cells in culture. Two such cycles were produced in less than 103 minutes and were stored within a single PTFE tube for incubation. Previous droplet-based screening approaches created limited chemical diversity without cells (128 combinations of 8 vs 16 compounds) for click chemistry applications (Wang et al., 2009). However, in the latter approach, sample plugs were separated by compressible air, which prevents the storage of many samples per tubing and sample tubes were exchanged manually after a maximum of eight reaction mixtures. This resulted in a production time of 17 s per sample without counting the time to exchange the sample tubing, which was not specified by the authors, but had to be carried out after always eight samples. To the best of our knowledge we thus present here the very first platform enabling the chemical genetic screening of human cells in a fully-integrated droplet-based microfluidic setup.

Small molecule screens often require long incubation times to elicit a specific cellular phenotype and therefore assay components are added only after hours or days of incubation. To this aim, we developed the first microfluidic fusion module that enables the controlled fusion of assay substrate droplets with trains of preformed plugs containing cells (cf. section **3.3**). This has not been shown previously, mainly because cells release high protein concentrations which cause a lot of wetting and thus interfere with the re-injection of samples into a second microfluidic chip after incubation. We solved this problem by injecting surfactant-laden carrier oil from additional side channels, which keeps the incoming plugs away from the channel walls and reduces wetting. Our fusion setup precludes the need for droplet synchronization that is required in other approaches to add reagents to target plugs. This is achieved by fusing a large number of small droplets with large sample plugs, i.e. a long plug fuses with more substrate droplets than a short one while the concentration of added substrate remains the same. Substrate droplets that are

released while an oil spacer passes the drop maker are stabilized by surfactant supplied in the carrier oil, which prevents them from fusing with each other. This means they can be easily detected by their length and therefore be excluded in data analysis.

When using our approach to perform chemical genetic screens for synergistic interactions of small molecules with defined cellular targets, we are faced with a trade-off between including different concentrations and sample diversity. On the one hand discovering, interactions between two drugs is more likely when screening several concentrations for each drug, which on the other hand would reduce the number of individual compounds used in a screen. Nevertheless, the likelihood of finding drug interactions from single drug concentrations can be increased by evaluating optimal working concentrations for every compound used in the screen. Moreover, once a first set of suitable concentrations has been characterized, the same drug combinations can be screened with different cell types. Even more intriguingly, a selected set of compounds could be used to directly screen drug combinations on individual patient samples to identify therapeutically beneficial drug interactions on a personalized level. Here, the panel of drugs could be composed of cancer therapeutics that are already used in the clinic, but have been reported to have varied effects on different patients with the same cancer type (van 't Veer and Bernards, 2008). Furthermore, some MMPs active in the tumor microenvironment are actually secreted by surrounding stromal cells rather than the tumor itself (Martin and Matrisian, 2007). This could be addressed by running the same screen on tumor cells as well as samples from surrounding tissue.

In ongoing experiments, which use our newly established microfluidic system in a chemical genetic screen of MMPs, a few challenges presented themselves. After detecting little effect on MMP activity when HT1080 cells were exposed to various drugs with targets in important cellular signaling pathways (cf. section **4.6.1**), we decided to use ostensibly more specific cytokines and growth factors. But we were so far unable to detect synergistic activation of MMPs, neither in the plate reader nor in plugs. One reason, why this might be the case, is that we used a broadband MMP FRET substrate in all of our experiments. However, fluorogenic substrates for individual MMPs do not exist for the same reasons that inhibitors for individual MMPs are absent. Thus, even though HT1080 cells are known to constitutively produce MMP-2 and MMP-9, it is very likely that a significant portion of our detected signal stems from other MMP family members such as MMP-1, MMP-5, MMP-14/MT1-MMP, MMP-15 and MMP-16, which have also been reported to be produced by HT1080 cells and potentially lead to a high background signal (Gervasi et al., 1996; Giambernardi et al., 1998). Additionally, since a lot of cross-regulation has been observed for MMPs, it is conceivable that the inhibition of one MMP would lead to the

activation of another, resulting in no significant change of overall substrate conversion (cf. **Figure 1.9**).

Consequently, we have started creating constructs containing the gene for ß-galactosidase (*lacZ*) under the control of the promoter sequences for MMP-2 and MMP-9. HT1080 cells stably transfected with such a construct will allow us to specifically measure the expression of particular MMPs, as was previously shown for similar constructs containing the luciferase gene (Yan et al., 2004). Since luminescence measurements require signal integration times in the range of seconds, we plan to use the conversion of fluorescein di-β-D-galactopyranoside (FDG) to fluorescein by ß-galactosidase as fluorescence-based reporter readout for MMP activity. FDG can cross the plasma membrane and enter cells where it is enzymatically converted and diffuses back out of the cells (He et al., 2005). This will allow us to use our established spectroscopic readout, since the whole plug would turn fluorescent upon activation of expression. Besides switching to a more specific readout of MMPs, we also plan to use different cell lines, which do not constitutively express certain types of MMPs and might therefore allow a clearer readout signal for the induction of expression of specific MMPs.

In addition to a more specific readout of MMP activity, we also aim to increase the number of compounds we can screen in a single experiment. So far, we have used only half of the available pins on the Braille display. By using all 32 available pin on the Braille display, the number of samples with unique combinatorial mixtures could therefore be easily increased to 407 (all possible pairs of 28 compounds + individual compounds). Furthermore, sample numbers could be increased on the existing chip by producing combinatorial mixtures of always three compounds which would already result in 232 unique samples. Importantly this could be achieved without the need for any additional equipment or significant changes in the sample production procedure. The larger number of sample plugs, however, would require the filling of more than one long sample tubing which can be easily achieved by manually replacing the filled sample tubing with an empty one and then continuing plug production. Alternatively, the number of samples could be even further increased by integrating an autosampler to infuse compounds from a 96-well plate into one of the inlets on the Braille chip. This technology is currently under development in the group (Ramesh Utharala & Federica Eduati).

The presented combinatorial chip enables us to run a fully combinatorial screen of 12 compounds using just 5×10^5 cells for the whole experiment or roughly 100 cells per plug. This is 10-times less cells than were used in a recent microtiter plate-based high throughput screen, which used 1536-well microtiter plates with a 1000 cells per well (Mathews Griner et al., 2014). Howev-

er, due to inherent technical problems of 1536-well microtiter plates (sample evaporation, cross-contamination through bridging between wells (Dove, 1999)), industry often still relies on 384- and 96-well plate formats, which require even more cells and reagents. Additionally, microtiter plate-based screens rely on bulky and expensive liquid handling robots with large dead volumes for sample solutions and are thus not amenable to the screening of expensive or rare compounds and cells. In conclusion, our microfluidic approach circumvents two limitations frequently encountered in conventional screens: It permits the use of rare samples such as primary cells or tumor biopsy-derived cells without the need of cell proliferation beforehand (Petit et al., 2013), while at the same time drastically reducing the amount of reagents required to carry out a complete screen.

Besides its application in the elucidation of cellular signaling pathways as described in this thesis, our technology could prove useful for any other experiment where combinations of small molecules are exploited. One field that would benefit from such an approach is the development of antibiotic combination therapy. Since their discovery nearly a century ago, antibiotics have been used extensively and in large quantities (3×10^6 kg administered to humans and 13×10^6 kg to animals per year in the United States alone). This has led to a spread of antibiotic resistance across the globe (Spellberg et al., 2013). One promising approach to stop (or at least to slow down) the emergence of antibiotic resistance is the use of combinations of antibiotics for the treatment of bacterial infections (Palmer and Kishony, 2013). This allows the use of lower overall antibiotic concentrations through synergistic drug effects, as well as making the occurrence of resistance less likely by simultaneously hitting two independent targets. But combinatorial interactions are not only important for the investigation of disease. Combinations of agonists can for instance also be used to interrogate cross-talk between cellular signaling pathways (Chatterjee et al., 2010). Finally, large efforts have been made in the stem cell community to identify combinations of small molecules that induce differentiation or re-programming of stem cells into specific cell fates, as well as the production of induced pluripotent stem cells (iPS) from somatic cells (Borowiak et al., 2009; Hou et al., 2013).

In parallel to the combinatorial chip discussed above, we developed a new semi-compartmentalization approach, which allows us to combine droplet-based microfluidics with long-term cell culture (cf. **Chapter 5**). Here, cells are no longer confined to the small volumes of plugs and therefore nutrient depletion and toxic compound accumulation over time are not an issue (Clausell-Tormos et al., 2008). This also means that cells are accessible to washing steps required in some assays (e.g. immunostaining assays). A further advantage of this approach is the possibility to image cells at high magnification, so that subcellular localization assays can be con-

ducted. This is not possible within droplets due to loss of focus caused by the cells floating around in the droplet and due to the movement of the plugs themselves, which prevents long exposure times. The Studer lab developed simple microfluidic chips called microfluidic stickers, which allow the user to turn a standard tissue culture dish into a continuous-phase microfluidic device by simply sticking the chip onto the surface of the cell culture (Morel et al., 2009). Our device uses a similarly easy setup, but combines combinatorial plug production (instead of continuous flow) with standard tissue culture techniques.

Several other methods to locally induce cells have been developed in the field of microfluidics. Juncker et al. developed a microfluidic probe (MFP), similar to a pipette, which can be used to stain or perturb subpopulations of cells within standard open tissue culture (**Figure 6.1 A** (Juncker et al., 2005). Here, a small microfluidic chip containing only two channels is fixed to the end of a robotic arm. The two channels have their openings at the tip of the chip. Liquids are infused through one channel (Q_I) and aspirated through the other (Q_A). When it is submerged into external liquid, a laminar flow is formed at the tip. Liquid flows from one channel port to the other and can be used to locally perturb cells in close proximity. However, this process is quite slow and cannot be used in high throughput applications (Qasaimeh et al., 2013). This device is very similar to a microfluidic device called "chemistrode", which was developed in the Ismagilov lab, except that the latter uses water-in-oil droplets instead of laminar flow to deliver and collect samples from tissue surfaces (Chen et al., 2008)).

Others developed methods to pattern microporous membranes, on which cells can be grown in the presence of compounds (Upadhyaya and Selvaganapathy, 2010). They fill a microfluidic channel with a sample compound and drive it through a porous membrane and into a gel with the help of an electric field (**Figure 6.1 B**). Alternatively, compounds can be delivered to cells simply by passive diffusion through the porous membrane (**Figure 6.1 C** (Evenou et al., 2012)). Here, the area of compound diffusion is defined by the shape of small wells in a removable membrane. Compound combinations can be applied by removing this membrane and applying another one (potentially with a different well pattern). However, since manual pipetting is required, the throughput and sample diversity in this approach are rather limited. Furthermore, Kusi-Appiah et al. used spotted arrays of drugs encapsulated in multilayer phospholipid vesicles onto dish surfaces. This allowed direct drug exposure of cells grown on the drug spots (Kusi-Appiah et al., 2012). All of these methods can be used to locally induce individual cells or subpopulations of cells within larger populations of cells. However, none of these methods allows a large set of compounds to be screened in a single experiment. Our device overcomes this limitation by combining it with our newly developed combinatorial chip.

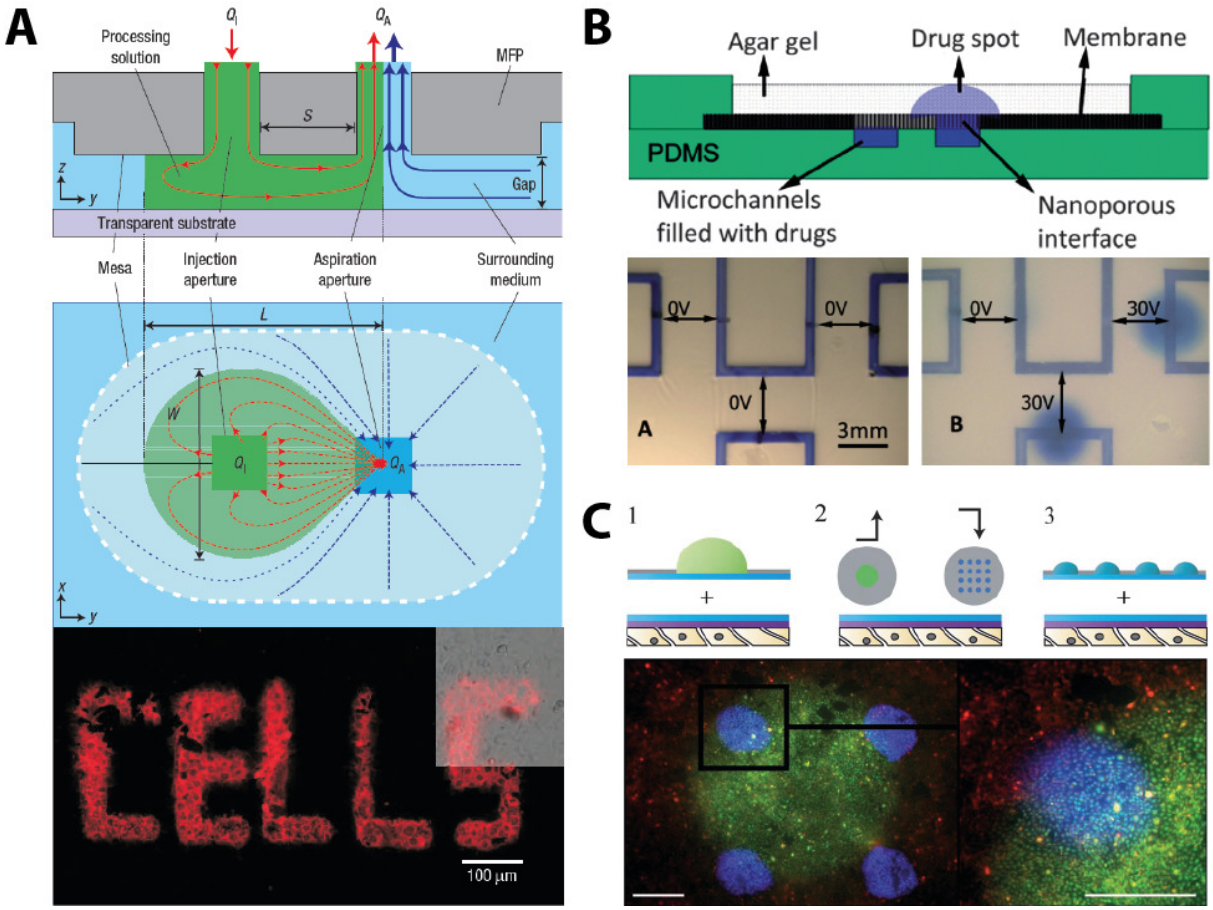

Figure 6.1 Different methods used to locally induce cells. A) A microfluidic probe (MFP) can be used to locally induce cells by creating a laminar flow of compound along the tip of the probe when submerged in liquid (Q_I: injected flow, Q_A: aspirated flow). **B)** Agar can be patterned with compounds by enhancing mass transport through a porous membrane by applying an electric field. **C)** Small wells in a removable membrane can be used to controllably expose cells to different compounds. Reproduced with permission from (Juncker et al., 2005) © Nature Publishing Group, (Upadhyaya and Selvaganapathy, 2010) © Royal Society of Chemistry, (Evenou et al., 2012) © Royal Society of Chemistry

Our technology is not limited to the format presented here. Rather, we think of semi-compartmentalization as a general concept for the delivery of small molecules to subpopulations of cells within a larger population or tissue. A minimal semi-compartmentalization device could consist of a simple straight channel filled with plugs of identical composition and produced by alternating aspiration of aqueous and carrier oil phase (Chen and Ismagilov, 2006). This setup would be sufficient to induce a specific phenotype in a small subpopulation of a confluent cell layer, to then observe the phenotype elicited by the surrounding cells. A different type of assay could be carried out by encapsulating one type of cells in plugs and letting them interact with a different cell type across the PDMS membrane. One population could for instance be expressing hydrophobic hormones like estrogen (e.g. granulosa cells), which are known to be absorbed into

PDMS, the other population could be monitored for changes in the expression of surface receptors within a fully confluent cell layer, e.g. estrogen receptors (Regehr et al., 2009). Granulosa cells were reported to secrete estrogen and progesterone in different ratios depending on the plating density, i.e. they secrete less estrogen and more progesterone the higher the culture density (Portela et al., 2010). Thus this behavior could be controlled by encapsulating cell suspensions with different cell densities. Such a setup would not be possible by simple co-cultivation of the two cell types and could lead to new insights into the dynamics of paracrine signaling. Other applications could be found in chemotaxis and neuronal growth, where plugs filled with small molecules could act as "road blocks" or "attractors" in predefined positions on a membrane (Li Jeon et al., 2002; Millet and Gillette, 2012).

7 MATERIALS & METHODS

7.1 Microfluidic device fabrication

7.1.1 Chip design and photomask printing

We used standard soft lithography techniques (Duffy et al., 1998) to manufacture all microfluidic devices out of polydimethylsiloxane (PDMS; Sylgard 184 silicone elastomer kit, Dow Corning Corp.). An overview of the process is shown in **Figure 7.1**. All microfluidic chips used in this work were designed using the computer aided design software AutoCAD (Autodesk Inc.) Individual modules were copied from designs existing in the group or designed from scratch to suit the individual tasks. The designs were then sent to an external company (Selba S.A., Versoix Switzerland) for photomask printing at very high resolution (25400 dpi) on transparency slides. Photomasks were printed either as positives or negatives, depending on the photoresist to be used in the manufacturing of molds (s. below).

7.1.2 Mold manufacturing

Molds for microfluidic devices requiring channels with a square cross section were fabricated from SU-8 negative photoresist (MicroChem Corp., Newton MA). The specific type of photoresist was chosen according to the required depth of the microfluidic channels (e.g. SU-8 2075 for channel depths between 75-150 μm). A spin coater (Laurell Technologies Corporation, North Wales PA) was used to coat silicon wafers (3" or 4"; Siltronix, France or Silicon Materials, Germany) to a specific thickness at spin speeds according to the manufacturer's manual. Wafers were heated to 140 °C to evaporate any organic solvents potentially remaining on the silicon wafer and left to cool for 5 min before proceeding with photoresist coating on the spin coater. After spinning, the photoresist was prebaked on a hotplate at 65 °C and 95 °C again for times indicated in the manufacturer's manual. The photomask with the channel design was placed on the wafer and both exposed to UV light using a mask aligner (Karl Suss MA45) to photo-cross-link exposed photoresist areas. The wafer was then baked again at 65 °C and 95 °C before development with mr-Dev 600 (micro resist technology GmbH, Berlin) and hard baking at 150 °C.

For rounded channel architectures (e.g. valves) we used the positive photoresist AZ 40XT (MicroChemicals GmbH, Ulm). This photoresist was used analogous to the SU-8 photoresist, but here positive photomasks were used. Silicon wafers were pre-coated with TI Prime (MicroChemicals GmbH) to improve adhesion of photoresist structures to the silicon substrate (alternatively this can be achieved by using an SU-8 photoresist of low viscosity, e.g. SU-8 2005). Rounded channels are made by a process called reflow by which the edges of the developed resist structures are heated beyond their softening point and thereby deform and become rounded.

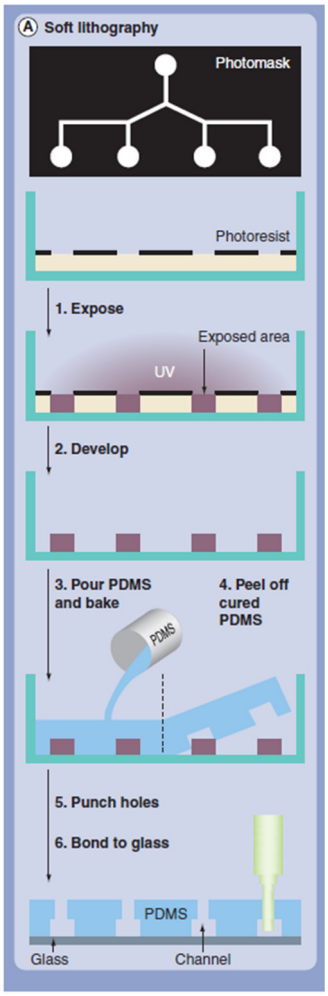

Figure 7.1 The workflow of soft lithography. Reproduced with permission **from** (Eicher and Merten, 2011). © Informa Healthcare

7.1.3 PDMS casting

Finished molds were placed in plastic Petri dishes which were then filled with a freshly prepared mixture of PDMS and curing agent (Sylgard 184 silicone elastomer kit, Dow Corning Corporation) at a ratio of 10:1 (w/w) and degassed in a desiccator until no gas bubbles could be seen floating to the surface anymore. The filled mold was then cross-linked overnight (or a minimum of two hours) in an oven at 65 °C.

7.1.4 PDMS membranes

PDMS membranes were produced by spinning liquid PDMS (elastomer:curing agent at a 20:1 ratio) onto a standard transparency slide (1/8 of a DIN A4 sheet) using a spin coater at 700 rpm for 30 s. The membranes were then baked at 65 °C over night.

7.1.5 Chip assembly

To produce a working microfluidic chip, the cast elastomer in the Petri dish was cut to shape using a scalpel and peeled out of the dish. Access ports for tubing and electrodes were punched out with a biopsy punch. The size of the biopsy punch was chosen according to the diameter of the tubing to be used in each experiment (e.g. a 0.75 mm punch was used in combination with a 0.8 mm tubing outer diameter). Pressurized air and adhesive tape was used to clear the chip of any residual PDMS debris left over from the punching out of access ports. Chips were bonded either to glass slides (Combinatorial chip: 50 × 70 × 1 mm, Menzel Gläser 50 OTG 90°, Thermo Fisher Scientific Inc., Germany ; Semi-compartmentalization chip: 70 × 70 × 0.17 mm, Paul Marienfeld GmbH & Co. KG, Germany) by exposing the structured surface and the glass slide or PDMS membrane to oxygen plasma generated in a plasma oven (Femto, Diener electronic GmbH + Co. KG, Germany) and then pressing the chip onto the glass slide/PDMS membrane before placing it at 65 °C for at least 1 min.

7.1.6 Channel surface treatment

Hydrophobic channel surfaces were created by flushing the chip with a 1% solution of 1H,1H,2H,2H-perfluorooctyltrichlorosilane (abcr GmbH & Co. KG, Germany) in Novec™ 7500 oil (3M Company, St. Paul MN). The channels were then rinsed with the oil used in the corresponding experiment. In some cases, aquapel (Autoserv, Germany) was used as an alternative to silane.

7.1.7 PTFE tubing

Polytetrafluoroethylene (PTFE) tubing was used in all microfluidic experiments to connect syringes containing liquids to inlet ports on the different chips (**Table 7.1**; Adtech Polymer Engineering Ltd, United Kingdom & APT Advanced Polymer Tubing GmbH, Germany).

Table 7.1 PTFE tubing sizes

Adtech Name	APT name/AWG size	Specifications (ID, OD; wall in mm)
UT3	P1000,30x0,101	0.3; 0.4; 0.10
UT6	P1000,60x0,101	0.6; 0.8; 0.10
HW30	AWG30S	0.32; 0.76; 0.23
TW24	AWG24T	0.59; 1.06; 0.25

7.2 Plug production

7.2.1 Cell encapsulation

Cells were harvested immediately before encapsulation by detaching cells with 10 mM EDTA (2 mL per T75 flask and 4 mL per T175 flask) solution (trypsin can act as a regulator of MMPs and should therefore be avoided (Vandooren et al., 2013)) after washing twice with PBS. The reaction was stopped by adding a 4-fold volume of PBS and sedimentation in a centrifuge at 1000 rpm for 5 min. Cells were then resuspended in 1 mL FS medium containing 0.1 % xanthan gum. An automated cell counter was used to determine cell concentration. Cells were then further diluted in FS medium containing xanthan gum and 0.02% Pluronic ® F-68 (Life Technologies GmbH, Germany) to a total volume of 6 mL with a cell concentration of 2×10^5-1×10^6 cells/mL. The cell suspension was then filtered using a 41 μm Steriflip ® nylon net filter (Merck Millipore) and cell density was determined again.

For cell encapsulation, 5 mL syringes were connected to PTFE tubing (UT6) without the use of needles. Rather, a PDMS cylinder was punched out of a monolithic PDMS piece with the use of a 5 mm biopsy punch and a connection port for the tubing created by puncturing the center of the cylinder with a 0.75 mm biopsy punch. The tubing was then connected to the PDMS cylinder and both glued with UV glue (Loctite UV glue, Dr. F. Krantz Rheinisches Mineralien-Kontor GmbH & Co. KG) to the tip of a 5 mL syringe in such a way that the end of the tubing is even with the end of the syringe barrel. A small magnetic stir bar was placed inside the syringe to enable stirring of the cell suspension during encapsulation with a magnetic stirrer (**Figure 3.2 C**). During cell encapsulation the cell syringe was continuously cooled with an ice pack.

7.2.2 Combinatorial plug production and incubation

5 mL syringes (BD) were freshly filled with the corresponding reagents for each experiment. Syringes were connected to HW30 PTFE tubing using a 27 gauge needle and placed on a syringe pumps (Harvard apparatus, Holliston MA or World Precision Instruments, Sarasota FL). All tubing was then "primed", i.e. the pumps were turned on until the liquid was visible at the end of the tubing. This step is performed to avoid air being trapped in the connection ports, which can cause problems when running the experiment. After channel surface treatment (described above) channels were filled with a dark blue dye to help in the alignment of valves contained in the Braille chip with pins on the Braille display. Once alignment was achieved, the Braille chip was fixed in position and all PTFE tubing connected to the syringes plugged into the connection

ports on the chip. Short pieces of tubing were connected to the waste outlets of the Braille chip. An additional short piece of UT6 tubing (20 cm) was connected to the sample outlet.

After connecting all tubing to the chip, the Braille chip control software (**Figure 3.5**) was started and all valves were tested for responsiveness. The short piece of UT6 tubing was then exchanged for a 6 m long stretch of UT6 tubing wrapped around a 1 L Schott bottle was connected to the sample outlet. This tubing served as incubation vessel for sample plugs. Plugs were produced by simultaneously infusing perfluorinated carrier oil Fluorinert ® FC-40 (Sigma-Aldrich, Germany) with 0.5% 1H,1H-perfluorooctanol 98% (PFO, abcr GmbH & Co. KG, Germany), aqueous phase and mineral oil (Sigma-Aldrich, Germany) as described in the Results section (section **3.2.2.2**). Generally, plugs containing mixtures of cells with two additional aqueous phases were produced at flow rates of 3 × 666-1100 µL/h and valve opening times of 1.5-2 s for the aqueous phase and 200 µL/h with valve opening times of 3 (with mineral oil) or 20 s (without mineral oil) for the carrier oil phase. After plug production finished, the end of this tubing was inserted into the plug inlet of the fusion chip and glued into position with Elastosil® E43 RTV-1 silicone rubber (Wacker Chemie AG, Germany) to seal the connection. Plugs were incubated in the tubing wrapped around the bottle for 48 hours at 37 °C and 5% CO_2 in a water saturated atmosphere.

7.2.3 Plug production for semi-compartmentalization

Plugs for the semi-compartmentalization approach were in principle generated in the same way as described above. Tubing containing plugs was glued to the semi-compartmentalization chip and dried overnight before loading the plugs on-chip. Additionally no mineral oil plugs were used in this setup. For some initial semi-compartmentalization experiments, we used an autosampler (Dionex UltiMate® 3000 Analytical Autosampler WPS-3000 SL, Thermo Fisher Scientific Inc.) to produce large plugs into UT3 tubing as published by Clausell-Tormos et al. (Clausell-Tormos et al., 2010). Samples were injected into the splitting chamber of a semi-compartmentalization chip (**Figure 5.2 C**) at 1000 µL/h while applying an aspirating flow rate of 800 µL/h from the adjacent outlet to split plugs into smaller volumes. Additionally, FC-40 carrier oil containing 1.5% PEG-PFPE was infused from a side channel to stabilize the loaded plugs and to reduce wetting.

7.3 Microscopy and fluorescence measurements

7.3.1 Light microscopy

We used a standard inverted light microscope (Eclipse Ti-S, Nikon GmbH., Germany) for imaging of microfluidic chips and their contents. A halogen fiber illuminator (Nikon Intensilight C-HGFI, Nikon GmbH, Germany) was used as a fluorescence light source in fluorescence microscopy. Images were acquired with a CCD camera (Hamamatsu ORCA-05G, Hamamatsu Photonics Deutschland GmbH, Germany) for long exposure times or a color high speed camera during microfluidic experiments with short exposure times (MotionBLITZ® EoSens® mini1, Mikrotron GmbH, Germany). We used a custom setup of μManager (https://www.micro-manager.org (Edelstein et al., 2001)) to control microscope components, such as the automated stage control (Prior ProScan III, Prior Scientific GmbH, Germany), shutters for bright field and fluorescence channels, as well as the CCD camera.

7.3.2 Optical setup for spectroscopic plug measurements

To perform spectroscopic readouts of plug contents we used a customized optical setup, a schematic of which is depicted in **Figure 7.2**. The optical setup comprises a standard inverted light microscope (Eclipse Ti-S, Nikon GmbH., Germany) attached to a vibration-reduced free optical breadboard. Three lasers with individual wavelengths (375 nm, 488 nm & 561 nm) allow simultaneous excitation of multiple fluorophores with corresponding excitation wavelengths. a standard inverted light microscope and three photomultiplier tubes (PMTs) to measure emitted fluorescent light in three wavelengths (blue, green, orange/red). Fluorescent measurements were performed either directly in the fusion channel or (if incubation was required) in the sample tubing. A custom LabView software was programmed for multi-color fluorescence readout in the range of hundreds of Hz for optimal readout and recording of fluorescent plug contents (Multi-channel data acquisition by Ramesh Utharala, Merten Group, EMBL Heidelberg). **Figure 7.3** shows the user interface of this new program. Recorded fluorescence data was analyzed in the statistical software R studio (R Studio Inc.) again using a custom software package (Federica Eduati, Saez-Rodriguz group, EMBL-EBI).

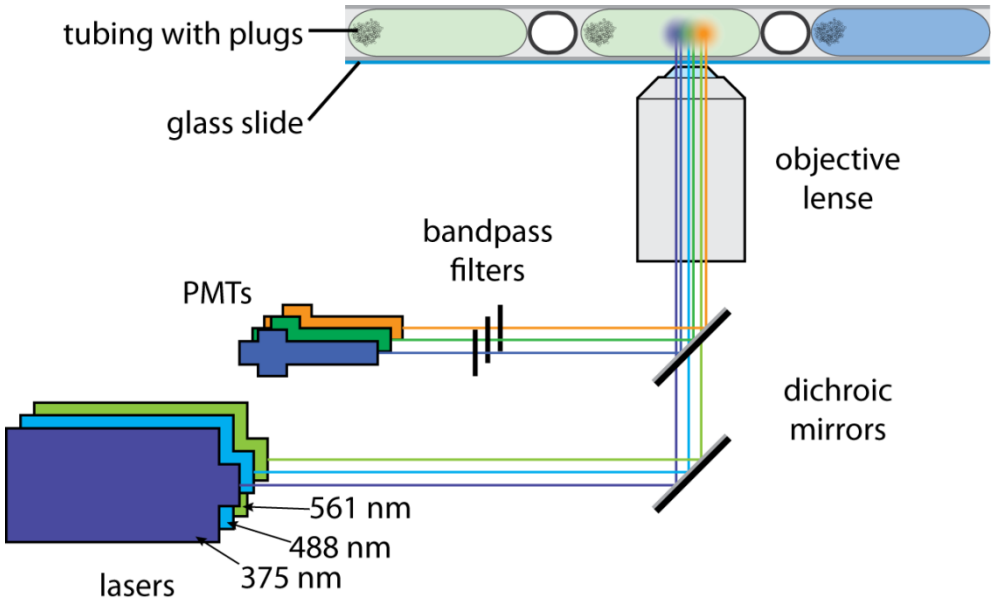

Figure 7.2 Scheme of the optical setup for fluorescent plug readout. Fluorescence of plugs in thin-walled PFTE tubing can be measured with PMTs after excitation by lasers in three different wavelengths (375 nm, 488 nm, 561 nm)

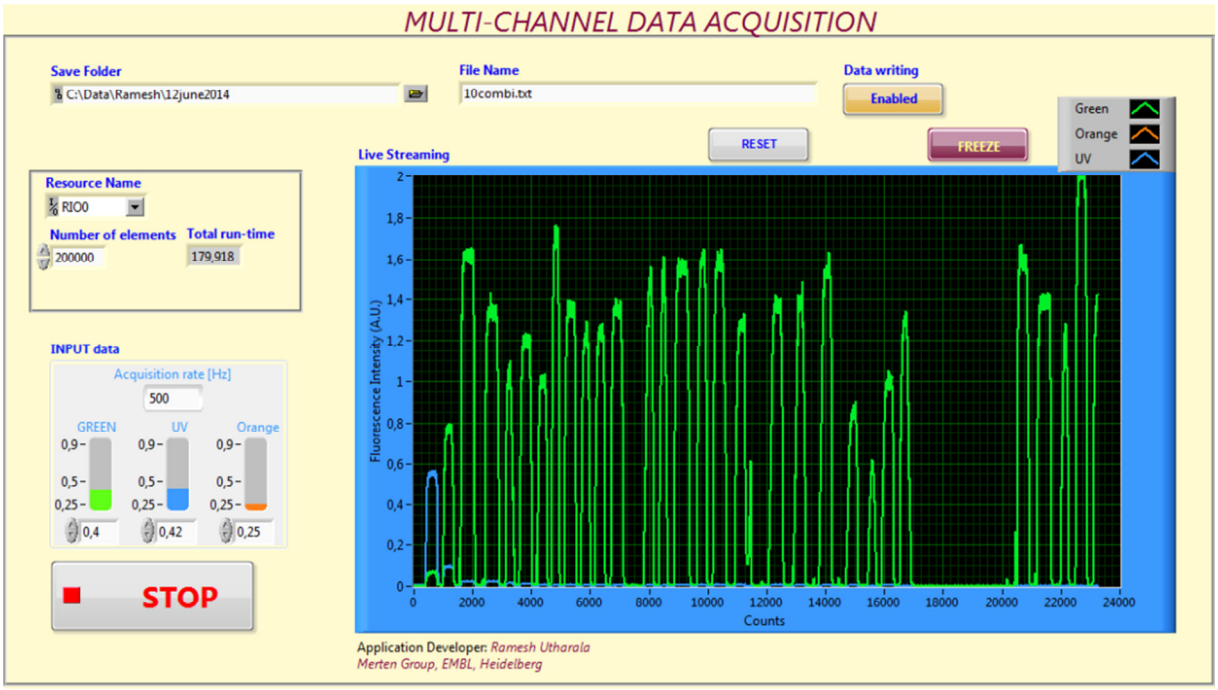

Figure 7.3 Screenshot of custom data acquisition software. This software allows simultaneous acquisition and recording of fluorescence intensity in three different channels.

7.3.3 Fluorescence measurements using a CCD camera

In order to conduct fluorescence measurements of plugs inside tubing, we used alternately triggered the bright field and fluorescence shutters at intervals of 300 ms and exposure times of 10 ms in a time-lapse sequence for the whole duration of one experiment.

7.3.4 Microtiter plate reader measurements

All microtiter plate reader experiments were carried out in a Tecan Safire^2 (Tecan Group, Ltd., Switzerland) or in a BioTek Synergy™ 4 (BioTek Instruments, Inc., Winooski VT).

7.4 Cell biology

7.4.1 HT1080 cells

HT1080 fibrosarcoma cells were purchased from ATCC® (CCL-121™ in the American Type Culture Collection; LGC Standards GmbH, Germany) and grown according to the company protocol.

7.4.2 HeLa cells

HeLa T-Rex™ cells were obtained as a courtesy of the Hentze group (Castello et al., 2012). These cells express GFP when treated with 1 μg/mL of tetracycline hydrochloride (Sigma-Aldrich, Germany).

7.4.3 Cell culture

Dulbecco's modified Eagle medium (DMEM; Life Technologies GmbH, Germany) containing 4.5 g/L D-glucose and L-glutamine and supplemented with sodium pyruvate 1 mM (Sigma-Aldrich, Germany), fetal bovine serum (FBS; Life Technologies GmbH, Germany) and penicillin/streptomycin (P/S; Life Technologies GmbH, Germany). DMEM was used for all standard tissue culture and in all experiments where not specifically indicated otherwise. Gibco® FreeStyle™ 293 Expression Medium (FS, Life Technologies GmbH, Germany) was supplemented with P/S and used in all experiments in which FBS would interfere, e.g. all experiments where cells were encapsulated or MMP FRET substrate measurements were made. Cells were thawed in 10 mL pre-warmed DMEM which was also used for ongoing tissue culture and incubated at 37 °C in a 5% CO_2 atmosphere saturated with water. To refresh the culture, cells were washed twice with phosphate buffered saline (PBS, EMBL lab kitchen) and incubated with trypsin-EDTA solution (1x; Sigma-Aldrich, Germany) or just 10 mM EDTA for up to 3 min at 37 °C. The reaction was then stopped with PBS and the cells spun down at 1000 rpm for 5 min at room temperature. The supernatant was removed and cells re-suspended in 1 mL of culture medium before splitting

the culture at ratios of 1:2 to 1:10. Cryostocks were made by freezing cells in complete DMEM supplemented with 5% DMSO in 1 mL cryotubes and stored at -80 °C.

7.4.4 Drugs

Table 7.2 Pathway drugs and their source. Drugs were dissolved in pure DMSO and stored at -20 °C

Name	Working concentration, µM	Source
5-methyl-2-(4-methylphenyl)-1H-benzimidazole (MPBD)	10	ChemBridge Corporation, San Diego CA
2-Amino-6-[2-(cyclopropylmethoxy)-6-hydroxyphenyl]-4-(4-piperidinyl)-3-pyridinecarbonitrile (ACHP)	1	Tocris Bioscience, Bristol UK
AZ 10417808	0.25	Tocris Bioscience, Bristol UK
Cyt387	5	Selleck Chemicals LLC, Houston TX
IKK-16	0.1	Selleck Chemicals LLC, Houston TX
Ivachtin	0.05	Tocris Bioscience, Bristol UK
IWR-1	5	Sigma-Aldrich, Germany
L-779,450	10	Tocris Bioscience, Bristol UK
Marimastat	50	Sigma-Aldrich, Germany
MK-2206	1	Selleck Chemicals LLC, Houston TX
Nutlin-3	30	Selleck Chemicals LLC, Houston TX
NVP-BSK805	0.1	Selleck Chemicals LLC, Houston TX
phorbol 12-myristate 13-acetate (PMA)	0.1	Sigma-Aldrich, Germany
PHT-427	25	Selleck Chemicals LLC, Houston TX
Pifithrin alpha	10	Sigma-Aldrich, Germany
Roscovitine	10	Sigma-Aldrich, Germany
SB590885	10	Selleck Chemicals LLC, Houston TX
Simvastatin	1	Sigma-Aldrich, Germany
Tunicamycin	5	Sigma-Aldrich, Germany
ZM306416	1	Tocris Bioscience, Bristol UK

7.4.5 Biologicals

All growth factors and cytokines (**Table 7.3**) were ordered from PeproTech (PeproTech Germany, Hamburg) and stock solutions were made according to company specifications for each individual compound. Aliquots were stored in working concentrations and volumes at 4 °C or -20 °C for long-term storage.

Table 7.3 Cytokines and growth factors

Compound name	Solvent	Working concentration
Bradykinin	0.1 M acetic acid	50 nM (50 ng/mL)
EGF	PBS + 0.1% BSA	16.1 nM (100 ng/mL)
IFN-β	PBS + 0.1% BSA	5 nM (100 ng/mL)
IFNγ	PBS + 0.1% BSA	592 pM (10 ng/mL)
IGF-1	PBS + 0.1% BSA	2.61 nM (20 ng/mL)
IL-10	5 mM Na-phosphate, pH 7.2	5.33 µM(100 ng/mL)
IL-1α	PBS + 0.1% BSA	554 pM (10 ng/mL)
IL-1β	PBS + 0.1% BSA	288 pM (5 ng/mL)
IL-6	PBS + 0.1% BSA	2.39 nM (50 ng/mL)
TGF-α	PBS + 0.1% BSA	4.5 nM (25 ng/mL)
TGF-β	10 mM citric acid, pH 3	391 pM (5 ng/mL)
TNF-α	PBS + 0.1% BSA	576 pM (10 ng/mL)

7.5 Data analysis

7.5.1 Image analysis

All image analysis in this thesis was conducted using FIJI (Fiji is just ImageJ). Image stitching was conducted with a FIJI plugin published by Preibisch et al.(Preibisch et al., 2009). Large sets of images recorded in a predefined grid with 20% overlap between frames were stitched together by using the "Grid/collection stitching" option of the plugin. We used either the linear blending or max. intensity fusion methods and computed the overlap with subpixel accuracy.

7.5.2 PMT data analysis

Data analysis for plug fluorescence was conducted with the BraDiPlus R package developed specifically for this purpose (Federica Eduati, Saez-Rodriguz group, EMBL-EBI). It allows semi-automated data analysis of raw fluorescence data coming from PMT measurements on our microfluidics workstation. The R package was routinely used to load fluorescence data and plot an overview of all data collected in an experiment. Based on this visual representation, we defined a fluorescence threshold above background signal levels and a minimal distance parameter for the label and assay channels in order to carry out automated label and sample peak identification. All identified sample sequences were then plotted individually in order to check the quality of peak detection.

8 REFERENCES

Abate, A.R., T. Hung, P. Mary, J.J. Agresti, and D.A. Weitz. 2010. High-throughput injection with microfluidics using picoinjectors. *Proc Natl Acad Sci USA*. 107:19163-19166.

Adamson, D.N., D. Mustafi, J.X.J. Zhang, B. Zheng, and R.F. Ismagilov. 2006. Production of arrays of chemically distinct nanolitre plugs via repeated splitting in microfluidic devices. *Lab Chip*. 6:1178-1186.

Agresti, J.J., E. Antipov, A.R. Abate, K. Ahn, A.C. Rowat, J.C. Baret, M. Marquez, A.M. Klibanov, A.D. Griffiths, and D.A. Weitz. 2010. Ultrahigh-throughput screening in drop-based microfluidics for directed evolution. *Proc Natl Acad Sci USA*. 107:4004-4009.

Ahn, K., J. Agresti, H. Chong, M. Marquez, and D.A. Weitz. 2006. Electrocoalescence of drops synchronized by size-dependent flow in microfluidic channels. *Appl Phys Lett*. 88.

Al-Lazikani, B., U. Banerji, and P. Workman. 2012. Combinatorial drug therapy for cancer in the post-genomic era. *Nat Biotech*. 30:679-692.

Alaimo, P.J., M.A. Shogren-Knaak, and K.M. Shokat. 2001. Chemical genetic approaches for the elucidation of signaling pathways. *Curr Opin Chem Biol*. 5:360-367.

Anna, S.L., N. Bontoux, and H.A. Stone. 2003. Formation of dispersions using "flow focusing" in microchannels. *Appl Phys Lett*. 82:364-366.

Avila, K., D. Moxey, A. de Lozar, M. Avila, D. Barkley, and B. Hof. 2011. The onset of turbulence in pipe flow. *Science*. 333:192-196.

Baffert, F., C.H. Regnier, A. De Pover, C. Pissot-Soldermann, G.A. Tavares, F. Blasco, J. Brueggen, P. Chene, P. Drueckes, D. Erdmann, P. Furet, M. Gerspacher, M. Lang, D. Ledieu, L. Nolan, S. Ruetz, J. Trappe, E. Vangrevelinghe, M. Wartmann, L. Wyder, F. Hofmann, and T. Radimerski. 2010. Potent and selective inhibition of polycythemia by the quinoxaline JAK2 inhibitor NVP-BSK805. *Mol Cancer Ther*. 9:1945-1955.

Baret, J.C., O.J. Miller, V. Taly, M. Ryckelynck, A. El-Harrak, L. Frenz, C. Rick, M.L. Samuels, J.B. Hutchison, J.J. Agresti, D.R. Link, D.A. Weitz, and A.D. Griffiths. 2009. Fluorescence-activated droplet sorting (FADS): efficient microfluidic cell sorting based on enzymatic activity. *Lab Chip*. 9:1850-1858.

Barkho, B.Z., A.E. Munoz, X. Li, L. Li, L.A. Cunningham, and X. Zhao. 2008. Endogenous Matrix Metalloproteinase (MMP)-3 and MMP-9 Promote the Differentiation and Migration of Adult Neural Progenitor Cells in Response to Chemokines. *STEM CELLS*. 26:3139-3149.

Bliss, C.I. 1939. THE TOXICITY OF POISONS APPLIED JOINTLY1. *Annals of Applied Biology*. 26:585-615.

Bodas, D., and C. Khan-Malek. 2006. Formation of more stable hydrophilic surfaces of PDMS by plasma and chemical treatments. *Microelectron Eng*. 83:1277-1279.

Boedicker, J.Q., L. Li, T.R. Kline, and R.F. Ismagilov. 2008. Detecting bacteria and determining their susceptibility to antibiotics by stochastic confinement in nanoliter droplets using plug-based microfluidics. *Lab Chip*. 8:1265-1272.

Borowiak, M., R. Maehr, S. Chen, A.E. Chen, W. Tang, J.L. Fox, S.L. Schreiber, and D.A. Melton. 2009. Small molecule efficiently direct endodermal differentiation of mouse and human embryonic stem cells. *Cell Stem Cell.* 4:348-358.

Brouzes, E., M. Medkova, N. Savenelli, D. Marran, M. Twardowski, J.B. Hutchison, J.M. Rothberg, D.R. Link, N. Perrimon, and M.L. Samuels. 2009. Droplet microfluidic technology for single-cell high-throughput screening. *Proc Natl Acad Sci USA.* 106:14195-14200.

Carlson, S.M., and F.M. White. 2011. Using small molecules and chemical genetics to interrogate signaling networks. *ACS Chem Biol.* 6:75-85.

Castello, A., B. Fischer, K. Eichelbaum, R. Horos, B.M. Beckmann, C. Strein, N.E. Davey, D.T. Humphreys, T. Preiss, L.M. Steinmetz, J. Krijgsveld, and M.W. Hentze. 2012. Insights into RNA Biology from an Atlas of Mammalian mRNA-Binding Proteins. *Cell.* 149:1393-1406.

Chatterjee, M.S., J.E. Purvis, L.F. Brass, and S.L. Diamond. 2010. Pairwise agonist scanning predicts cellular signaling responses to combinatorial stimuli. *Nat Biotech.* 28:727-732.

Chen, B., M.E. Dodge, W. Tang, J. Lu, Z. Ma, C.W. Fan, S. Wei, W. Hao, J. Kilgore, N.S. Williams, M.G. Roth, J.F. Amatruda, C. Chen, and L. Lum. 2009. Small molecule-mediated disruption of Wnt-dependent signaling in tissue regeneration and cancer. *Nat Chem Biol.* 5:100-107.

Chen, D., W. Du, Y. Liu, W. Liu, A. Kuznetsov, F.E. Mendez, L.H. Philipson, and R.F. Ismagilov. 2008. The chemistrode: A droplet-based microfluidic device for stimulation and recording with high temporal, spatial, and chemical resolution. *Proc Natl Acad Sci USA.* 105:16843-16848.

Chen, D.L., C.J. Gerdts, and R.F. Ismagilov. 2005. Using microfluidics to observe the effect of mixing on nucleation of protein crystals. *J Am Chem Soc.* 127:9672-9673.

Chen, D.L., and R.F. Ismagilov. 2006. Microfluidic cartridges preloaded with nanoliter plugs of reagents: an alternative to 96-well plates for screening. *Curr Opin Chem Biol.* 10:226-231.

Choudhury, D., D. van Noort, C. Iliescu, B. Zheng, K.L. Poon, S. Korzh, V. Korzh, and H. Yu. 2012. Fish and Chips: a microfluidic perfusion platform for monitoring zebrafish development. *Lab Chip.* 12:892-900.

Chu, L.Y., A.S. Utada, R.K. Shah, J.W. Kim, and D.A. Weitz. 2007. Controllable monodisperse multiple emulsions. *Angew Chem Int Ed Engl.* 46:8970-8974.

Clausell-Tormos, J., A.D. Griffiths, and C.A. Merten. 2010. An automated two-phase microfluidic system for kinetic analyses and the screening of compound libraries. *Lab Chip.* 10:1302-1307.

Clausell-Tormos, J., D. Lieber, J.C. Baret, A. El-Harrak, O.J. Miller, L. Frenz, J. Blouwolff, K.J. Humphry, S. Koster, H. Duan, C. Holtze, D.A. Weitz, A.D. Griffiths, and C.A. Merten. 2008. Droplet-based microfluidic platforms for the encapsulation and screening of Mammalian cells and multicellular organisms. *Chem Biol.* 15:427-437.

Cokol, M., H.N. Chua, M. Tasan, B. Mutlu, Z.B. Weinstein, Y. Suzuki, M.E. Nergiz, M. Costanzo, A. Baryshnikova, G. Giaever, C. Nislow, C.L. Myers, B.J. Andrews, C. Boone, and F.P. Roth. 2011. Systematic exploration of synergistic drug pairs. *Mol Syst Biol.* 7:544.

Cortez, D.M., M.D. Feldman, S. Mummidi, A.J. Valente, B. Steffensen, M. Vincenti, J.L. Barnes, and B. Chandrasekar. 2007. IL-17 stimulates MMP-1 expression in primary human cardiac fibroblasts via p38 MAPK- and ERK1/2-dependent C/EBP-beta , NF-kappaB, and AP-1 activation. *Am J Physiol Heart Circ Physiol.* 293:H3356-3365.

Coussens, L.M., B. Fingleton, and L.M. Matrisian. 2002. Matrix metalloproteinase inhibitors and cancer: trials and tribulations. *Science*. 295:2387-2392.

Darbyshire, J.H. 1996. Delta: a randomised double-blind controlled trial comparing combinations of zidovudine plus didanosine or zalcitabine with zidovudine alone in HIV-infected individuals. *The Lancet*. 348:283-291.

Dove, A. 1999. Drug screening[mdash]beyond the bottleneck. *Nat Biotech*. 17:859-863.

Duffy, D.C., J.C. McDonald, O.J. Schueller, and G.M. Whitesides. 1998. Rapid Prototyping of Microfluidic Systems in Poly(dimethylsiloxane). *Anal Chem*. 70:4974-4984.

Edelstein, A., N. Amodaj, K. Hoover, R. Vale, and N. Stuurman. 2001. Computer Control of Microscopes Using μManager. *In* Current Protocols in Molecular Biology. John Wiley & Sons, Inc.

Eggers, J., J.R. Lister, and H.A. Stone. 1999. Coalescence of liquid drops. *J Fluid Mech*. 401:293-310.

Eicher, D., and C.A. Merten. 2011. Microfluidic devices for diagnostic applications. *Expert Rev Mol Diagn*. 11:505-519.

El Debs, B., R. Utharala, I.V. Balyasnikova, A.D. Griffiths, and C.A. Merten. 2012. Functional single-cell hybridoma screening using droplet-based microfluidics. *Proc Natl Acad Sci USA*. 109:11570-11575.

Eow, J.S., and M. Ghadiri. 2003. Drop-drop coalescence in an electric field: the effects of applied electric field and electrode geometry. *Colloid Surface A*. 219:253-279.

Evenou, F., J.M. Di Meglio, B. Ladoux, and P. Hersen. 2012. Micro-patterned porous substrates for cell-based assays. *Lab Chip*. 12:1717-1722.

Eyer, K., P. Kuhn, C. Hanke, and P.S. Dittrich. 2012. A microchamber array for single cell isolation and analysis of intracellular biomolecules. *Lab Chip*. 12:765-772.

Flores, G.V., H. Duan, H. Yan, R. Nagaraj, W. Fu, Y. Zou, M. Noll, and U. Banerjee. 2000. Combinatorial Signaling in the Specification of Unique Cell Fates. *Cell*. 103:75-85.

Frenz, L., K. Blank, E. Brouzes, and A.D. Griffiths. 2009. Reliable microfluidic on-chip incubation of droplets in delay-lines. *Lab Chip*. 9:1344-1348.

Fukuda, H., S. Mochizuki, H. Abe, H.J. Okano, C. Hara-Miyauchi, H. Okano, N. Yamaguchi, M. Nakayama, J. D'Armiento, and Y. Okada. 2011. Host-derived MMP-13 exhibits a protective role in lung metastasis of melanoma cells by local endostatin production. *Brit J Cancer*. 105:1615-1624.

Funfak, A., A. Brosing, M. Brand, and J.M. Kohler. 2007. Micro fluid segment technique for screening and development studies on Danio rerio embryos. *Lab Chip*. 7:1132-1138.

Futai, N., W. Gu, J.W. Song, and S. Takayama. 2006. Handheld recirculation system and customized media for microfluidic cell culture. *Lab Chip*. 6:149-154.

Gervasi, D.C., A. Raz, M. Dehem, M. Yang, M. Kurkinen, and R. Fridman. 1996. Carbohydrate-Mediated Regulation of Matrix Metalloproteinase-2 Activation in Normal Human Fibroblasts and Fibrosarcoma Cells. *Biochem Biophys Res Commun.* 228:530-538.

Giambernardi, T.A., G.M. Grant, G.P. Taylor, R.J. Hay, V.M. Maher, J.J. McCormick, and R.J. Klebe. 1998. Overview of matrix metalloproteinase expression in cultured human cells. *Matrix Biol.* 16:483-496.

Gómez-Sjöberg, R., A.A. Leyrat, D.M. Pirone, C.S. Chen, and S.R. Quake. 2007. Versatile, Fully Automated, Microfluidic Cell Culture System. *Anal Chem.* 79:8557-8563.

Gu, W., X.Y. Zhu, N. Futai, B.S. Cho, and S. Takayama. 2004. Computerized microfluidic cell culture using elastomeric channels and Braille displays. *Proc Natl Acad Sci USA.* 101:15861-15866.

Gueders, M.M., M. Balbin, N. Rocks, J.-M. Foidart, P. Gosset, R. Louis, S. Shapiro, C. Lopez-Otin, A. Noël, and D.D. Cataldo. 2005. Matrix Metalloproteinase-8 Deficiency Promotes Granulocytic Allergen-Induced Airway Inflammation. *J Immunol.* 175:2589-2597.

Haas, T.L., M. Milkiewicz, S.J. Davis, A.L. Zhou, S. Egginton, M.D. Brown, J.A. Madri, and O. Hudlicka. 2000. Matrix metalloproteinase activity is required for activity-induced angiogenesis in rat skeletal muscle. *Am J Physiol* 279:H1540-H1547.

Han, Y.P., T.L. Tuan, H. Wu, M. Hughes, and W.L. Garner. 2001. TNF-alpha stimulates activation of pro-MMP2 in human skin through NF-(kappa)B mediated induction of MT1-MMP. *J Cell Sci.* 114:131-139.

Harris, J.E., M. Fernandez-Vilaseca, P.T. Elkington, D.E. Horncastle, M.B. Graeber, and J.S. Friedland. 2007. IFNgamma synergizes with IL-1beta to up-regulate MMP-9 secretion in a cellular model of central nervous system tuberculosis. *FASEB J.* 21:356-365.

He, M.Y., J.S. Edgar, G.D.M. Jeffries, R.M. Lorenz, J.P. Shelby, and D.T. Chiu. 2005. Selective encapsulation of single cells and subcellular organelles into picoliter- and femtoliter-volume droplets. *Anal Chem.* 77:1539-1544.

Hennequin, L.F., A.P. Thomas, C. Johnstone, E.S. Stokes, P.A. Ple, J.J. Lohmann, D.J. Ogilvie, M. Dukes, S.R. Wedge, J.O. Curwen, J. Kendrew, and C. Lambert-van der Brempt. 1999. Design and structure-activity relationship of a new class of potent VEGF receptor tyrosine kinase inhibitors. *J Med Chem.* 42:5369-5389.

Heo, Y.S., L.M. Cabrera, J.W. Song, N. Futai, Y.-C. Tung, G.D. Smith, and S. Takayama. 2006. Characterization and Resolution of Evaporation-Mediated Osmolality Shifts That Constrain Microfluidic Cell Culture in Poly(dimethylsiloxane) Devices. *Anal Chem.* 79:1126-1134.

Heyries, K.A., C. Tropini, M. Vaninsberghe, C. Doolin, O.I. Petriv, A. Singhal, K. Leung, C.B. Hughesman, and C.L. Hansen. 2011. Megapixel digital PCR. *Nat Methods.* 8:649-651.

Hirai, H., H. Sootome, Y. Nakatsuru, K. Miyama, S. Taguchi, K. Tsujioka, Y. Ueno, H. Hatch, P.K. Majumder, B.S. Pan, and H. Kotani. 2010. MK-2206, an allosteric Akt inhibitor, enhances antitumor efficacy by standard chemotherapeutic agents or molecular targeted drugs in vitro and in vivo. *Mol Cancer Ther.* 9:1956-1967.

Hotary, K.B., E.D. Allen, P.C. Brooks, N.S. Datta, M.W. Long, and S.J. Weiss. 2003. Membrane Type I Matrix Metalloproteinase Usurps Tumor Growth Control Imposed by the Three-Dimensional Extracellular Matrix. *Cell*. 114:33-45.

Hou, P.P., Y.Q. Li, X. Zhang, C. Liu, J.Y. Guan, H.G. Li, T. Zhao, J.Q. Ye, W.F. Yang, K. Liu, J. Ge, J. Xu, Q. Zhang, Y. Zhao, and H.K. Deng. 2013. Pluripotent Stem Cells Induced from Mouse Somatic Cells by Small-Molecule Compounds. *Science*. 341:651-654.

Hu, J., P.E. Van den Steen, Q.X. Sang, and G. Opdenakker. 2007. Matrix metalloproteinase inhibitors as therapy for inflammatory and vascular diseases. *Nat Rev Drug Discov*. 6:480-498.

Huebner, A., D. Bratton, G. Whyte, M. Yang, A.J. deMello, C. Abell, and F. Hollfelder. 2009. Static microdroplet arrays: a microfluidic device for droplet trapping, incubation and release for enzymatic and cell-based assays. *Lab Chip*. 9:692-698.

Huh, D., D.C. Leslie, B.D. Matthews, J.P. Fraser, S. Jurek, G.A. Hamilton, K.S. Thorneloe, M.A. McAlexander, and D.E. Ingber. 2012a. A Human Disease Model of Drug Toxicity–Induced Pulmonary Edema in a Lung-on-a-Chip Microdevice. *Sci Transl Med*. 4:159ra147.

Huh, D., B.D. Matthews, A. Mammoto, M. Montoya-Zavala, H.Y. Hsin, and D.E. Ingber. 2010. Reconstituting organ-level lung functions on a chip. *Science*. 328:1662-1668.

Huh, D., Y.-s. Torisawa, G.A. Hamilton, H.J. Kim, and D.E. Ingber. 2012b. Microengineered physiological biomimicry: Organs-on-Chips. *Lab Chip*. 12:2156-2164.

Huhtala, P., A. Tuuttila, L.T. Chow, J. Lohi, J. Keski-Oja, and K. Tryggvason. 1991. Complete structure of the human gene for 92-kDa type IV collagenase. Divergent regulation of expression for the 92- and 72-kilodalton enzyme genes in HT-1080 cells. *J Biol Chem*. 266:16485-16490.

Jakiela, S., T.S. Kaminski, O. Cybulski, D.B. Weibel, and P. Garstecki. 2013. Bacterial growth and adaptation in microdroplet chemostats. *Angew Chem Int Ed*. 52:8908-8911.

Jeon, N.L., S.K.W. Dertinger, D.T. Chiu, I.S. Choi, A.D. Stroock, and G.M. Whitesides. 2000. Generation of Solution and Surface Gradients Using Microfluidic Systems. *Langmuir*. 16:8311-8316.

Joensson, H.N., M.L. Samuels, E.R. Brouzes, M. Medkova, M. Uhlen, D.R. Link, and H. Andersson-Svahn. 2009. Detection and Analysis of Low-Abundance Cell-Surface Biomarkers Using Enzymatic Amplification in Microfluidic Droplets. *Angew Chem Int Edit*. 48:2518-2521.

Juncker, D., H. Schmid, and E. Delamarche. 2005. Multipurpose microfluidic probe. *Nat Mater*. 4:622-628.

Kessenbrock, K., V. Plaks, and Z. Werb. 2010. Matrix metalloproteinases: regulators of the tumor microenvironment. *Cell*. 141:52-67.

Kolb, H.C., M.G. Finn, and K.B. Sharpless. 2001. Click chemistry: Diverse chemical function from a few good reactions. *Angew Chem Int Edit*. 40:2004-+.

Komarov, P.G., E.A. Komarova, R.V. Kondratov, K. Christov-Tselkov, J.S. Coon, M.V. Chernov, and A.V. Gudkov. 1999. A chemical inhibitor of p53 that protects mice from the side effects of cancer therapy. *Science*. 285:1733-1737.

Kravchenko, D.V., Y.A. Kuzovkova, V.M. Kysil, S.E. Tkachenko, S. Maliarchouk, I.M. Okun, K.V. Balakin, and A.V. Ivachtchenko. 2005. Synthesis and structure-activity relationship of 4-substituted 2-(2-

acetyloxyethyl)-8-(morpholine-4-sulfonyl)pyrrolo[3,4-c]quinoline-1,3-diones as potent caspase-3 inhibitors. *J Med Chem*. 48:3680-3683.

Kusi-Appiah, A.E., N. Vafai, P.J. Cranfill, M.W. Davidson, and S. Lenhert. 2012. Lipid multilayer microarrays for in vitro liposomal drug delivery and screening. *Biomaterials*. 33:4187-4194.

Lehar, J., G.R. Zimmermann, A.S. Krueger, R.A. Molnar, J.T. Ledell, A.M. Heilbut, G.F. Short, 3rd, L.C. Giusti, G.P. Nolan, O.A. Magid, M.S. Lee, A.A. Borisy, B.R. Stockwell, and C.T. Keith. 2007. Chemical combination effects predict connectivity in biological systems. *Mol Sys Biol*. 3:80.

Lei, Y., Y. Liu, W. Wang, W. Wu, and Z. Li. 2011. Studies on Parylene C-caulked PDMS (pcPDMS) for low permeability required microfluidics applications. *Lab Chip*. 11:1385-1388.

Li, A., S. Dubey, M.L. Varney, B.J. Dave, and R.K. Singh. 2003. IL-8 directly enhanced endothelial cell survival, proliferation, and matrix metalloproteinases production and regulated angiogenesis. *J Immunol*. 170:3369-3376.

Li Jeon, N., H. Baskaran, S.K.W. Dertinger, G.M. Whitesides, L. Van De Water, and M. Toner. 2002. Neutrophil chemotaxis in linear and complex gradients of interleukin-8 formed in a microfabricated device. *Nat Biotech*. 20:826-830.

Li, L., J.Q. Boedicker, and R.F. Ismagilov. 2007. Using a multijunction microfluidic device to inject substrate into an array of preformed plugs without cross-contamination: Comparing theory and experiments. *Anal Chem*. 79:2756-2761.

Lin, W.C., Y.C. Chuang, Y.S. Chang, M.D. Lai, Y.N. Teng, I.J. Su, C.C. Wang, K.H. Lee, and J.H. Hung. 2012. Endoplasmic reticulum stress stimulates p53 expression through NF-kappaB activation. *PloS one*. 7:e39120.

Link, D.R., S.L. Anna, D.A. Weitz, and H.A. Stone. 2004. Geometrically Mediated Breakup of Drops in Microfluidic Devices. *Phys Rev Lett*. 92:054503.

Link, D.R., E. Grasland-Mongrain, A. Duri, F. Sarrazin, Z. Cheng, G. Cristobal, M. Marquez, and D.A. Weitz. 2006. Electric Control of Droplets in Microfluidic Devices. *Angew Chem Int Ed*. 45:2556-2560.

Lipinski, C.A., F. Lombardo, B.W. Dominy, and P.J. Feeney. 2012. Experimental and computational approaches to estimate solubility and permeability in drug discovery and development settings. *Adv Drug Deliver Rev*. 64:4-17.

Loewe, S. 1928. Die quantitativen Probleme der Pharmakologie. *Ergebnisse der Physiologie*. 27:47-187.

Lohi, J., K. Lehti, J. Westermarck, V.M. Kahari, and J. Keski-Oja. 1996. Regulation of membrane-type matrix metalloproteinase-1 expression by growth factors and phorbol 12-myristate 13-acetate. *Eur J Biochem*. 239:239-247.

Lucchetta, E.M., J.H. Lee, L.A. Fu, N.H. Patel, and R.F. Ismagilov. 2005. Dynamics of Drosophila embryonic patterning network perturbed in space and time using microfluidics. *Nature*. 434:1134-1138.

Macarron, R., M.N. Banks, D. Bojanic, D.J. Burns, D.A. Cirovic, T. Garyantes, D.V. Green, R.P. Hertzberg, W.P. Janzen, J.W. Paslay, U. Schopfer, and G.S. Sittampalam. 2011. Impact of high-throughput screening in biomedical research. *Nat Rev Drug Discov.* 10:188-195.

Malo, N., J.A. Hanley, S. Cerquozzi, J. Pelletier, and R. Nadon. 2006. Statistical practice in high-throughput screening data analysis. *Nat Biotech.* 24:167-175.

Manz, A., N. Graber, and H.M. Widmer. 1990. Miniaturized total chemical analysis systems: A novel concept for chemical sensing. *Sens Actuators, B.* 1:244-248.

Martin, A.J., and R.L. Synge. 1941. A new form of chromatogram employing two liquid phases: A theory of chromatography. 2. Application to the micro-determination of the higher monoamino-acids in proteins. *Biochem J.* 35:1358-1368.

Martin, K., T. Henkel, V. Baier, A. Grodrian, T. Schon, M. Roth, J. Michael Kohler, and J. Metze. 2003. Generation of larger numbers of separated microbial populations by cultivation in segmented-flow microdevices. *Lab Chip.* 3:202-207.

Martin, M.D., and L.M. Matrisian. 2007. The other side of MMPs: protective roles in tumor progression. *Cancer Metastasis Rev.* 26:717-724.

Martinez, A.W., S.T. Phillips, M.J. Butte, and G.M. Whitesides. 2007. Patterned paper as a platform for inexpensive, low-volume, portable bioassays. *Angew Chem Int Edit.* 46:1318-1320.

Mathews Griner, L.A., R. Guha, P. Shinn, R.M. Young, J.M. Keller, D. Liu, I.S. Goldlust, A. Yasgar, C. McKnight, M.B. Boxer, D.Y. Duveau, J.K. Jiang, S. Michael, T. Mierzwa, W. Huang, M.J. Walsh, B.T. Mott, P. Patel, W. Leister, D.J. Maloney, C.A. Leclair, G. Rai, A. Jadhav, B.D. Peyser, C.P. Austin, S.E. Martin, A. Simeonov, M. Ferrer, L.M. Staudt, and C.J. Thomas. 2014. High-throughput combinatorial screening identifies drugs that cooperate with ibrutinib to kill activated B-cell-like diffuse large B-cell lymphoma cells. *Proc Natl Acad Sci USA.* 111:2349-2354.

Mazutis, L., J.C. Baret, and A.D. Griffiths. 2009. A fast and efficient microfluidic system for highly selective one-to-one droplet fusion. *Lab Chip.* 9:2665-2672.

Meier, M., E.M. Lucchetta, and R.F. Ismagilov. 2010. Chemical stimulation of the Arabidopsis thaliana root using multi-laminar flow on a microfluidic chip. *Lab Chip.* 10:2147-2153.

Meijer, L., A. Borgne, O. Mulner, J.P. Chong, J.J. Blow, N. Inagaki, M. Inagaki, J.G. Delcros, and J.P. Moulinoux. 1997. Biochemical and cellular effects of roscovitine, a potent and selective inhibitor of the cyclin-dependent kinases cdc2, cdk2 and cdk5. *Eur J Biochem.* 243:527-536.

Meuillet, E.J., S. Zuohe, R. Lemos, N. Ihle, J. Kingston, R. Watkins, S.A. Moses, S. Zhang, L. Du-Cuny, R. Herbst, J.J. Jacoby, L.L. Zhou, A.M. Ahad, E.A. Mash, D.L. Kirkpatrick, and G. Powis. 2010. Molecular pharmacology and antitumor activity of PHT-427, a novel Akt/phosphatidylinositide-dependent protein kinase 1 pleckstrin homology domain inhibitor. *Mol Cancer Ther.* 9:706-717.

Millet, L.J., and M.U. Gillette. 2012. New perspectives on neuronal development via microfluidic environments. *Trends Neurosci.* 35:752-761.

Moll, U.M., G.L. Youngleib, K.B. Rosinski, and J.P. Quigley. 1990. Tumor Promoter-stimulated Mr 92,000 Gelatinase Secreted by Normal and Malignant Human Cells: Isolation and Characterization of the Enzyme from HT1080 Tumor Cells. *Cancer research*. 50:6162-6170.

Morel, M., D. Bartolo, J.-C. Galas, M. Dahan, and V. Studer. 2009. Microfluidic stickers for cell- and tissue-based assays in microchannels. *Lab Chip*. 9:1011-1013.

Mott, J.D., and Z. Werb. 2004. Regulation of matrix biology by matrix metalloproteinases. *Curr Opin Cell Biol*. 16:558-564.

Mukhopadhyay, R. 2007. When PDMS isn't the best. What are its weaknesses, and which other polymers can researchers add to their toolboxes? *Anal Chem*. 79:3248-3253.

Nagase, H., R. Visse, and G. Murphy. 2006. Structure and function of matrix metalloproteinases and TIMPs. *Cardiovasc Res*. 69:562-573.

Nair, R.R., H. Avila, X. Ma, Z. Wang, M. Lennartz, B.G. Darnay, D.D. Boyd, and C. Yan. 2008. A novel high-throughput screening system identifies a small molecule repressive for matrix metalloproteinase-9 expression. *Mol Pharmacol*. 73:919-929.

Nall, J.R., and J.W. Lathrop. 1958. Photolithographic fabrication techniques for transistors which are an integral part of a printed circuit. *Electron Devices, IRE Transactions on*. 5:117-117.

Niu, X., S. Gulati, J.B. Edel, and A.J. deMello. 2008. Pillar-induced droplet merging in microfluidic circuits. *Lab Chip*. 8:1837-1841.

Okada, M., H. Yamawaki, and Y. Hara. 2010. Angiotensin II enhances interleukin-1 beta-induced MMP-9 secretion in adult rat cardiac fibroblasts. *J Vet Med Sci*. 72:735-739.

Okada, Y., Y. Gonoji, K. Naka, K. Tomita, I. Nakanishi, K. Iwata, K. Yamashita, and T. Hayakawa. 1992. Matrix metalloproteinase 9 (92-kDa gelatinase/type IV collagenase) from HT 1080 human fibrosarcoma cells. Purification and activation of the precursor and enzymic properties. *J Biol Chem*. 267:21712-21719.

Overall, C.M., and O. Kleifeld. 2006. Tumour microenvironment - Opinion - Validating matrix metalloproteinases as drug targets and anti-targets for cancer therapy. *Nat Rev Cancer*. 6:227-239.

Overall, C.M., and C. Lopez-Otin. 2002. Strategies for MMP inhibition in cancer: innovations for the post-trial era. *Nat Rev Cancer*. 2:657-672.

Palmer, A.C., and R. Kishony. 2013. Understanding, predicting and manipulating the genotypic evolution of antibiotic resistance. *Nat Rev Genet*. 14:243-248.

Pardanani, A., T. Lasho, G. Smith, C.J. Burns, E. Fantino, and A. Tefferi. 2009. CYT387, a selective JAK1/JAK2 inhibitor: in vitro assessment of kinase selectivity and preclinical studies using cell lines and primary cells from polycythemia vera patients. *Leukemia*. 23:1441-1445.

Petit, V., G. Massonnet, Z. Maciorowski, J. Touhami, A. Thuleau, F. Nemati, J. Laval, S. Chateau-Joubert, J.-L. Servely, D. Vallerand, J.-J. Fontaine, N. Taylor, J.-L. Battini, M. Sitbon, and D. Decaudin. 2013. Optimization of tumor xenograft dissociation for the profiling of cell surface markers and nutrient transporters. *Lab Invest*. 93:611-621.

Portela, V.M., G. Zamberlam, and C.A. Price. 2010. Cell plating density alters the ratio of estrogenic to progestagenic enzyme gene expression in cultured granulosa cells. *Fertil Steril.* 93:2050-2055.

Preibisch, S., S. Saalfeld, and P. Tomancak. 2009. Globally optimal stitching of tiled 3D microscopic image acquisitions. *Bioinformatics.* 25:1463-1465.

Proudfoot, J.R. 2005. The evolution of synthetic oral drug properties. *Bioorg Med Chem Lett.* 15:1087-1090.

Qasaimeh, M.A., S.G. Ricoult, and D. Juncker. 2013. Microfluidic probes for use in life sciences and medicine. *Lab Chip.* 13:40-50.

Randall, G.C., and P.S. Doyle. 2005. Permeation-driven flow in poly(dimethylsiloxane) microfluidic devices. *Proc Natl Acad Sci USA.* 102:10813-10818.

Regehr, K.J., M. Domenech, J.T. Koepsel, K.C. Carver, S.J. Ellison-Zelski, W.L. Murphy, L.A. Schuler, E.T. Alarid, and D.J. Beebe. 2009. Biological implications of polydimethylsiloxane-based microfluidic cell culture. *Lab Chip.* 9:2132-2139.

Roman, G.T., and C.T. Culbertson. 2006. Surface engineering of poly(dimethylsiloxane) microfluidic devices using transition metal sol-gel chemistry. *Langmuir.* 22:4445-4451.

Roman, G.T., T. Hlaus, K.J. Bass, T.G. Seelhammer, and C.T. Culbertson. 2005. Sol−Gel Modified Poly(dimethylsiloxane) Microfluidic Devices with High Electroosmotic Mobilities and Hydrophilic Channel Wall Characteristics. *Anal Chem.* 77:1414-1422.

Roth, I., and S.J. Fisher. 1999. IL-10 is an autocrine inhibitor of human placental cytotrophoblast MMP-9 production and invasion. *Dev Biol.* 205:194-204.

Sanda, T., S. Iida, H. Ogura, K. Asamitsu, T. Murata, K.B. Bacon, R. Ueda, and T. Okamoto. 2005. Growth Inhibition of Multiple Myeloma Cells by a Novel IκB Kinase Inhibitor. *Clin Cancer Res.* 11:1974-1982.

Schaerli, Y., R.C. Wootton, T. Robinson, V. Stein, C. Dunsby, M.A.A. Neil, P.M.W. French, A.J. deMello, C. Abell, and F. Hollfelder. 2009. Continuous-Flow Polymerase Chain Reaction of Single-Copy DNA in Microfluidic Microdroplets. *Anal Chem.* 81:302-306.

Schenone, M., V. Dancik, B.K. Wagner, and P.A. Clemons. 2013. Target identification and mechanism of action in chemical biology and drug discovery. *Nat Chem Biol.* 9:232-240.

Schreiber, S.L. 1998. Chemical genetics resulting from a passion for synthetic organic chemistry. *Bioorg Med Chem.* 6:1127-1152.

Schreiber, S.L. 2003. The small-molecule approach to biology. *Chem Eng News.* 81:51-+.

Scott, C.W., C. Sobotka-Briner, D.E. Wilkins, R.T. Jacobs, J.J. Folmer, W.J. Frazee, R.V. Bhat, S.V. Ghanekar, and D. Aharony. 2003. Novel Small Molecule Inhibitors of Caspase-3 Block Cellular and Biochemical Features of Apoptosis. *J Pharmacol Exp Ther.* 304:433-440.

Shi, J., E. Schmitt-Talbot, D.A. DiMattia, and R.G. Dullea. 2004. The differential effects of IL-1 and TNF-alpha on proinflammatory cytokine and matrix metalloproteinase expression in human chondrosarcoma cells. *Inflamm Res.* 53:377-389.

Shim, J.U., S.N. Patil, J.T. Hodgkinson, S.D. Bowden, D.R. Spring, M. Welch, W.T. Huck, F. Hollfelder, and C. Abell. 2011. Controlling the contents of microdroplets by exploiting the permeability of PDMS. *Lab Chip*. 11:1132-1137.

Shuman Moss, L.A., S. Jensen-Taubman, and W.G. Stetler-Stevenson. 2012. Matrix Metalloproteinases: Changing Roles in Tumor Progression and Metastasis. *Am J Pathol*. 181:1895-1899.

Skhiri, Y., P. Gruner, B. Semin, Q. Brosseau, D. Pekin, L. Mazutis, V. Goust, F. Kleinschmidt, A. El Harrak, J.B. Hutchison, E. Mayot, J.F. Bartolo, A.D. Griffiths, V. Taly, and J.C. Baret. 2012. Dynamics of molecular transport by surfactants in emulsions. *Soft Matter*. 8:10618-10627.

Song, H., and R.F. Ismagilov. 2003. Millisecond kinetics on a microfluidic chip using nanoliters of reagents. *J Am Chem Soc*. 125:14613-14619.

Song, H., J.D. Tice, and R.F. Ismagilov. 2003. A microfluidic system for controlling reaction networks in time. *Angew Chem Int Edit*. 42:768-772.

Spellberg, B., J.G. Bartlett, and D.N. Gilbert. 2013. The Future of Antibiotics and Resistance. *N Engl J Med* 368:299-302.

Steward, W.P. 1999. Marimastat (BB2516): current status of development. *Cancer Chemother Pharmacol*. 43 Suppl:S56-60.

Stuve, O., N.P. Dooley, J.H. Uhm, J.P. Antel, G.S. Francis, G. Williams, and V.W. Yong. 1996. Interferon beta-1b decreases the migration of T lymphocytes in vitro: effects on matrix metalloproteinase-9. *Ann Neurol*. 40:853-863.

Takayama, S., E. Ostuni, P. LeDuc, K. Naruse, D.E. Ingber, and G.M. Whitesides. 2001. Subcellular positioning of small molecules. *Nature*. 411:1016.

Takle, A.K., M.J.B. Brown, S. Davies, D.K. Dean, G. Francis, A. Gaiba, A.W. Hird, F.D. King, P.J. Lovell, A. Naylor, A.D. Reith, J.G. Steadman, and D.M. Wilson. 2006. The identification of potent and selective imidazole-based inhibitors of B-Raf kinase. *Bioorg Med Chem Lett*. 16:378-381.

Tan, Y.-C., J.S. Fisher, A.I. Lee, V. Cristini, and A.P. Lee. 2004. Design of microfluidic channel geometries for the control of droplet volume, chemical concentration, and sorting. *Lab Chip*. 4:292-298.

Thorsen, T., R.W. Roberts, F.H. Arnold, and S.R. Quake. 2001. Dynamic pattern formation in a vesicle-generating microfluidic device. *Phys Rev Lett*. 86:4163-4166.

Toepke, M.W., and D.J. Beebe. 2006. PDMS absorption of small molecules and consequences in microfluidic applications. *Lab Chip*. 6:1484-1486.

Tung, Y.-C., Y.-s. Torisawa, N. Futai, and S. Takayama. 2007. Small volume low mechanical stress cytometry using computer-controlled Braille display microfluidics. *Lab Chip*. 7:1497-1503.

Umbanhowar, P.B., V. Prasad, and D.A. Weitz. 2000. Monodisperse emulsion generation via drop break off in a coflowing stream. *Langmuir*. 16:347-351.

Unger, M.A., H.P. Chou, T. Thorsen, A. Scherer, and S.R. Quake. 2000. Monolithic microfabricated valves and pumps by multilayer soft lithography. *Science*. 288:113-116.

Upadhyaya, S., and P.R. Selvaganapathy. 2010. Microfluidic devices for cell based high throughput screening. *Lab Chip*. 10:341-348.

Utada, A.S., E. Lorenceau, D.R. Link, P.D. Kaplan, H.A. Stone, and D.A. Weitz. 2005. Monodisperse double emulsions generated from a microcapillary device. *Science*. 308:537-541.

Uttamsingh, S., X. Bao, K.T. Nguyen, M. Bhanot, J. Gong, J.L. Chan, F. Liu, T.T. Chu, and L.H. Wang. 2008. Synergistic effect between EGF and TGF-beta1 in inducing oncogenic properties of intestinal epithelial cells. *Oncogene*. 27:2626-2634.

van 't Veer, L.J., and R. Bernards. 2008. Enabling personalized cancer medicine through analysis of gene-expression patterns. *Nature*. 452:564-570.

Van den Steen, P.E., B. Dubois, I. Nelissen, P.M. Rudd, R.A. Dwek, and G. Opdenakker. 2002. Biochemistry and molecular biology of gelatinase B or matrix metalloproteinase-9 (MMP-9). *Crit Rev Biochem Mol Biol*. 37:375-536.

VanDersarl, J.J., A.M. Xu, and N.A. Melosh. 2011. Rapid spatial and temporal controlled signal delivery over large cell culture areas. *Lab Chip*. 11:3057-3063.

Vandooren, J., P.E. Van den Steen, and G. Opdenakker. 2013. Biochemistry and molecular biology of gelatinase B or matrix metalloproteinase-9 (MMP-9): the next decade. *Crit Rev Biochem Mol Biol*. 48:222-272.

Vassilev, L.T., B.T. Vu, B. Graves, D. Carvajal, F. Podlaski, Z. Filipovic, N. Kong, U. Kammlott, C. Lukacs, C. Klein, N. Fotouhi, and E.A. Liu. 2004. In vivo activation of the p53 pathway by small-molecule antagonists of MDM2. *Science*. 303:844-848.

Vu, T.H., J.M. Shipley, G. Bergers, J.E. Berger, J.A. Helms, D. Hanahan, S.D. Shapiro, R.M. Senior, and Z. Werb. 1998. MMP-9/Gelatinase B Is a Key Regulator of Growth Plate Angiogenesis and Apoptosis of Hypertrophic Chondrocytes. *Cell*. 93:411-422.

Vyawahare, S., A.D. Griffiths, and C.A. Merten. 2010. Miniaturization and Parallelization of Biological and Chemical Assays in Microfluidic Devices. *Chem Biol*. 17:1052-1065.

Waelchli, R., B. Bollbuck, C. Bruns, T. Buhl, J. Eder, R. Felfel, R. Hersperger, P. Janser, L. Revesz, H.G. Zerwes, and A. Schlapbach. 2006. Design and preparation of 2-benzamido-pyrimidines as inhibitors of IKK. *Bioorg Med Chem Lett*. 16:108-112.

Walsh, L.A., and S. Damjanovski. 2011. IGF-1 increases invasive potential of MCF 7 breast cancer cells and induces activation of latent TGF-beta1 resulting in epithelial to mesenchymal transition. *Cell Commun Signal*. 9:10.

Wang, J., H.C. Fan, B. Behr, and Stephen R. Quake. 2012a. Genome-wide Single-Cell Analysis of Recombination Activity and De Novo Mutation Rates in Human Sperm. *Cell*. 150:402-412.

Wang, J.D., N.J. Douville, S. Takayama, and M. ElSayed. 2012b. Quantitative analysis of molecular absorption into PDMS microfluidic channels. *Ann Biomed Eng*. 40:1862-1873.

Wang, J.Y., G.D. Sui, V.P. Mocharla, R.J. Lin, M.E. Phelps, H.C. Kolb, and H.R. Tseng. 2006. Integrated microfluidics for parallel screening of an in situ click chemistry library. *Angew Chem Int Edit*. 45:5276-5281.

Wang, Y., W.-Y. Lin, K. Liu, R.J. Lin, M. Selke, H.C. Kolb, N. Zhang, X.-Z. Zhao, M.E. Phelps, C.K.F. Shen, K.F. Faull, and H.-R. Tseng. 2009. An integrated microfluidic device for large-scale in situ click chemistry screening. *Lab Chip*. 9:2281-2285.

Whitesides, G.M. 2006. The origins and the future of microfluidics. *Nature*. 442:368-373.

Wolf, K., Y.I. Wu, Y. Liu, J. Geiger, E. Tam, C. Overall, M.S. Stack, and P. Friedl. 2007. Multi-step pericellular proteolysis controls the transition from individual to collective cancer cell invasion. *Nat Cell Biol*. 9:893-904.

Woronoff, G., A. El Harrak, E. Mayot, O. Schicke, O.J. Miller, P. Soumillion, A.D. Griffiths, and M. Ryckelynck. 2011. New Generation of Amino Coumarin Methyl Sulfonate-Based Fluorogenic Substrates for Amidase Assays in Droplet-Based Microfluidic Applications. *Anal Chem*. 83:2852-2857.

Xia, Y.N., and G.M. Whitesides. 1998. Soft lithography. *Angew Chem Int Edit*. 37:551-575.

Yan, C., and D.D. Boyd. 2007. Regulation of matrix metalloproteinase gene expression. *J Cell Physiol*. 211:19-26.

Yan, C., H. Wang, B. Aggarwal, and D.D. Boyd. 2004. A novel homologous recombination system to study 92 kDa type IV collagenase transcription demonstrates that the NF-kappaB motif drives the transition from a repressed to an activated state of gene expression. *FASEB J*. 18:540-541.

Yeh, P., A.I. Tschumi, and R. Kishony. 2006. Functional classification of drugs by properties of their pairwise interactions. *Nat Genet*. 38:489-494.

Yeh, P.J., M.J. Hegreness, A.P. Aiden, and R. Kishony. 2009. SYSTEMS MICROBIOLOGY - OPINION Drug interactions and the evolution of antibiotic resistance. *Nat Rev Microbiol*. 7:460-466.

Yoo, J., C.E. Rodriguez Perez, W. Nie, J. Sinnett-Smith, and E. Rozengurt. 2011. Protein kinase D1 mediates synergistic MMP-3 expression induced by TNF-alpha and bradykinin in human colonic myofibroblasts. *Biochem Biophys Res Commun*. 413:30-35.

Zucker, S., and J. Cao. 2009. Selective matrix metalloproteinase (MMP) inhibitors in cancer therapy Ready for prime time? *Cancer Biol Ther*. 8:2371-2373.

9 ABBREVATIONS

5-FAM	5-Carboxyfluorescein
Abu	2-Aminobutyric acid
Ala	Alanine
AP-1	Activator protein-1
ATCC	American type culture collection
BF	Bright field
BSA	Bovine serum albumin
CAD	Computer-aided design
CCD	Charge-coupled device
Cha	Cyclohexylamine
Dab	2,4-Diaminobutyric acid
DMEM	Dulbecco's modified Eagles Medium
DMSO	Dimethylsulfoxide
dpi	Dots per inch
EDTA	Ethylenediaminetetraacetic acid
EGF	Epidermal growth factor
EGFR	Epidermal growth factor receptor
EMBL	European molecular biology laboratory
FBS	Fetal bovine serum
FDG	Fluorescein di-β-D-galactopyranoside
FL	Fluorescent channel
FRET	Förster resonance energy transfer
FS	Gibco® FreeStyle™ 293 Expression Medium
GFP	Green fluorescent protein
His	Histidine
IFN	Interferon
IL	Interleukin
Lys	Lysine
MMP	Matrix metalloproteinase
MPBD	5-methyl-2-(4-methylphenyl)-1H-benzimidazole
NR	Nile red
PBS	Phosphate buffered saline
PCR	Polymerase chain reaction
PDMS	Polydimethylsiloxane

PEG	Polyethylene glycol
PFO	Perfluorooctanol
PFPE	Perfluoropolyether
PMA	Phorbol 12-myristate 13-acetate
PMT	Photomultiplier tube
Pro	Proline
PTFE	Polytetrafluoroethylene
RFU	Relative fluorescence unit
rpm	Rounds per minute
Smc	S-methyl-L-cysteine
SR	Sulforhodamine B
Tet	Tetracycline
TGF	Transforming growth factor
TNF	Tumor necrosis factor
UV	Ultraviolet

10 APPENDIX

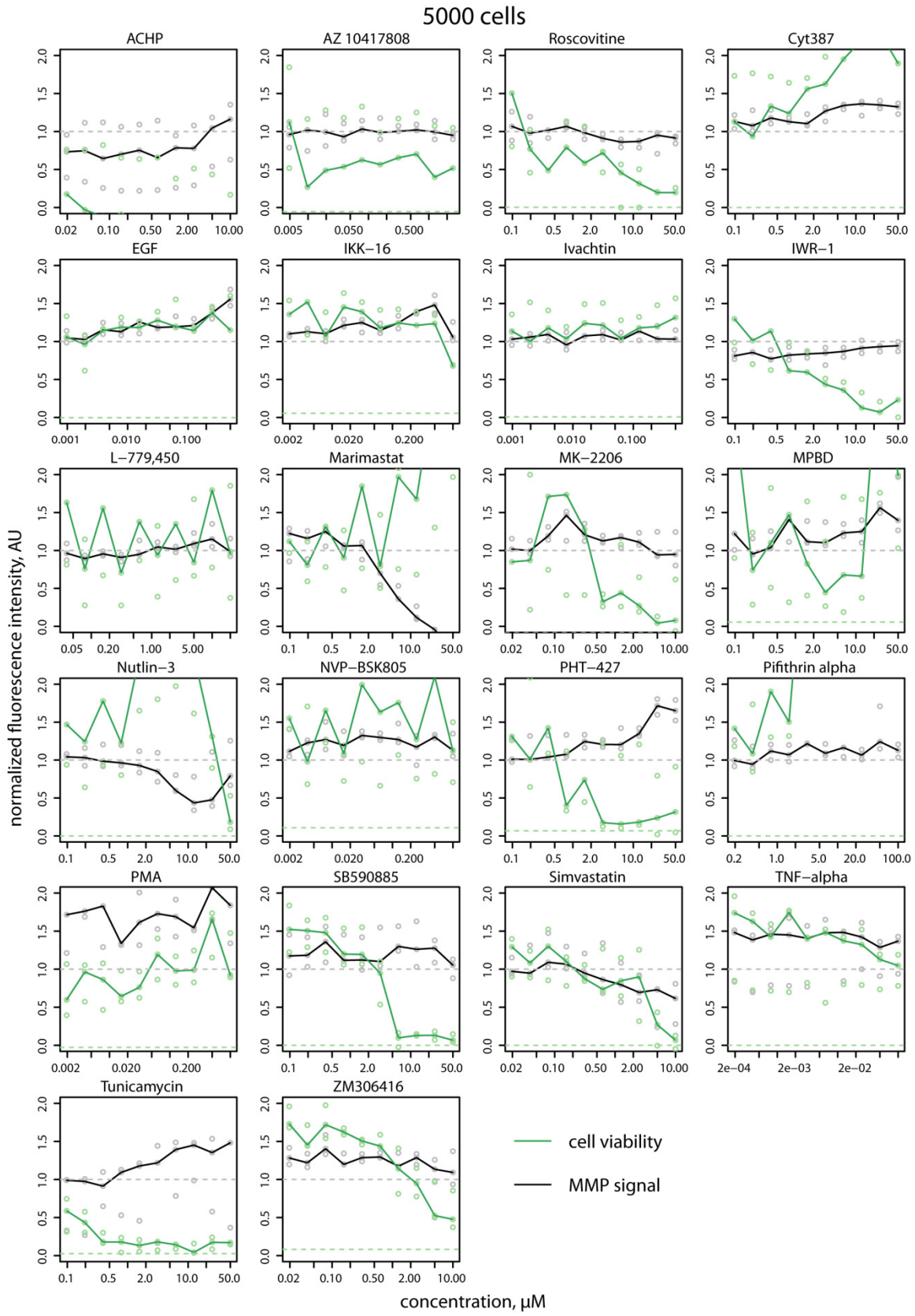

Figure 10.1 Individual plots for all detected drug combination samples in a 6 vs 6 drug screen. The name of each combination is indicated above every individual plot. Green lines show MMP FRET substrate fluorescence and red circles indicate individual detected plug signals. 5000 HT1080 cells were seeded in each well.

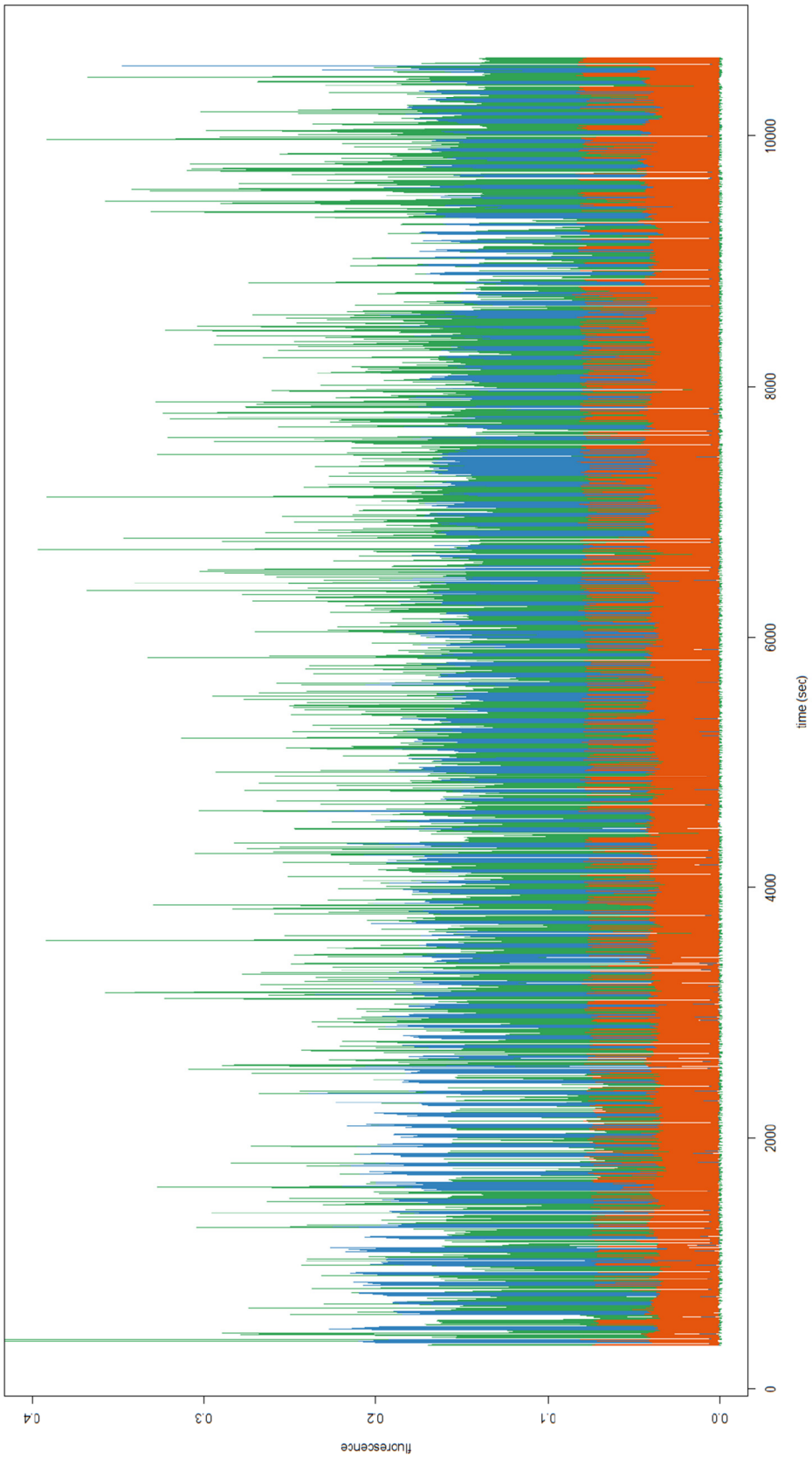

Figure 10.2 Overview of the recorded fluorescence data for a full combinatorial screen of twelve compounds. Fluorescence was measured simultaneously in the green (525±22.5 nm), orange (594+ nm) and blue (448±10 nm) fluorescence channels. Depicted are all fluorescence signals recorded over the course of a complete experiment.

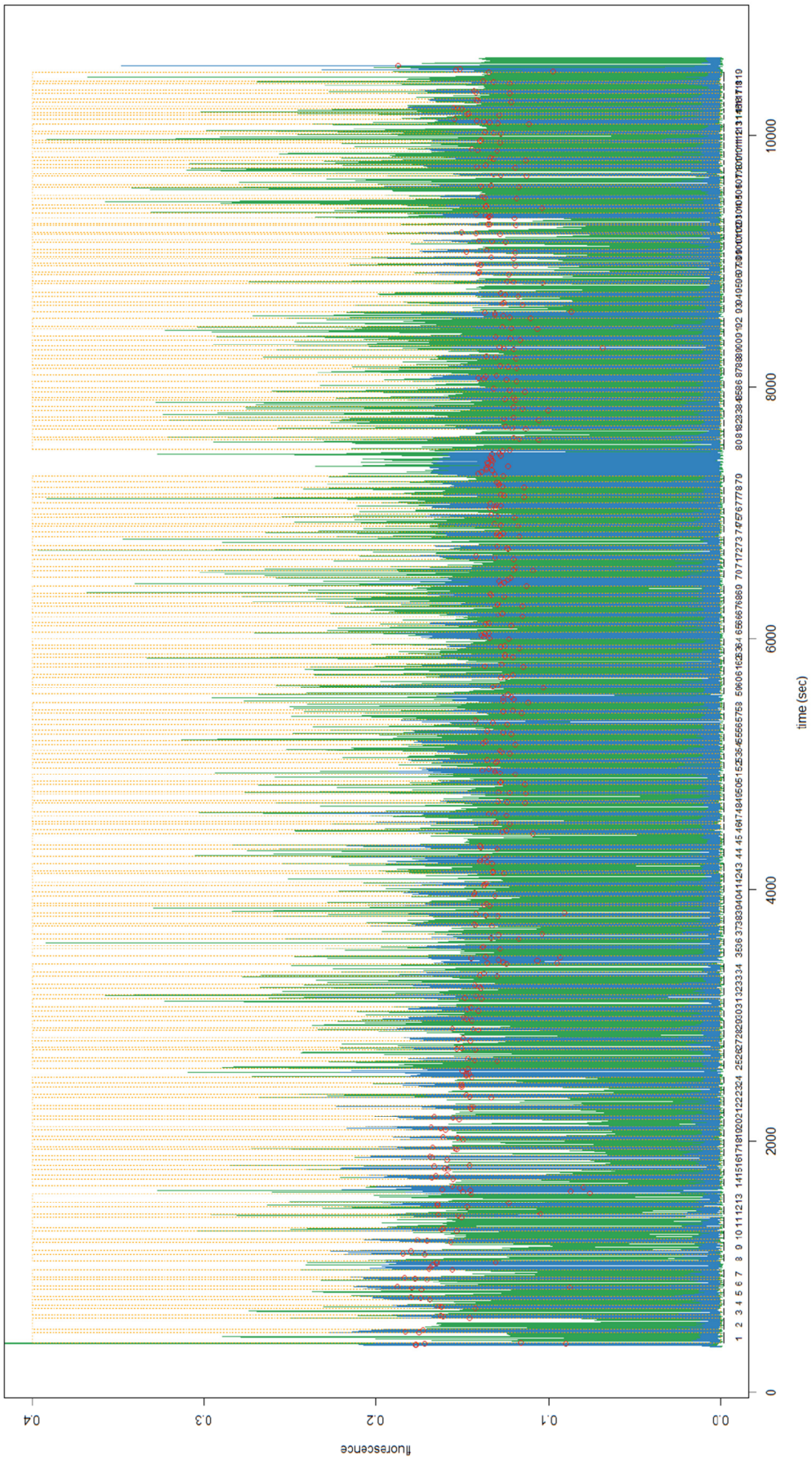

Figure 10.3 Overview of detected sample and label plugs in a full combinatorial screen of 12 compounds.

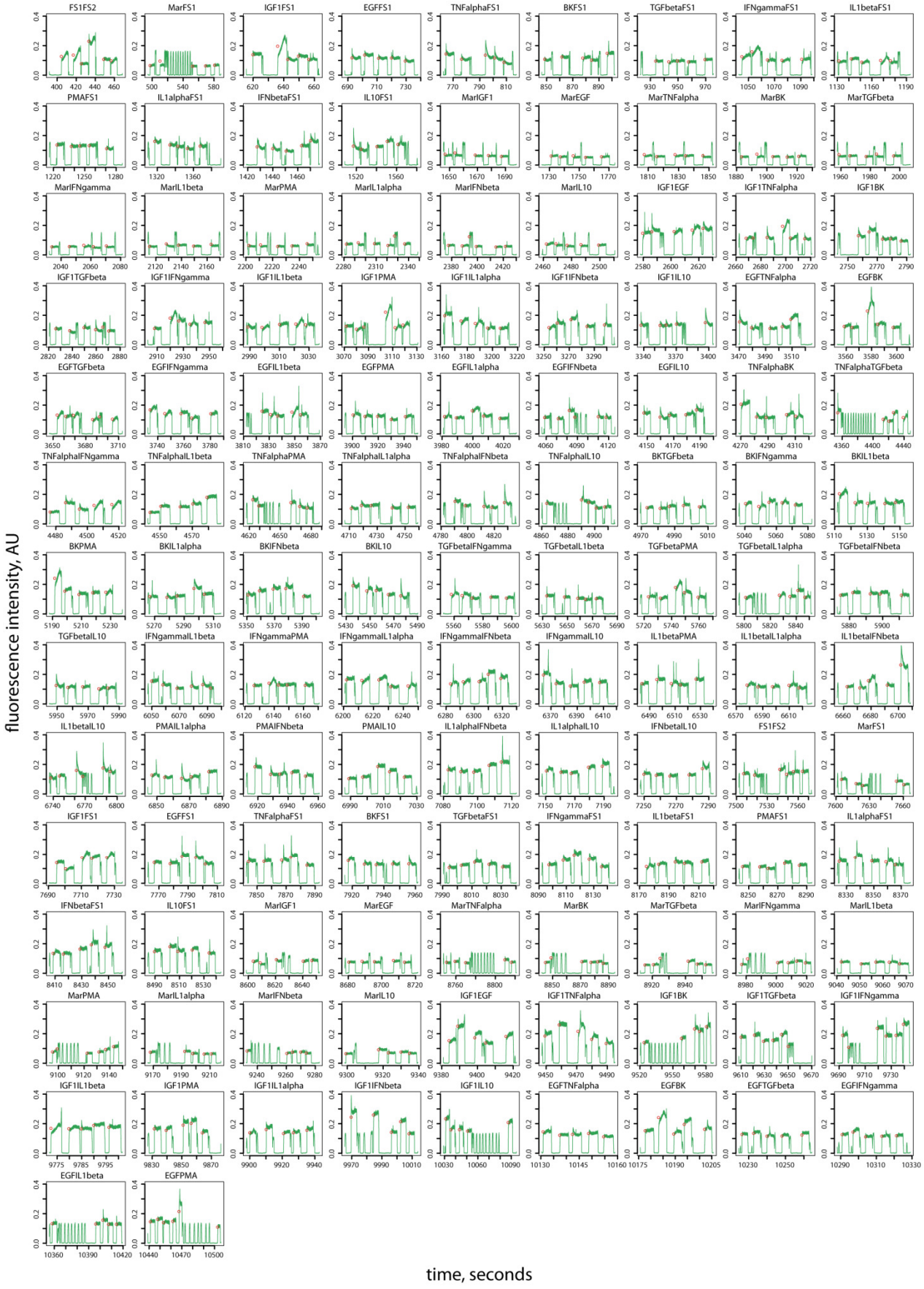

Figure 10.4 Individual plots for all detected drug combination samples in a full combinatorial MMP activity screen.